Microfluidic Bioreactor to Simulate Fluid Flow in a Tissue Engineered Heart Valve

A Major Qualifying Project

Submitted to the Faculty of
WORCESTER POLYTECHNIC INSTITUTE

In partial fulfillment of the requirements
for the Degree of Bachelor of Science

Submitted By:

Sydney Hertel

Sydney Hertel

Isaac Petruzziello

Isaac Petruzziello

Miranda Pitta

Miranda Pitta

Emily Sansoucy

Emily Sansoucy

Date: May 3, 2022
Approved:

_____   _____

Prof. Kristen L. Billiar, Advisor

This report represents the work of one or more WPI undergraduate students submitted to the faculty as evidence of completion of a degree requirement. WPI routinely publishes these reports on the web without editorial or peer review

Table of Contents

Authorship

Section	Author	Editor
I. Introduction	Sydney	Emily
II. Heart Valves, Heart Valve Disease, & Flow	Emily	Sydney
II. Current Existing Treatments	Miranda	Isaac
II. Tissue Engineered Heart Valves	Sydney	Emily
II. EndMT	Isaac	Miranda
II. Fluidic Pumps	Isaac	Sydney
II. Device Measuring Shear Stress on Cells	Isaac	Emily
II. State of the Art and Project Direction	Emily	Isaac
III. Design Process	Emily	Sydney
IV. Initial and Final Device Design	Sydney	Miranda
IV. PDMS Casting and Plasma Treatment	Miranda	Emily
IV. Design Testing; Gel Placement	Sydney	Miranda
IV. Characterization of Silicon Wafer	Miranda	Isaac
IV. Commercial Device Tested Upon	Sydney	Isaac
IV. Flow Through Decellularization in Transwell Plates	Miranda	Sydney
IV. Decellularization in AIM Biotech idenTx 3 Chip	Emily	Sydney
IV. Producing a Microfluidic Gravity Pump	Isaac	Miranda
IV. Programming of Solenoid Pinch Valves	Isaac	Sydney
V. Additional Considerations	Emily	Miranda
VI. Future Directions	Emily	Isaac

List of Figures

List of Tables

Acknowledgements

We would like to first thank our project advisor, Professor Kristen Billiar for his guidance and support throughout the duration of the project. We also want to thank Rozanne Mungai for serving as the project mentor. Her patience, guidance, and expertise contributed greatly to the success of this project.

Additionally, we want to acknowledge our gratitude to Professor Dirk Albrecht for his knowledge in the technical aspects of microfluidic devices. We also appreciate the help from Jyotsna Patel for her guidance in histology procedures and Eric Larsen and James Eakin for their help in the photolithography aspect of our project. With the gracious assistance from Taimoor Afzal we were able to create a circuit within our final designs. We would also like to give a final thanks to Lisa Wall, our lab manager, for her assistance in gathering the necessary equipment for the project. Our project would not have been possible without these individuals' support, guidance, and knowledge.

Abstract

Heart valve disease is a serious medical condition that causes improper flow of blood in the heart and affects millions of people globally. Although over 290,000 heart valve replacement surgeries are conducted annually worldwide, current valve replacement options are hindered by significant limitations and dangerous side effects. Tissue engineered heart valves (TEHV) offer great promise in producing improved valve replacements. Consisting of a fibrous matrix repopulated with the patient's cells, these valve replacements would be able to remodel and grow with the patient. Shear forces due to complex blood flow patterns around TEHV have been theorized to affect host cell repopulation of the decellularized engineered matrix. *In vitro* experiments are needed to study the effects of the flow patterns in a controlled manner, yet no high-throughput systems that allow for matrix decellularization and detailed observation of valvular cell proliferation, migration and differentiation exist. To fulfill this need, we developed a microfluidic system made up of a microfluidic chip and a gravity pump. The PDMS chip has a central chamber in which a fibroblast seeded hydrogel can be cultured, allowing it to create a cell derived matrix, and then decellularized by utilizing fluid channels parallel to the gel chamber. It was demonstrated that the decellularization process removes all cell materials below the ability to detect using fluorescent nuclear and cytoskeletal stains. We verified that the gravity pump can produce steady and oscillatory shear flow patterns relevant to healthy and diseased native heart conditions (0.2-2.0 Pa, 1 Hz). The pump consists of fluid reservoirs placed at customizable heights to allow for the ease of manipulating flow rates, and pinch valves to reverse the direction of flow in the device. Using this system, the attachment, migration, and differentiation of multiple cell types through engineered matrices can be studied to improve the design of TEHVs.

I. Introduction

Heart valve disease is a prevalent issue facing the population today and its incidence is expected to increase with the rising population, as well as the rising age of the population (Lincoln & Garg, 2014). As the only effective treatment is implantation of a new heart valve, over 290,000 valve replacement surgeries are conducted per year worldwide (Hasan et al., 2014). Current implantable heart valve replacements can be mechanical or bioprosthetic, however both are associated with a multitude of detrimental health consequences (Butcher et al., 2011). Additionally, there are pressing limitations to who is eligible to receive these implants due to their lack of versatility. One example is that mechanical valve implants cannot be placed in those who cannot tolerate taking anticoagulant medications, an essential drug to prevent blood clotting, for the duration of their lives, such as pregnant people, people intending to be pregnant at any point of their life, or elderly patients (Harris et al., 2015). Bioprosthetic valve implants also have their share of limitations. Only lasting ten to fifteen years, they require multiple surgeries throughout a patient's life (Hasan et al., 2018). These valves also do not grow with the patient, meaning pediatric patients would need multiple replacement surgeries as they grow older. For these reasons, tissue engineered heart valve research is crucial in developing long-lasting heart valve replacements.

It is essential that tissue engineered constructs are able to function under the hemodynamic forces present in human hearts. Therefore a thorough understanding of how mechanical forces impact cellular function in the heart valve is vital. Shear stresses due to steady and oscillatory blood flow patterns in the heart are of particular interest as they have been demonstrated to act as the catalyst for many valvular cell signaling pathways (Arjunon et al., 2013). For instance, shear stresses have been suggested to influence endothelial to mesenchymal transition (EndMT), a process by which endothelial cells (ECs) naturally found on the outer layer of the heart valve obtain characteristics of mesenchymal cells, which alters the structure of the valvular tissue and modifies its functionality (Kovacic, 2019). This process has been known to cause challenges in the functionality of engineered constructs (Muylaert et al., 2016).

To quantify EndMT the migration of cells into the extracellular matrix (ECM), a method to measure the migration and phenotype of cells must be developed. One means of accomplishing this task is through the implementation of a fluidic bioreactor. Fluidic bioreactors can be used to measure the migration of cells into a fibrous gel when fluid flows over a sample (Sucosky et al., 2008). Existing fluidic bioreactors that perform these particular functions vary in their abilities. Many are only able to simulate a flow over a two-dimensional matrix, which is an inaccurate comparison to three-dimensional conditions in the body (Cukierman et al., 2001). Furthermore, current fluidic bioreactor devices lack the ability to run a multitude of trials simultaneously, the ability to easily image cell migration, the ability to decellularize gels *in situ* and the ability to test steady and oscillatory flow patterns.

Due to the limitations of current microfluidic bioreactors, a newly designed microfluidic bioreactor that combats these limitations is needed. Though there is a range of highly functional fluidic bioreactors, very few have all of the features necessary to properly examine EndMT. Our

goal is to develop a microfluidic bioreactor that is able to measure migration of cells into a three-dimensional matrix and also permit the tracking of cell phenotype. Ideally, this device will also be a precise and effective tool to decellularize fibrous gels *in situ*. This microfluidic bioreactor will also be able to conduct multiple trials at once. Additionally, the device will be able to produce controlled steady and oscillatory flow patterns and the resulting shear stresses, both of which are found in the presence of native heart valve tissue.

II. Literature Review

A. Heart Valves, Heart Valve Disease & Flow

Valvular heart disease is a serious medical condition accounting for an estimated 20,000 deaths per year in the United States (Lloyd-Jones et al., 2010; Hinton & Yutzey, 2011). While all of the valves in the heart have the potential to be affected by this condition, the disease of the aortic valve is most common and therefore needs to be further studied (Hinton & Yutzey, 2011). In the United States, there is a 2.5% prevalence of aortic valve disease in the population which is expected to increase with the increasing population and age of the population (Hinton & Yutzey, 2011; Lincoln & Garg, 2014; Lloyd-Jones et al., 2010; Vahanian et al., 2007).

There are two major pathological mechanisms associated with valvular heart disease, stenosis and regurgitation (Hinton & Yutzey, 2011). Both of these mechanisms alter the flow of blood through the heart, thus leading to serious complications if left untreated (Hinton & Yutzey, 2011; Peeters et al., 2018). In stenosis, calcification of the heart valve prevents the valve from opening properly, which in turn restricts the outward flow of blood through the valve and creates an elevated pressure gradient across the valve (Arjunon et al., 2013; Hinton & Yutzey, 2011). Although calcification was originally proposed to be a passive result of aging, it is now believed that molecular and chemical pathways play a more significant role in the onset of calcification. The exact mechanism is still unknown (Peeters et al., 2018). In regurgitation, improper closing of the heart valve leads to backwards flow of blood. Figure 1 shows a schematic of healthy and diseased valves.
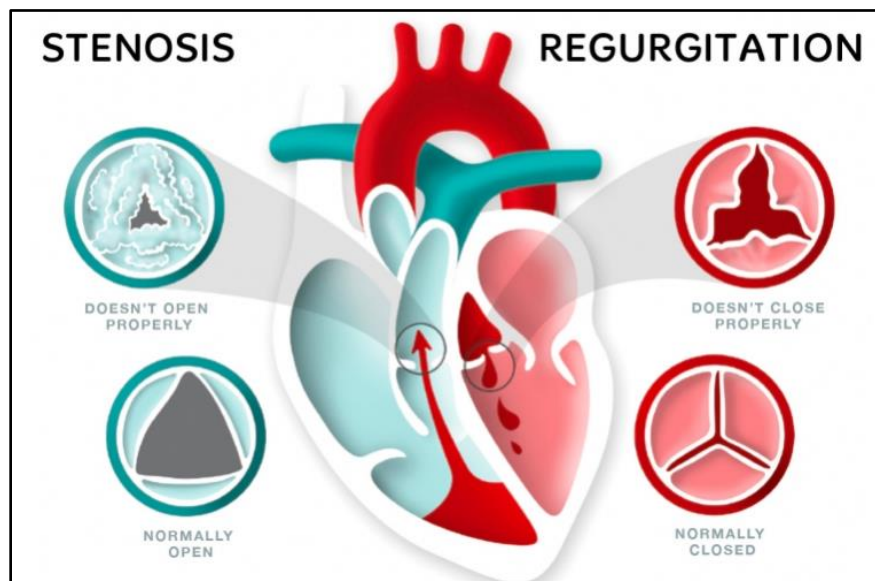
Figure 1: Heart Valve Stenosis and Regurgitation. A representation of a heart valve experiencing stenosis (upper left) is compared to a healthy valve in an open state (lower left). The representation of a heart valve experiencing regurgitation (upper right) is compared to a healthy valve in a closed state (lower right). Used with permission of the National Heart Foundation of New Zealand. heartfoundation.org.nz.

The human heart contains four distinct heart valves. The mitral and tricuspid valves are atrioventricular valves and are located between the atria and the ventricles, while the aortic and pulmonary valves are semilunar valves located between the ventricles and great arteries (Hinton & Yutzey, 2011). All of the valves work to maintain unidirectional flow of blood through the heart (Arjunon et al., 2013; Hinton & Yutzey, 2011). The thickness of the heart valve differs slightly based on valve type and location, however the aortic valve is typically less than 1mm in thickness (Hinton & Yutzey, 2011). The main components of heart valves are the three-dimensional extracellular matrix, valvular interstitial cells (VICs) and valvular endothelial cells (VECs) (Hinton & Yutzey, 2011; Peeters et al., 2018). The extracellular matrix, or ECM, is a stratified web of proteins which provides a scaffold for cell growth. This must be strong enough to withstand the forces of blood flow, but flexible enough that the leaflet yields, allowing the heart valve to open (Walker et al., 2004). Endothelial cells form a monolayer on the outside of the ECM and are responsible for regulating nutrient exchange and hemostasis (Peeters et al., 2018). VICs make up the majority of the structure of heart valves, perform most of the remodeling and excrete ECM components (Walker et al., 2004). More in depth descriptions of each of these components can be found in Appendix A.

It has been well reported that mechanical forces play a significant role in the regulation of the heart valve (Arjunon et al., 2013). A healthy heart undergoes various mechanical stresses based on the stage of the cardiac cycle. When the valve is closed, tensile forces are present in the valve leaflets and hemostatic pressure is applied. As the valves open and close, they experience flexure. Finally, as blood passes through the valve, shear stress is applied to the VECs as a result of the friction present between the blood and the valvular walls (Arjunon et al., 2013; Hinton & Yutzey, 2011). During the blood flow process, one side of the heart valve experiences oscillatory flow, while the other experiences steady flow. Steady flow is indicative of a smooth flow pattern in which fluid particles follow the path of the particles preceding them (Islam & Hossain, 2021). Conversely, oscillatory flow is defined as flow patterns of fluctuating magnitude which follow trajectories in both forward and backwards directions (Hsu et al., 2020). During systole, the aorta is open to allow flow out of the heart valve, resulting in the flow being tangential to the valve leaflets. During diastole, the valve is closed, meaning the flow pushes on the valve leaflets directly. This direct pressure will be raised in systole to cause the valves to open. The forces experienced by the aortic valve during the systolic phase are diagrammed in Figure 2. Forces regulate the proteins expressed by the VECs. It is speculated that the different shear forces experienced on either side of the leaflet contributes to the differing gene transcription profiles detected from VECs on either side of the leaflet (Arjunon et al., 2013).
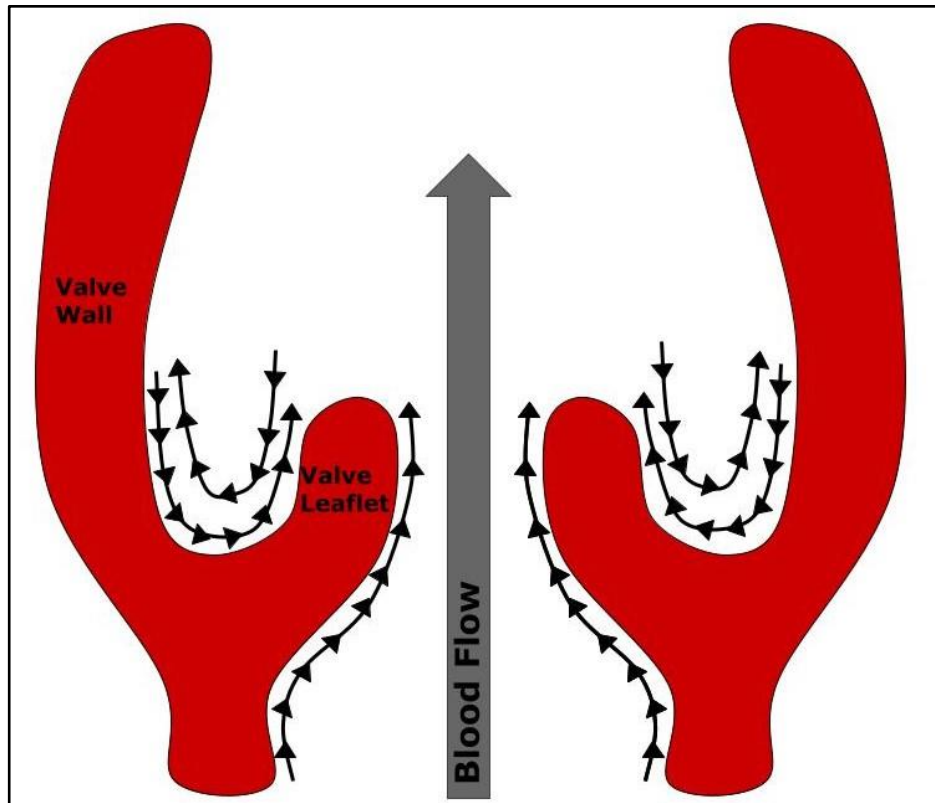
Figure 2: Shear Forces on Aortic Valves. The mechanical forces that the aortic valve experiences upon the opening of the heart valve. Steady shear is exerted on the underside of the leaflets, and oscillatory flow is exerted on the topside of the leaflets. Image adapted from Arjunon et al., 2013 and used with copyright approval from Springer.

Irregular flow and corresponding shear patterns inflicted onto the valvular walls has been speculated to contribute to the pathology of valvular heart disease (Arjunon et al., 2013; Hinton & Yutzey, 2011; Peeters et al., 2018). Specifically, altered shear stress patterns have been linked to ECM maladaptation, altered EC protein expression, EC damage, EC activation and EC proliferation (Arjunon et al., 2013; Hinton & Yutzey, 2011; Peeters et al., 2018). These abnormalities caused by irregular flow are associated with valvular heart disease, although not all of the mechanisms linking them are fully understood. For instance, EC damage induces an inflammatory response which can become a trigger for the initiation of valve calcification and stenosis (Peeters et al., 2018). Likewise, maladaptive ECM remodeling has been linked to calcified aortic valves (Brecs et al., 2018). Furthermore, the progression of stenosis or regurgitation of the heart valve is further amplified by the altered flow patterns that these conditions cause (Peeters et al., 2018). Therefore, it is clear that understanding the impact shear stress has on heart valve function is paramount to understanding the mechanisms which lead to valvular heart disease.

13

B. Current Existing Treatments

As the mechanisms behind heart valve disease are not yet fully understood, treatments for the condition are limited. The only viable treatment for severe heart valve disease is a heart valve replacement. Medications and valve repair surgery may slow the progression of heart valve disease, but will never stop it (Zhu & Grande-Allen, 2018). Valve replacement is currently used for treating both stenosis and regurgitation. Options for replacement valves fall into two categories, mechanical valves and bioprosthetic valves (Cukierman et al., 2001).

Mechanical valves are typically made of pyrolytic carbon-coated metals (Ahmed, 2017). Their structure is that of metal leaflets held inside of a suture ring. Shear forces are created by blood passing through the valve which causes platelet lysis and protein aggregation (Butcher et al., 2011). Platelet activation leads to blood clotting, which is extremely dangerous as it can cause pain, stroke, pulmonary embolism, deep vein thrombosis, or in very severe cases, death (Ellis, 2014). To prevent clotting, blood-thinning medications are required for life after valve replacement surgery (Hasan et al., 2018). With these drugs, patients have a 2-5% annual cumulative risk of serious bleeding events like hemorrhage, stroke, or infarction (Butcher et al., 2011). Blood thinners are generally considered unsafe to take during pregnancy, so people who are pregnant or plan on becoming pregnant in their lifetimes are not eligible to receive a mechanical heart valve replacement (Harris et al., 2015). Additionally, those with uncontrolled high blood pressure or stomach ulcers can also not take blood thinners and are not eligible for mechanical valve replacements (Butcher et al., 2011). Typically, if there are no complications, patients can live with mechanical valves for 20-30 years (Ahmed, 2017; Hasan et al., 2018). However, this means a pediatric patient would require several replacement surgeries throughout their lifetime.

Another category of heart valve replacement options is bioprosthetic valves. These can be a human allograft, bovine xenograft, or porcine xenograft valve (Zhu & Grande-Allen, 2018). Bioprosthetic valves can be implanted with or without the use of a stent. Stented valves have a synthetic sewing ring, which is used to sew it into the body. Stentless valves retain the tissue around the valve, which can be sewn into the body in a similar fashion (Butcher et al., 2011). Bioprosthetic valves have a lower chance of thrombosis compared to mechanical valves because they don't have mechanical leaflet hinges (Hasan et al., 2018). The valve is a tissue graft and because of this there is a risk of structural degradation (Schoen, 2012, Butcher et al., 2011). In conjunction, these patients' valves are prone to accumulation of proteins and lipids which can again lead to a diseased state (Hasan et al., 2018). Bioprosthetic valves are not recommended for people who are very active, as this causes extra strain on the valve. These valves only last approximately 10-15 years, after which they must be replaced, meaning they are inadequate for pediatric patients (Harris et al., 2015). Typically they are recommended for people ages 60 or older who get little regular physical activity and those who cannot tolerate blood thinners (Butcher et al., 2011).

One benefit of bioprosthetic valves over mechanical valves is that they can be implanted using a procedure called transcatheter aortic valve replacement (TAVR) where the diseased

valve is not removed and instead the graft valve is placed inside the diseased valve (Harris et al., 2015). This approach is far less invasive because it can be done without opening the chest cavity, allowing patients who are not eligible to undergo open heart surgery to still receive treatment. At this time there is no significant difference in mortality rates between patients who undergo TAVR and those that undergo traditional valve replacement surgery (Mc Morrow et al., 2020). It has been found in numerous studies that TAVR is not statistically inferior to other valve replacement methods (Makkar et al., 2012; Reardon et al., 2017).

The current risks associated with the aforementioned valves create the need for tissue engineered heart valves (TEHV). Neither mechanical nor bioprosthetic valves can grow with the body, meaning children would need multiple valve replacements over their childhood (Hasan et al., 2018). Both options run the risk of reoperation, especially in younger patients. They also pose a risk for those who cannot tolerate blood thinning medications but are still active, as there is no option that doesn't present a large risk of reoperation (Harris et al., 2015). Tissue engineered heart valves present a way to create replacement heart valves that are biocompatible, long lasting and lower risk than traditional heart valve replacements.

C. Tissue Engineered Heart Valves

Tissue engineering is the concept of using new biomaterials to restore, maintain, improve, or replace biological tissues (Mendelson & Schoen, 2006). Tissue engineering allows for cell growth, nutrient supply access, waste removal, migration, proliferation and differentiation in the newly created structure (Mendelson & Schoen, 2006). Additionally, tissue engineered biomaterials are able to grow with patients (Cheung et al., 2015; Mendelson & Schoen, 2006).

A well-established approach to tissue engineering involves the application of three-dimensional scaffolds which serve as structural supports for the promotion of cellular attachment and proliferation (Vesely, 2005). As the field of tissue engineering has progressed, various synthetic scaffolding materials have been explored for use in tissue engineered heart valves. The types of scaffolds typically employed for tissue engineered heart valves are 3D porous scaffolds, fibrous scaffolds and hydrogels (Shinoka & Miyachi, 2016).

Synthetic materials have the advantage of customizability in terms of material properties, however they are limited in their ability to mimic the natural structures found *in vivo*. The list of synthetic scaffold materials that have been applied to the engineering of heart valves are vast and range from felt to more recently established bioresorbable polymers (Merryman, 2015; Shinoka & Miyachi, 2016). Bioresorbable scaffolding materials are designed to be gradually replaced with living tissue as the degradation byproducts are reabsorbed into the body (Vesely, 2005). Similarly, a variety of manufacturing processes including particulate leaching, solvent casting and electrospinning have been used to construct the scaffolds (Shinoka & Miyachi, 2016). These processes create pores in the materials to better facilitate cell adherence to the scaffold. Woven meshes composed of polymers such as polyglactin have also been explored for this application (Shinoka & Miyachi, 2016). Furthermore, to improve the mechanical properties of the tissue

engineered heart valves, a concept known as preconditioning can be implemented. In preconditioning, a bioreactor is utilized to expose the tissue engineered construct to the *in vivo* mechanical conditions prior to implantation in the body (Stassen et al., 2017). Preconditioning has been demonstrated to improve cell adhesion to vascular grafts (Baguneid et al., 2004).

To improve the structure of scaffolds so that they better represent native structures, biologically derived scaffolds can be explored. One method of tissue engineering is to utilize the preexisting extracellular structures in all tissue types to repopulate with cells of choice. This allows the new cellular structure to form in the correct orientation around the scaffold. This scaffold, called the extracellular matrix (ECM) functions as the structural component of the tissue as well as the regulatory body. The ECM regulates migration, proliferation and differentiation, controls communication between cells and separates different types of tissue (Fernández-Pérez & Ahearne, 2019). The ECM is composed of a complex and diverse set of molecules. There are three main classes of ECM components, glycosaminoglycans (GAGs), fibrous proteins and proteoglycans. GAGS are polysaccharides and they are responsible for cellular signaling (Casale & Crane, 2021). There are many types of fibrous proteins, including collagens and elastins. These make up structural components of ECM. Proteoglycans, such as fibrogen, are responsible for adhering cells to the fibrous proteins. Each type of tissue has a uniquely shaped ECM to support it (Badylak et al., 2009).

One of the major components of tissue engineering is the scaffold upon which the new tissue will be built. One such scaffold is a decellularized extracellular matrix. This preserves the tissue's native environment. The decellularization process removes living cells from the heart valve tissue, leaving behind only the ECM. This provides a scaffold for autologous cells to repopulate (Taylor et al., 2018). This method of decellularization is used to study cell growth, migration and proliferation of different cell types seeded onto the decellularized extracellular matrix (dECM). dECM can be obtained from many species, making it relatively easy to procure (Taylor et al., 2018). The dECM retains functional ECM proteins, allowing researchers to mimic a natural environment for cellular growth (Taylor et al., 2018). dECM also contains growth factors such as transforming growth factor beta (TGF-β) and vascular endothelial growth factor (VEGF), which encourage the differentiation of cells into different cell types and encourage vascular growth (Fernández-Pérez & Ahearne, 2019). Necessary mechanical support for these processes is provided, including proper vascular structure (Taylor et al., 2018). It has been proven that dECM facilitates constructive remodeling of the cellular tissue in both human and animal models (Badylak et al., 2009).

Several *in vivo* studies of dECM engineered heart valves in sheep models have been conducted. In these studies, decellularized tissues are implanted and allowed to remodel *in vivo*. However, abnormal remodeling in these implanted valves has been demonstrated to contribute to leaflet retraction or leaflet thickening (Flanagan et al., 2009; Gottlieb et al., 2010; Reimer et al., 2017; Syedain et al., 2015). In the case of leaflet retraction, the valves resemble a heart valve afflicted by regurgitation and leaflet thickening resembles a heart valve affected by stenosis. Additionally, an *in vivo* 2021 study implanted TEHV composed of decellularized ECM into

sheep for 52 weeks. The valves were stained and imaged for the presence of both valvular interstitial cells and endothelial cells. While some host cell repopulation was documented, this repopulation was not sufficient (Syedain et al., 2021). Thus, more research is required to understand the mechanisms behind this aberrant remodeling.

Current animal models have shown the promise of TEHVs *in vivo*. In a study conducted by Reimer et al., 2017, pediatric TEHV were constructed and implanted into the main pulmonary artery of a growing lamb. The valves functioned well for up to eight weeks, after which leaflet shortening, partial leaflet recellularization and cell phenotype changes were observed. Full recellularization of valve roots have been seen, but typically the leaflet itself remains mostly acellular (VeDepo et al., 2017, Reimer et al., 2017). Based on these observations, recellularization is believed to begin at the vessel wall (Motta et al., 2020, VeDepo et al., 2017). However, it has also been found that an endothelial layer of cells accumulates on the surface of the leaflets which is likely due to circulating cells adhering to the leaflets (Syedain et al., 2021). It is not currently known what signaling factors cause VECs to infiltrate the leaflet surface and therefore the process of recellularization must be studied.

Decellularization and repopulation are major steps in the development of TEHV. In order to use tissue engineering effectively, the structural, biological and chemical properties of the cells repopulating the matrix must be taken into consideration. One such process which affects these cells is EndMT, which has numerous effects on the composition, structure and functionality of the TEHV.

D. EndMT

Tissue engineered heart valves are inserted into the patient either pre-populated with endothelial cells or decellularized entirely. A major question in the development of TEHV is how they are repopulated. One hypothesis is that circulating cells in the bloodstream attach to the surface of the matrix and a process known as endothelial to mesenchymal transition (EndMT) causes them to invade, populating the interior. EndMT is the process by which endothelial cells (ECs) transition into mesenchymal-like cells in response to environmental and intracellular factors (Kovacic, 2019). This process both increases the structural integrity of the TEHV and may result in several disease states due to a lack of endothelial cells on the external layer. ECs line the inside of the heart, heart valves and blood vessels. They are responsible for producing chemicals which inhibit blood clotting and play a significant role in the structure of the heart and cardiovascular network (Pober, 2007). Mesenchymal cells are a variety of multipotent stem cell which can differentiate into many kinds of cells including osteocytes, a cell type found in bone (Tonk, 2020). The newly transitioned cells display chemical markers typically associated with mesenchymal cells, such as α-SMA and calponin. The loss of ECs can cause structural complications, especially within heart valves, which may cause a transition into a diseased state such as regurgitation or stenosis. A loss of regulatory chemicals from ECs can also lead to an increase in blood clots. The calcification of a heart valve leads to increased stress on the valve, as well as increasing the effects of stenosis.

The process of EndMT is observed in two primary manners. The first is ECM invasion, where the newly transitioned cells recede from the surface of the matrix towards the interior (Kovacic, 2019). This can be observed with traditional microscopy. The second is by monitoring the proteome of the cells. ECs have several hallmark proteins, as do mesenchymal cells. Two of the more well documented endothelial proteins are CD31 and VE-cadherin. Proteins made by mesenchymal cells that also facilitate imaging include α-Smooth muscle actin (α-SMA) and calponin (Kovacic, 2019). These proteins can be marked through immunofluorescence techniques, making them distinguishable under fluorescent light. Immunofluorescence is a subset of histology in which specific proteins within a tissue sample are targeted with antibodies (Goding, 1996; Joshi & Yu, 2017). Using a combination of these methods, an accurate picture of the cell transition rate can be obtained.

Several growth factors have been reported in relation to EndMT. One of the most notable is transforming growth factor beta (TGF-β) as it has been shown to cause changes in cell behavior and expression, as well as increase rates of EndMT (Mina et al., 2016). TGF-β binds to proteins on the cell's surface which then phosphorylate SMAD proteins, a family of regulator proteins that aid in transcription. The SMAD protein family then acts as transcription factors, either encouraging or repressing transcription of certain genes, depending on the specific protein (Hata, 2016). The SMAD complex created in response to TGF-β interacts which EndMT inhibitors such as ZEB1 and TWIST. These interactions result in the changes in expression which lead to EndMT (Kovacic, 2019). More mesenchymal markers and behaviors begin to appear, such as invasion and the production of collagen. Other elements known to have an effect on EndMT include oxidative stress, glucose levels within a cell, and endothelin. However, this project will focus predominantly on the effects of shear stress exerted by steady and oscillatory fluid flow on ECs.

Shear stress due to steady and oscillatory fluid flow has been reported to increase the rates of EndMT (Mina et al., 2016). Since these are the flow varieties most likely to be seen *in vivo*, the data gathered on EndMT under these conditions are the most applicable in relation to TEHV. By measuring the rates at which fluid is flowing over the cells and the rate at which EndMT occurs, the optimal conditions for triggering or preventing EndMT can be found. This allows effective *in vivo* development for TEHV.

E. Fluidic Pumps

A fluidic pump is required to generate the necessary flow to stimulate fluid within the heart. Typically, pumps used for fluidic bioreactors have the capability to produce both steady flow, pulsatile, oscillatory flow, at a wide range of flow rates. It is also important that a pump used with cells or cell media, be sterile and thus not come in direct contact with the fluid. Common pumps for this application are peristaltic pumps, syringe pumps, gravity pumps, vacuum pumps and pressure pumps.

Peristaltic pumps function by the use of a motor with rollers that flexible tubing is wrapped around. As the motor rotates, liquid is pushed through the tubing as shown in Appendix

B (Byun et al., 2014). With this motor setup, peristaltic pumps can be programmed to produce steady, pulsatile, and oscillatory flow, based on the pattern of rotation performed by the motor; a constant rotation for steady flow, pausing for pulsatile flow and occasionally reversing for oscillation (Behrens et al., 2020; McMillan, 2017). As peristaltic pumps have rollers, the fluid only comes in contact with the tubing, retaining sterility (Byun et al., 2014). A variety of peristaltic pumps exist and many have more than one motor, allowing multiple tubing to be connected and multiple trials to run in parallel. One negative of peristaltic pumps is that due to the nature of the design, the flow cannot be perfectly steady as a result of the motors rotation, even when set to move at a constant pace.

Another common type of pump used in macro and microfluidics is the syringe pump, which functions by a piston pushing on a syringe to create flow through, as shown in Appendix B. Most commonly the piston is screw driven, giving it the ability to perform steady, pulsatile and oscillatory flow by pushing the piston, stopping the piston and pulling the piston (Alizadehgiashi et al., 2018; Byun et al., 2014). These pumps are also programmable to increase precision, however deformation of the syringe causes smaller flow rates to be difficult to measure precisely (Byun et al., 2014). Additionally syringe pumps are closed systems, and fluids such as cell media cannot be refreshed during use (McMillan, 2017).

A more simplified type of pump is the gravity pump, as shown in Figure 3. These pumps can be very inexpensive (or easily handmade), as all that is needed is tubing and fluid. Gravity pumps are able to generate a wide range of flow rates with varying tubing length, tubing diameter, or by changing the height difference between the two ends of the tubing (Byun et al., 2014). They can also be set up to run over long periods and can be open systems to allow for fluid to be continuously added (Byun et al., 2014). Gravity pumps have been used to generate steady and pulsatile flow and can be developed to also generate oscillatory flow (Kim et al., 2017). There are models which use a feature called an oscillator to create pulsatile flow (Kim et al., 2017). A variation on this design would produce oscillation by the use of a rocker plate. The movement of the plate would allow fluid to move in an oscillatory pattern through the device and would likely have a great increase in throughput.
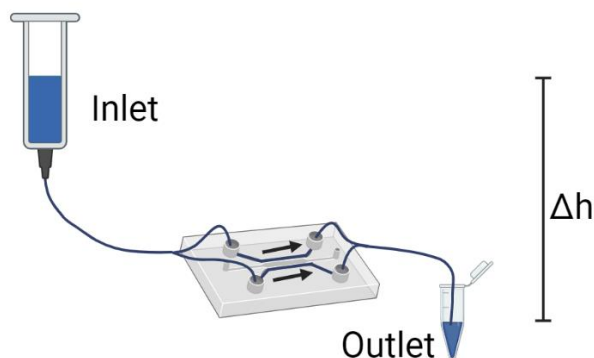

Figure 3: Gravity Pump. This pump operates by use of gravity by creating a height difference between inlet and outlet. Image created with BioRender.com.

Another pump, the pressure pump, is driven by an external pressure source of gas, such as an air tank or flow controller, as shown in Appendix B. Essentially, gas becomes pressurized in a reservoir containing liquid, so the liquid flows through tubing (Casquillas G., 2021). Steady and pulsatile flow are commonly generated using a pressure pump, however oscillatory flow can also be generated by changing the pressure differences at the tubing inlet and outlet (Mavrogiannis et al., 2016). In order to measure a precise flow rate, a flow controller, to generate the pressure, or flow sensor, to measure the pressure, is necessary (Casquillas G., 2021). Another drawback is the potential for backflow of liquid caused by pressure imbalances.

Vacuum pumps work similarly to pressure pumps. Instead of pushing fluid through tubing, they generate negative pressure which draws or pulls fluid through the system, as shown in Appendix B (Byun et al., 2014). This allows for the system to be open, allowing liquid to be continuously added to the setup. Steady and pulsatile flow are commonly generated using a vacuum pump, however, oscillatory flow could be generated by altering the setup of the system (Seo et al., 2019). These pumps do also require a flow controller or flow sensor to measure the precise flow rate.

All of the pumps discussed can be employed to expose cells to fluidic flow conditions. To accomplish this the pumps can be paired with microfluidic devices.

F. Devices Applying Shear Stress on Cells

In order to produce steady and oscillatory forces and analyze how they affect cells in EndMT, fluidic bioreactors are utilized. Fluidic bioreactors are used to simulate biological processes, in this case, simulating fluid flow *in vitro* (Mendelson & Schoen, 2006). Testing *in vitro* allows for stable and controlled testing over an extended period of time (Peterson, 2014).

Fluidic bioreactors can measure data in two-dimensions or three-dimensions. Most fluidic studies are conducted under two-dimensional conditions, as it is easier to simulate and gather data. Two-dimensional flow devices usually consist of fluid flowing over one layer of cells (i.e. in a flat petri dish), while a three-dimensional flow device has a 3D matrix for cell migration (Sabbagh-yazdi et al., 2007). Three-dimensional flow modeling is also referred to as computational fluid dynamics (CFD) (Cukierman et al., 2001). CFD is a better simulation of how fluids flow through the body and is able to better mediate cell adhesion, however, it is more difficult to model (Cukierman et al., 2001).

Current fluidic bioreactors exist at either a macroscopic or microscopic scale. Macro-fluidic devices are larger in size and are typically able to measure multiple trials of cell migration at one time (Sucosky et al., 2008). The Cone and Plate Device is a macro-fluidic bioreactor in which steady and oscillatory flow patterns are generated by a rotating cone placed in the medium, as shown in Figure 4. The cone rotates unidirectionally and bidirectionally to generate shear stress from both steady and oscillatory flow (Kouzbari et al., 2019; Sucosky et al., 2008). Gels are placed on the bottom plate and cells are seeded on the gels. Cell migration into a gel is measured by removing the gels from the fluid and utilizing microscopy to quantify how far into

the gel they have moved (Kouzbari et al., 2019; Sucosky et al., 2008). A table of the strengths and limitations of this device can be found in Appendix C.
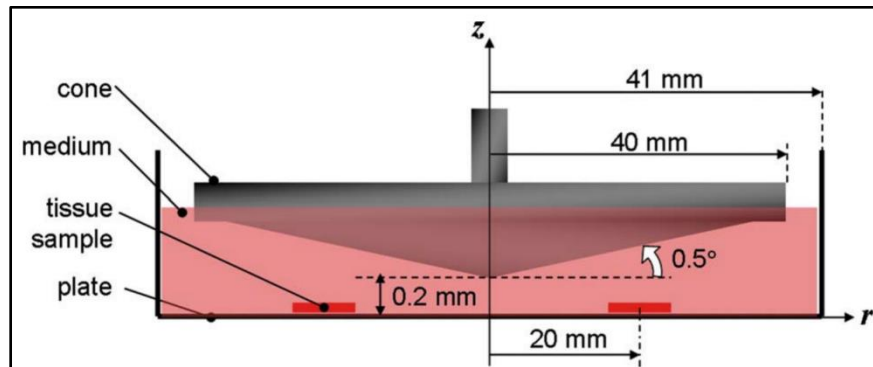
Figure 4: Schematic of Cone and Plate Fluidic Bioreactor. The gels and cells are seeded on the plate (shown in red) where multiple trials can fit. The cone rotates and generates flow. Unidirectional rotation generates steady flow, while bidirectional rotation generates oscillatory flow (Sucosky et al., 2008). Image used with copyright permission of American Society of Mechanical Engineers.

Macro-fluidic bioreactors have some limitations. The most important disadvantage to note is that the fluid flow is not uniform (Sucosky et al., 2008). As the flow is generated via rotation of the cone, the fluid flowing closer to the center of the plate will be faster than the fluid flowing on the outer edges of the plate. This causes gels placed in different areas to undergo different flow conditions and thus placements of the gels must be very precise. Additionally, as this device is a closed system with no inlets or outlets for media the device must be stopped frequently to replace media (Sucosky et al., 2008).

Oppositely, microfluidic bioreactors have many advantages and are able to very closely simulate the conditions within the heart. Microfluidic bioreactors are commonly used to measure cell migration because they can be designed to fit on a microscope slide, allowing for easy cellular imaging. One example of these devices is shown in Figure 5, in which fluid flows in channels surrounded by polydimethylsiloxane (PDMS) and a glass slide (Huesa et al., 2010). A fluid pump generates a pressure gradient that forces fluid to flow through channels and past gel chambers where cells are seeded (Mahler et al., 2014; Ramaswamy et al., 2014). These pumps are able to control the flow rates and create shear forces from both steady and oscillatory flow (Mahler et al., 2014; Ramaswamy et al., 2014).
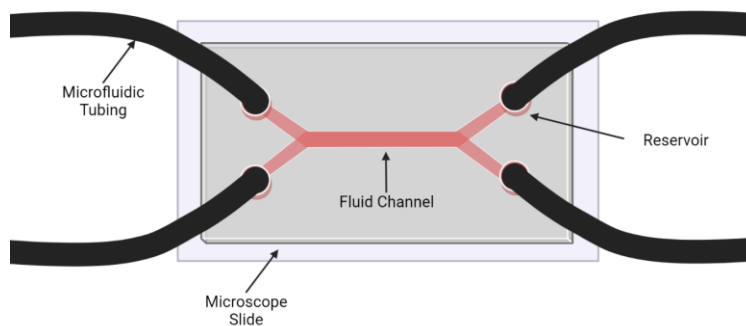
Figure 5: Schematic of a Pump Activated Microfluidic Bioreactor. A PDMS piece is developed in a mold so that the underside has channels cut into it. It is then bonded onto a glass slide to close the device. Fluid comes through microfluidic tubing and into the inlet reservoirs on the left. Fluid is then pushed into the microfluidic channels in pink. Finally, the fluid comes out the outlet tubing on the right. Image created with BioRender.com.

PDMS microfluidic bioreactors are commonly used for studying cell migration and there are currently a wide variety of designs that have been developed and tested. For instance, a very simple design has two fluid channels and a gel chamber, as shown in Figure 6. This device was designed to study capillary morphogenesis, a process that occurs during wound healing and development (Vickerman et al., 2008). An advantage of this design is that the two fluid channels flow past a singular gel chamber that has staggered square pillars to hold the gel in place. By altering the fluid flow rate through the channels, this device allows for the control of shear stress and interstitial flow through the gel (Vickerman et al., 2008). A drawback of this design is that the gel needs to be precisely pipetted into the gel chamber using a microscope and micropipette, all of which is contained within a cell culture hood. This design is also of limited throughput, as only one trial can be run at a time (Vickerman et al., 2008). A table of the strengths and limitations of this device can be found in Appendix C.


Figure 6: PDMS Microfluidic Design Developed in Vickerman et al., 2008. This device consists of a gel chamber placed between two microfluidic channels. At the ends of the fluid channels there are connector ports which allow the device to be connected to an external pump. Within the gel chamber micropillars are present to support a soft hydrogel (Vickerman et al., 2008). Used with permission of the Royal Society of Chemistry.

Another design which was developed by Farahat et al. and utilized by Polacheck et al. was aimed at studying the migration of mammary adenocarcinoma cells in a collagen gel. High interstitial fluid pressure is associated with solid tumors and has been linked to cell migration (Farahat et al., 2012; Polacheck et al., 2014). To simulate this interstitial pressure, a 60 Pa pressure gradient was generated across the gel. This pressure gradient was established by running cell media in one channel at a higher flow rate than that of the other cell media channel. This device is specially designed to easily place a collagen hydrogel. Gel inlet and outlet channels as displayed in Figure 7 allow the user to more easily pipette the gel into the chamber. Furthermore, the presence of trapezoidal pillars along the edge of the channel prevents the overspill of the collagen into the media channels via capillary action. However, this design is severely limited by its throughput, as only one trial can be run at a time (Polacheck et al., 2014). A table of the strengths and limitations of this device can be found in Appendix C.
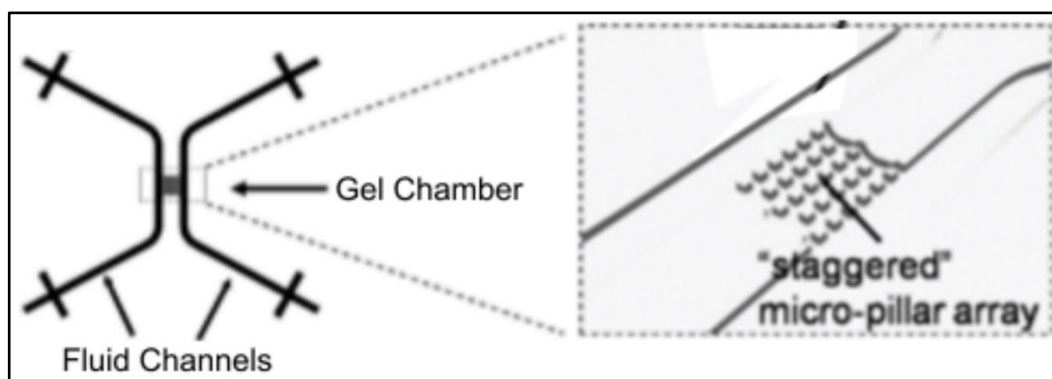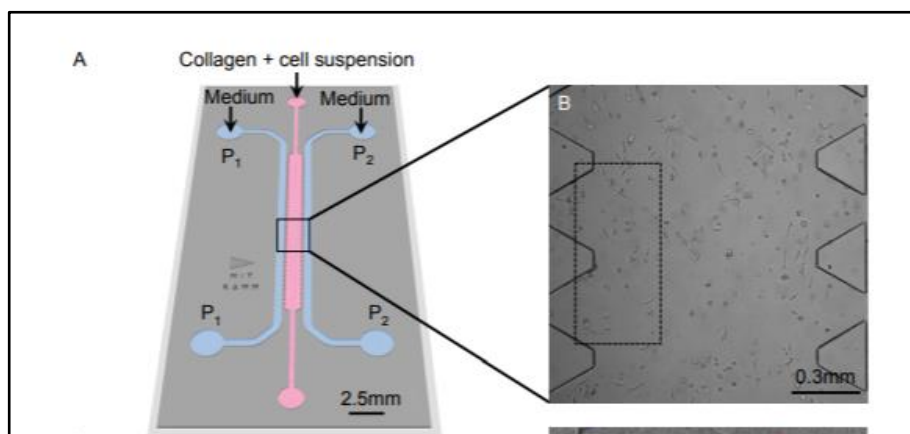

Figure 7: PDMS Microfluidic Design developed by Farahat et al., 2012, and used in Polacheck et al., 2014. This device features a collagen gel channel (indicated in pink) located between two channels for the flow of cell media (indicated in blue). Inlet and outlet ports on the collagen chamber facilitate the placement of collagen into the device to allow for easy placement. The design within the chamber, shown on the right, shows trapezoidal pillars placed on the outer edge of the gel chamber to hold the gels in place. Used with permission of the Proceedings of the National Academy of Sciences (Farahat et al., 2012; Polacheck et al., 2014).

Another device with gel inlets and channels is shown in Figure 8 and was developed by Chung et al. This device was developed to test the effects of several factors on endothelial cell migration through a 3D collagen gel matrix (Chung et al., 2009). Three channels are employed for this purpose. The central channel is for the flow of a suspension of cells in cell media, the leftmost channel is the control channel where media is flowed, and the rightmost channel is the condition channel where the media containing the desired variable is flown. On each side of the control channel there are channels where the collagen gel scaffold can be placed. The design also includes inlet ports for the gels. After placing the gels in the chambers, the team placed a droplet of cell media on each of the ports to prevent evaporation. As the three channels were filled with

media, the migration of the cells through the collagen scaffold was traced and following the experiment the cells were stained for easy imaging (Chung et al., 2009). A benefit of this device is that it permits the co-culture of two different cell types at the same time. This is accomplished through culturing one cell type in the cell channel and another in the condition channel. This design has a throughput of 2, as there are two control and two condition gel chambers. A benefit of this design is that it is able to test the control and independent variable concurrently. A table of the strengths and limitations of this device can be found in Appendix C.
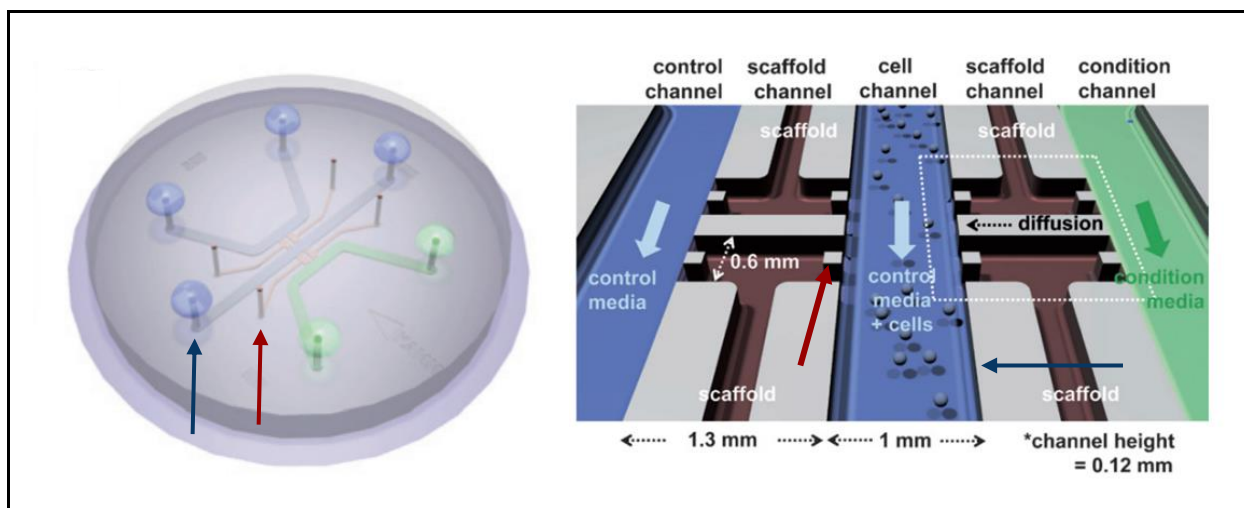
Figure 8: PDMS Microfluidic Design Developed in Chung et al., 2009. This device consists of three fluidic channels and two gel channels (gel channels indicated by a red arrow in the left image). The center fluid channel, (indicated by blue arrows) is designed for the flow of a suspension of cells in media. Between the gel channel and fluid channels are gel chambers, as shown in the image on the right in brown. In each gel chamber there is a post (indicated by the red arrow in the right image) made to hold the gel in place (Chung et al., 2009). Used with permission of the Royal Society of Chemistry.

Lastly, another PDMS microfluidic device which was developed by Mina et al., uses a simple PDMS design to generate shear flow, as shown in Figure 9 (Mina et al., 2016). There is a single flow channel which runs over a single culture well. The bottom of this well is plasma sealed to a microscope slide, which will sit on the bottom of the device during testing. The major benefit of this device is that imaging the migration of the cells is greatly simplified with the addition of the glass slide. This allows for a microscope to be set to a certain depth and the cells at that depth to be counted to measure invasion rates (Mina, 2016). The main drawback of this device is its small throughput size. Having only one culture well, the device limits itself to one trial at a time. As seen with Mahler's fluidic bioreactor, multiple chambers could be added along a single flow channel and likely no discernable difference would be seen (Mahler et al, 2014). A table of the strengths and limitations of this device can be found in Appendix C.

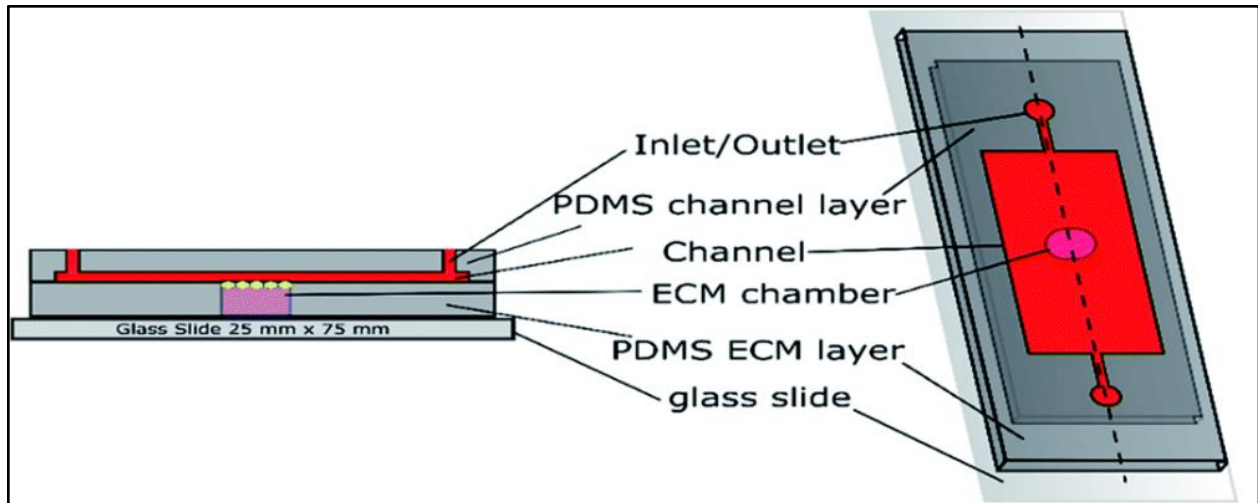Figure 9: PDMS Microfluidic Design Developed in Mina et al., 2016. This device has one gel chamber that sits deeper in the device than the fluid channels where gels and cells are seeded. Tubing is connected to the inlet and outlet and liquid flows through the channel, indicated in red, over the gel chamber (Mina, et al., 2016). Used with permission of the Royal Society of Chemistry.

Based on the comparisons of the devices listed in Appendix C, it was concluded that a microfluidic device is necessary to measure rates of EndMT and cell migration using a cell derived matrix *in situ*. General advantages of microfluidics are that they require a smaller volume of reagents and that their small size allows for portability and application in many laboratories. Additionally, these devices are relatively cheap to produce (Streets & Huang, 2013).

G. The State of the Art and Project Direction

Evaluating what has caused success in similar research applications is crucial in setting a direction for this project. The current treatments for heart valve disease are lacking in a way that a tissue engineered solution could improve. There are studies being done on TEHV generation, insertion, and functionality which have encountered challenges in repopulation of decellularized tissues. A major factor in the repopulation of TEHV is EndMT, which needs to be further studied in an *in vitro* model. Various components including a pumping system and microfluidic device will be incorporated into a design to produce a system capable of measuring endothelial cell migration into a decellularized matrix. This design will take influence from the microfluidic bioreactors that came before it to test EndMT in an observable and controlled environment.

25

III.   Design Process

A. Initial Client Statement

The goal of this project is to design a fluidic bioreactor to test the effects of shear stress caused by different magnitudes of steady flow and oscillatory flow on endothelial cells. This device would ideally simulate a 3D environment, similar to fluid flow in heart chambers. This device should be inexpensive and easy for the user to place gels and seed cells, as well as confine the gels within the gel chamber. *In situ* decellularization is desired. It should also allow for cellular fixing, staining and imaging within the device to measure cell migration and phenotype. Ideally, twelve trials of flow over gel samples should occur simultaneously.

B. Design Objectives

The Objective Table, shown below as Table 1, is based on the client's requests in the development of the fluidic bioreactor. Objectives are on the left side, and the weight value on the right represents the importance of that objective. The criteria are weighted from one to five; five being of the highest importance, one being of least importance.

The overall requirements as detailed by our client are that the device is able to produce a range of shear stresses, as shown in Table 2, produce both steady and oscillatory flow, and be precise in measuring and generating flow rates. Ideally, 60 to 72 oscillations per minute will be produced during oscillatory flow, as that is an average range of human heart rates (Avram et al., 2019). Additionally, it is very important that gel in the device stays in place, cells can be decellularized *in situ*, and cells can be imaged within the device by fixing and staining *in situ*.

Table 1: Objective Table

Criteria	Weight
Produce a range of shear stresses	5
Produce both steady and oscillatory flow	5
Precision of flow rates/applied shear	5
Gels contained in the chamber	5
In situ decellularization	5
Ability to image cells in the device	5
Fix and stain *in situ*	5
Ability to place cells on the gel matrix	4

Criteria	Weight
Precision of oscillations	3
More than 1 simultaneous trial	3
Ease of gel placement	2
Ease of use	2
$1000 budget	1

Table 2: Table of Flow Parameters

Flow Pattern		Magnitude of Shear Stress (Pa)	
	Static (Control)	0	
	Steady	0.2	2.0
	Oscillatory (60-72 bpm)	0.2	2.0

C. Shear Stresses

The three categories of the above objective tree are related to the required shear stresses within the device. A range of shear stresses, between 0.2 pascal and 2.0 pascal, as shown in Table 2, are required as they replicate the average resting heart rate (Mahler et al, 2014). Both steady and oscillatory flow must also be generated, as both types of flow are applied against heart valves. Finally, it is extremely important that the flow rates and shear stresses applied are accurate and precise. These values will be needed to accurately analyze results and develop conclusions. These criteria were all weighted with 5, as they are all absolute requirements in developing a device. The precision of oscillations was given a weight of 3, as it was taken into consideration that heart rates vary in different people at different times.

D. Device Setup

Another important factor of the device is how it is set up. This covers criteria related to the gel chambers and the ability to image the cells *in situ*. It is very important that the gels are placed precisely and remain contained in the gel chamber, to prevent the cells from being moved or disrupted during testing. The ease of gel placement was given a weight of 2, because the precision of gel placement is more important than the user being able to easily place them.

Imaging the cell *in situ* was given a weight of 5, as it is vital that the cells and gels are not disrupted prior to being imaged. This would cause inaccurate results.

E. Decellularization

The client also seeks to employ the use of a decellularized extracellular matrix as the medium through which the cells migrate. Ideally, the client wishes for the decellularization process to occur in the device itself as a means to simplify the experimental procedure. From this it follows that using a decellularized matrix in the design is ranked at a 5.

F. EndMT Quantification

To analyze the effects of EndMT, the client requests that the device allows for the measurement of migration and tracking of cellular phenotype. It follows that the ability to image, fix and stain the cells *in situ* are ranked at a 5 as these are fundamental to the desired experimental procedure.

G. Throughput

The final general category of criteria characterizes the throughput of the device. Commonly, microfluidic designs only have one gel chamber, allowing for only one trial to run at a time. A weight of 3 was given to this criteria to increase throughput to more than one trial measured simultaneously.

H. Ease of Use & Budget

A further criterion is the overall ease of use of the device. This is ranked as a 2, because while an easier operational strategy would be beneficial, this criterion can be compromised to improve the functionality of the device. Finally, the price criterion of $1000 is ranked at a 1, as the client prioritizes the functionality of the device over the cost of the device.

I. Need Statement

The dynamic mechanical environment of the heart valve plays a significant role in the regulation of healthy valve structure and function. As such, biomedical engineers that seek to develop functional tissue engineered heart valves must consider the hemodynamic forces that are exerted onto the heart valve during the stages of the cardiac cycle. A particular focus of these engineers is on the mechanisms behind the transition of endothelial cells to mesenchymal cells (EndMT) in heart valves as it can lead to stenosis and regurgitation of the heart valve (Hinton & Yutzey, 2011). Modeling the hemodynamic forces of the heart valve for research purposes is a significant challenge, as many current models are limited to a 2D plane. Thus, there is a need for a 3D model of fluid flow on valvular endothelial cells that is capable of characterizing the effects of shear stress on EndMT.

J. Revised Client Statement

The goal is to design a microfluidic device aimed at studying the effects of both steady and oscillatory flow on endothelial cells. The device should produce a wall shear stress of 0.2 and 2.0 pascals in the microchannels. Furthermore, the device requires a fluidic pump which can ideally produce 60-72 oscillations/minute. The microfluidic channels should allow the placement of fibrous gel to simulate a 3D environment and allow for the culturing and decellularization of cells *in situ*. Decellularization should be achieved after a fibroblast seeded gel has been allowed to culture for two weeks. After decellularization, endothelial cell placement will occur. Ease of use should be prioritized in regards to gel placement and cell seeding. The device must also permit the imaging of the cells in the gels to quantify cell migration and phenotype. The number of simultaneous trials should be maximized.

IV.   Designs and Proof of Concepts

To meet the needs of our client, a microfluidic device was produced in order to best simulate the flow conditions in a native heart valve. This allows for valvular cells to be seeded within the device, and measurements to be taken of their migration into a cell-derived extracellular matrix. The purpose of the hydrogel is to act similarly to valvular tissue that cells are able to move within, as previously stated in the Literature Review. To best mimic the conditions of the native heart valve as well as that of decellularized tissue seen in many preliminary tissue-based heart valve designs, fibroblasts will be seeded in a fibrin gel, placed into the device, and allowed to remodel for two weeks prior to being decellularized *in situ*. Endothelial cell migration into the dECM will be measured. Within the device, gel inlets and channels will allow for ease of placement of the gel into the device. Pillars will sit on the outer edge of a chamber to create surface tension that holds the gel in place.

A. Initial Device Design Alternatives

To develop microfluidic devices, the process of photolithography was used. Photolithography is a process of microfabrication where a photoresist is placed onto a substrate or silicon wafer, a photomask is placed on top and UV light is used to cure the photoresist in the open areas of the mask (Chen et al., 2003). After this step, developer is used to dissolve all unexposed photoresist. At the end of the process a silicon wafer with features determined by the mask shape is created. Photolithography is often used for micro scale precise printing, such as for circuit boards. In order to print the designs, Autodesk AutoCAD 2022 Software was used to create a photomask.

To meet our goal of creating a device that is high throughput, easy to load gels and seed cells, and facilitate proper fluid flow, we created several different iterations of designs. Within each design there are circular inlets and outlets, rectangular gel chambers, fluid channels that run alongside the gel chambers and gel channels that flow into and/or out of the gel chambers. Each of the inlets and outlets are 1mm in diameter to fit a standard pipette tip to place the fluids. This allowed for a 1mm outer diameter piece of tubing to be placed in the inlets and outlets that can connect to a pump to flow the fluids through the device. The gel chambers range in dimensions but were all approximately 3 mm^2 in area. This allows for enough valvular cells to be placed and give them room to migrate through the hydrogel. Inside the gel chambers there are trapezoidal pillars that will use surface tension to hold the gels in place and stop them from spilling into the fluid channels. Trapezoidal pillars were used as they will increase the surface area of the pillars and surface tension to hold the gels. Each of the fluid channels are 500 µm wide. The silicon wafer was printed so all channels and chambers were 200 µm in depth, which allowed for room for the valvular cells to migrate within the device.

Design 1, as shown in the Figure 10 below, allows for placing of gels into each of the three individual gel chambers by inserting a pipette into the gel inlets and pushing the gel into place. The gel outlets accommodate for overflow of gel. Both the gel inlet channels and gel outlet channels are 500 µm in width. Multiple gels chambers in the same device allows for a higher throughput of trials, as three can be done in series in the same device.

Figure 10: AutoCAD Design 1. Design 1 has a gel inlet and outlet for each of the three gel chambers, which sit between the fluid channels are 1 mm by 3 mm. The fluid channels on the top and bottom of the device are 17 mm in length.

Design 2, as shown in Figure 11, has four gel chambers and four gel inlets. The first gel inlet is where gel will flow into the chamber. The gel inlet channel is 500 µm wide and the gel outlet channel is 250 µm wide. This connects to the next gel inlet. This is to accommodate gel overflow. This differs from Design 1, as it allows for room for an additional gel chamber to be placed on the device to increase throughput. There is one final gel outlet to accommodate for final gel overflow.

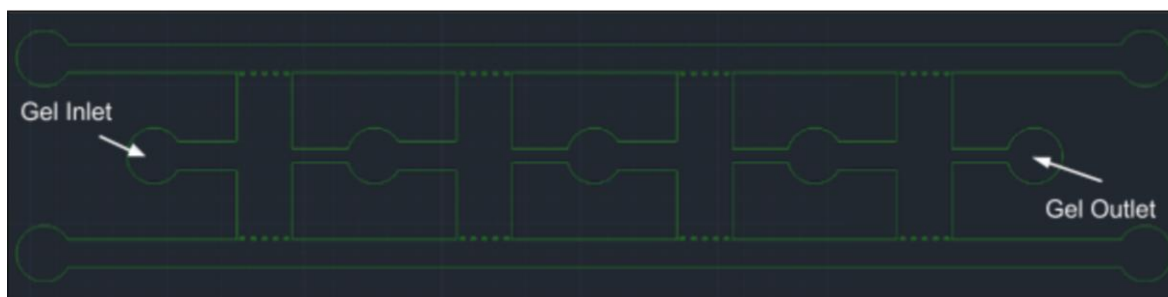Figure 11: AutoCAD Design 2. Design 2 has a gel inlet for each of the four gel chambers. The chambers are 1 mm by 3 mm. The fluid channels in this device are 20 mm in length.

Design 3, as shown in Figure 12, has four gel chambers, but only one gel inlet and one gel outlet. This allows for all the gel chambers to be filled at the same time by pushing the gels through the gel channels consecutively.
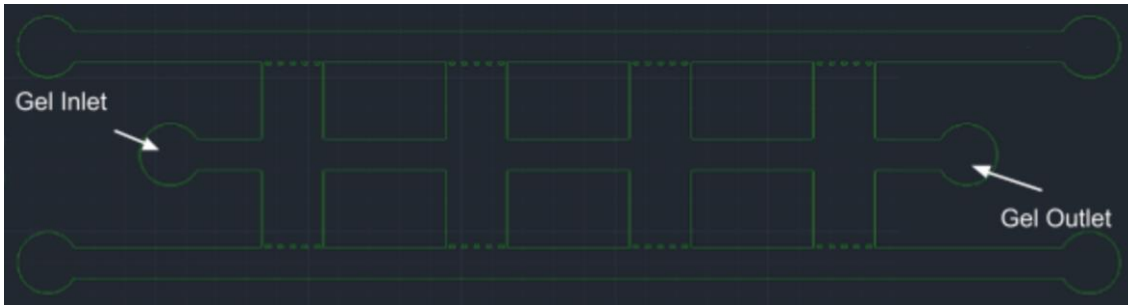
Figure 12: AutoCAD Design 3. Design 3 has a gel inlet that is used to fill all four gel chambers. The gel chambers are 1 mm by 3 mm. The fluid channels in this device are 17 mm in length.

Design 4, as shown in Figure 13, has four gel chambers, as shown below, a gel inlet and a gel outlet for each chamber. The design varies in that there are two fluid channels, one branching into four and one requiring external tubing. The first fluid inlet is used to flow fluid into the device, then branches to reach each of the gel chambers. The second fluid inlet is indicated by the number '1.' Here, a tube will be placed into the device and fluid will flow down to the fluid outlet indicated by the number '2.' External tubing will connect the fluid outlet to the next fluid inlet (external tubing connects both indicated by the number '2'). Then, external tubing will connect inlets indicated by the number '3' and again for those numbered '4.' Finally, the outlet indicated by the number '5,' will be the final fluid outlet. This design was created to increase throughput, but differs from Designs 1, 2, and 3 because the devices are in parallel rather than in series. This was done so each gel chamber could be exposed to fresh media in the flow channels, rather than having the same media passing by each gel.
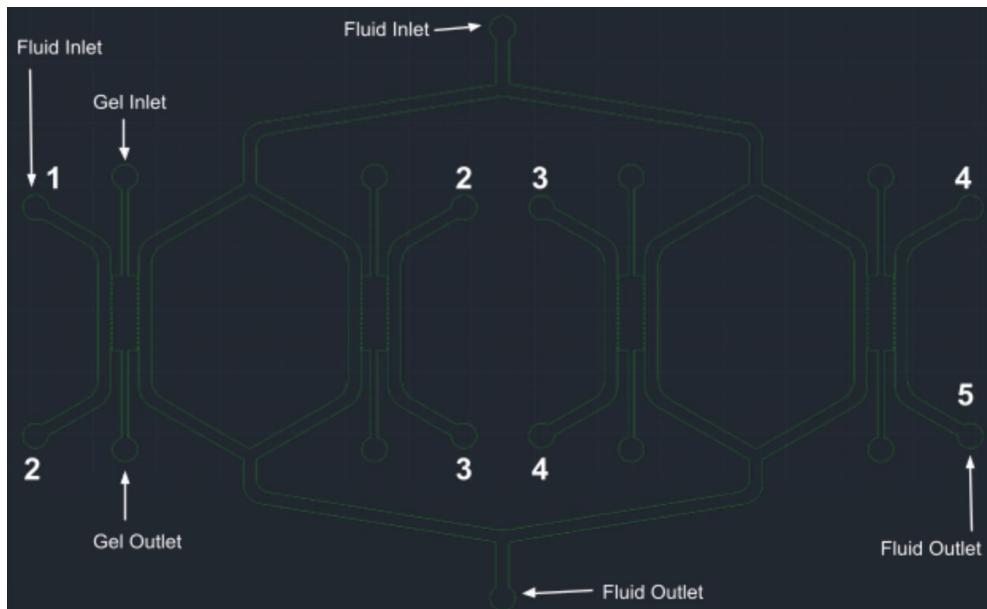

Figure 13: AutoCAD Design 4. Design 4 has a gel inlets and outlets for each of the four chambers. External tubing connects the fluid channels indicated with the same number, such as '2' connected to '2'. The gel chambers are 3 mm by 1 mm.

The remaining nine designs were modifications of the gel chamber, to test the ease of gel placement and how well the gels stay in place, as shown in Appendix D. Each of the designs have a gel chamber that is 3 mm by 1 mm and has fluid channels on either side. They also all have 500 µm wide gel inlet and outlet channels. The exterior pillars on the devices were intended to confine the gel in the chamber using surface tension. Different distances between the pillars were tested to see which configuration was able to hold the gel in place while also maximizing surface area for gel adhesion. Pillar widths were 100 µm, and pillar spacing ranged from 100 µm to 150 µm. It was theorized that the gels may compact during experiments, and therefore interior pillars were tested inside the gel chamber to hold the gel in place. Interior pillars were square with lengths of 100 µm, and were tested at distances apart ranging from 100 µm to 230 µm. Overall, four configurations without interior pillars and five configurations with interior pillars were tested. All devices were printed on one silicon wafer, which can be seen in Figure 14 below.
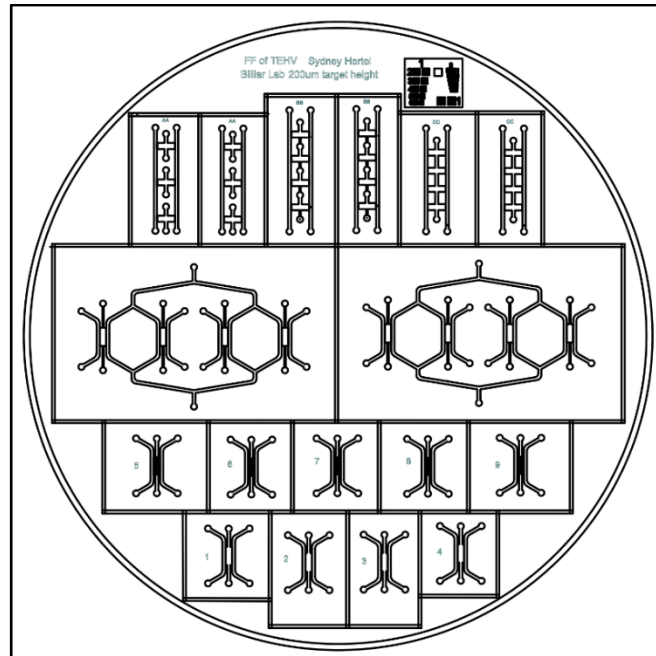

Figure 14: AutoCAD Design of Printed Silicon Wafer. The diameter of this silicon wafer is 4 inches (101.6 mm). A scale bar is plated at the top of the wafer to show measurements during imaging.

B. Final Device Design

Upon testing of our devices, modifications were made to improve our features. Figure 15 below shows our final, optimal design. This design had trapezoidal exterior pillars that were 100µm at the base and spaced out 100 µm. All inlets and outlets were 1 mm in diameter. Fluid channels were modified to have curves, so they were not located close together, causing potential issues with placing fluids. The connection between gel inlets and gel chamber was slightly modified to encourage gel to stay confined within the chamber.
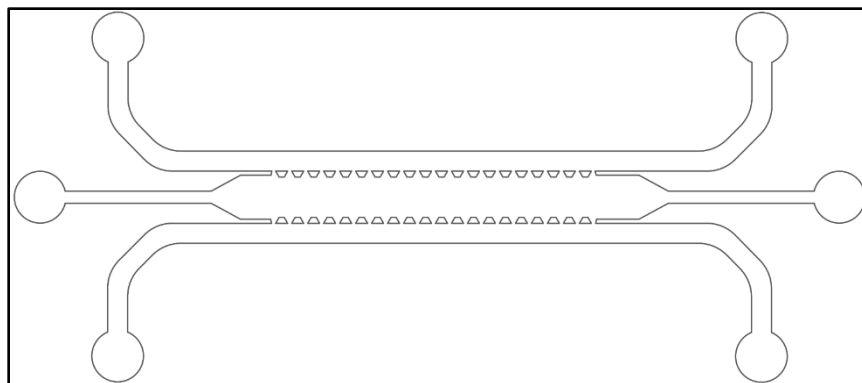
Figure 15: Final Device Design.

C. PDMS Casting and Plasma Treatment

The devices were made out of polydimethylsiloxane (PDMS). PDMS is a biocompatible polymer that is often used for cell culture because it is cheap, biocompatible, optically transparent, gas permeable and easy to fabricate (Torino et al., 2018). The polymer is easily produced out of two components; a liquid silicone rubber base and a curing agent, at a 10:1 ratio. When the two are mixed, they are poured over the silicon wafer. Then the polymer chains begin crosslinking and a solid polymer is formed, in this time the PDMS is placed in a vacuum chamber to remove air bubbles. PDMS is then cured in an oven at 65 ℃ overnight due to the volume of PDMS produced (Torino et al., 2018). The final polymer is flexible yet still strong and optically clear. The PDMS will take on the shape of whatever mold it is poured into and due to its rigidity is able to accurately produce the shape and size of microchannels.

The PDMS pieces were prepared for device testing by using plasma treatment to chemically bind a glass coverslip on top of the channels. In a laminar flow hood, the PDMS devices were cut out with a scalpel and carefully removed from the wafer. As each design has inlets and outlets for the fluid channels, a 1 mm biopsy punch was used to carefully punch these out while the device was placed face down on a cutting board. Once the inlets and outlets were removed, the PDMS pieces were cleaned to prepare for plasma treatment. This was done by individually spraying each piece with ethanol, wiping it with a Kimwipe, then spraying again with ethanol and finally drying it with pressurized air. Scotch tape was placed over the clean PDMS to prevent any dust from clinging to it. The same steps were repeated with glass coverslips that will be bound to the PDMS. After all pieces were cleaned and wrapped in tape, individually, the tape was removed off of one side of the cover slip and the face of the PDMS with the design and carefully placed into the plasma cleaner. The device was turned on and a vacuum was pulled in the chamber. The plasma was turned on high and was run for 60 seconds. When removed, the glass coverslip was quickly placed on top of the PDMS to chemically adhere. These steps were repeated for the remainder of the devices. After a few minutes, the glass coverslip was bound to the PDMS and the scotch tape could be carefully removed. Full procedures on PDMS casting and plasma treating can be found in Appendix E.

D. Design Testing: Gel Placement

In order to test the feasibility of the initial design, a test was performed to flow fluid through the gel inlets and into the gel chamber, to ensure there was enough surface tension to hold the fluid within the pillars of the gel chamber. This is essential, as the final application of the device requires a hydrogel with valvular cells to be seeded within the chamber so that fluid can run alongside the gel in the fluid channels.

The final hydrogel tested, which will be used in the final application of the device, was fibrin gel. Prior to placing fibrin gel, water and gelatin were used, as they are both more cost effective for proof of concept testing. Gelatin was used as it is more viscous than water and can be prepared to have a similar viscosity to that of the fibrin gel.

A variety of methods were used when placing the gels in order to decrease the pressure of the fluid being injected. The initial method, which is most commonly used in this application, is injecting a pipette with the fluid into the gel inlet and slowly pushing down on the pipette to inject. Other methods tried included using a pipette tip attached to a vacuum to pull the fluid from the gel outlet, using a gravity pump to allow gravity to pull fluid in from the gel inlet, or placing a droplet of fluid over the gel inlet so gravity would slowly pull the fluid into the gel chamber.

No combination of the design of the device, type of fluid, or method of placement resulted in the fluid remaining within the gel chamber. Figure 16 and Figure 17 show the placement of fibrin gel into a device with only exterior trapezoidal pillars and with both exterior trapezoidal pillars and interior square pillars, respectively. In both figures, the gel entered from the gel inlet and was pushed into the gel chamber. Immediately, the gel overflowed past the pillars and into the fluid channel. No signs of surface tension were present to hold the gel in place.
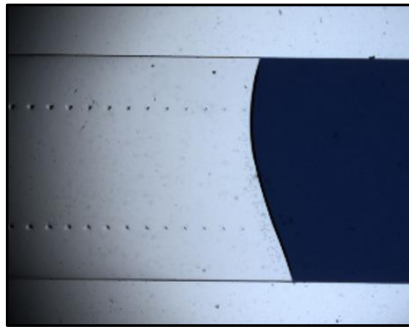

Figure 16: Gel Placement in Device with No Interior Pillars. When fibrin gel was pushed into the gel chamber of this device, it immediately overflowed into the fluid channel, exhibiting no signs of surface tension from the pillars.
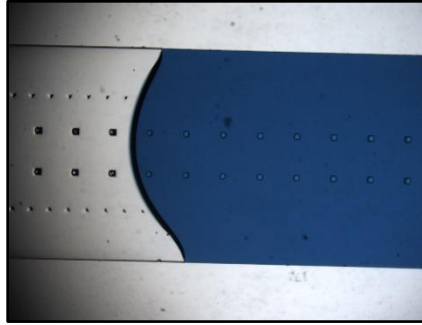
Figure 17: Gel Placement in Device with Interior Pillars. When fibrin gel was pushed into the gel chamber of this device, it immediately overflowed into the fluid channel, exhibiting no signs of surface tension from the pillars.

Upon completion of testing, it was apparent that there was an issue with the pillars as they were not producing the desired surface tension to hold the gels in place. Due to the presence of fluid above the pillars, the team hypothesized that the photolithography or PDMS casting process could be causing the pillars to be shorter than the desired height of 200 μm. This could cause the pillars to not be adhering to the glass coverslip, allowing fluid to flow right over them and leak from the gel chamber. Another explanation could be that during the photolithography printing process, the edges of the pillars are printed at an angle rather than forming a 90° angle with the base of the device. This would cause the pillars to taper out and become very thin and lose their shape towards their upper regions. This would cause the surface tension to decrease substantially towards the top of the device. Additionally, this tapering could also be contributing to the lack of bonding seen between the pillars and the glass coverslip. Further testing was required to understand this phenomenon.

E. Characterization of Silicon Wafer

To determine the root cause of the undesirable pillar properties, the team performed a characterization of the silicon wafer used to cast the PDMS devices. Imaging each of the three silicon wafers the team had access to, was performed to assess the quality of the wafers. Two wafers were of Rozanne Mungai's designs (one at 120 μm depth and one at 200 μm depth) and one was of the team's design (200 μm), described in the Initial Device Design Alternatives section of this paper. This characterization was performed as a result of the PDMS pillars not holding fluid in the gel chamber. This was to test the hypothesis that the pillars were not at the same height as the rest of the device, causing them to not fully adhere to the coverslip and allowing fluid to flow over the pillars.

In order to image the silicon wafer and measure the depths of the pillars, a KLA Tencor Alpha Step D-600 stylus profilometer, a Keyence VHX-7000 digital microscope, a Zygo Nexview NX2 optical profilometer and a Zeiss Stemi 2000-C Stereo microscope was used. Several challenges arose during the imaging process due to the optical properties of silicon and the narrow depths of the pillar negatives.

The dimensions of the stylus of the Alpha Step profilometer exceeded that of the 200 µm deep pillar holes in the silicon wafers. Thus, the determination of depth of the pillars was unable to be conducted with this technology. However, the team was able to measure the height of the 120 µm depth wafer, which determined that the wafer was approximately 115 µm in depth. Variations in depth of different pillars may be due to where on the wafer they are located, as the spin lithography process causes the outer regions of the wafer to be thicker than the inner regions.

The Keyence VHX-7000 digital microscope was also employed to visualize the wafers. Figure 18 shows the results of the imaging of the team's 200 µm deep wafer for a design with interior pillars. The microscope software reported that the wafer had a height of 318.03 µm, as shown in Figure 18, however this measurement was impacted by the presence of optical artifacts protruding from the surface of the image which caused the height reported by the software to be greater than the actual height.
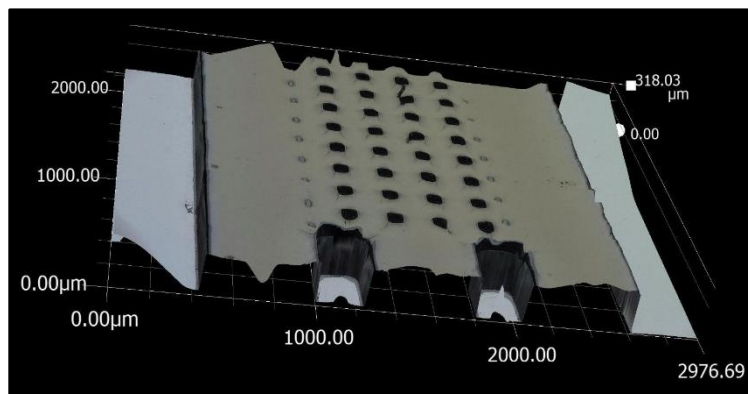

Figure 18: Three-Dimensional Model of 200 µm Device using Keyence Microscope. While imaging using the Keyence VHX-7000 digital microscope, it was noticed that the wafer had a height of 318.03 µm, likely due to the presence of optical artifacts.

Measuring the depth of the 200 µm pillar negatives proved to be not possible with this Keyence microscope as the light was unable to penetrate into the narrow pillar holes. Thus, the team tried out a third microscope, the Zygo Nexview NX2 optical profilometer. As there had been challenges measuring the 200 µm deep wafer, the team started off by imaging the 120 µm deep wafer. The results of this imaging are displayed in Figure 19. The software was able to image to the bottom of the pillar negatives and reported that the pillar depths were roughly 112 µm, as reported by the graphical output in Figure 19.
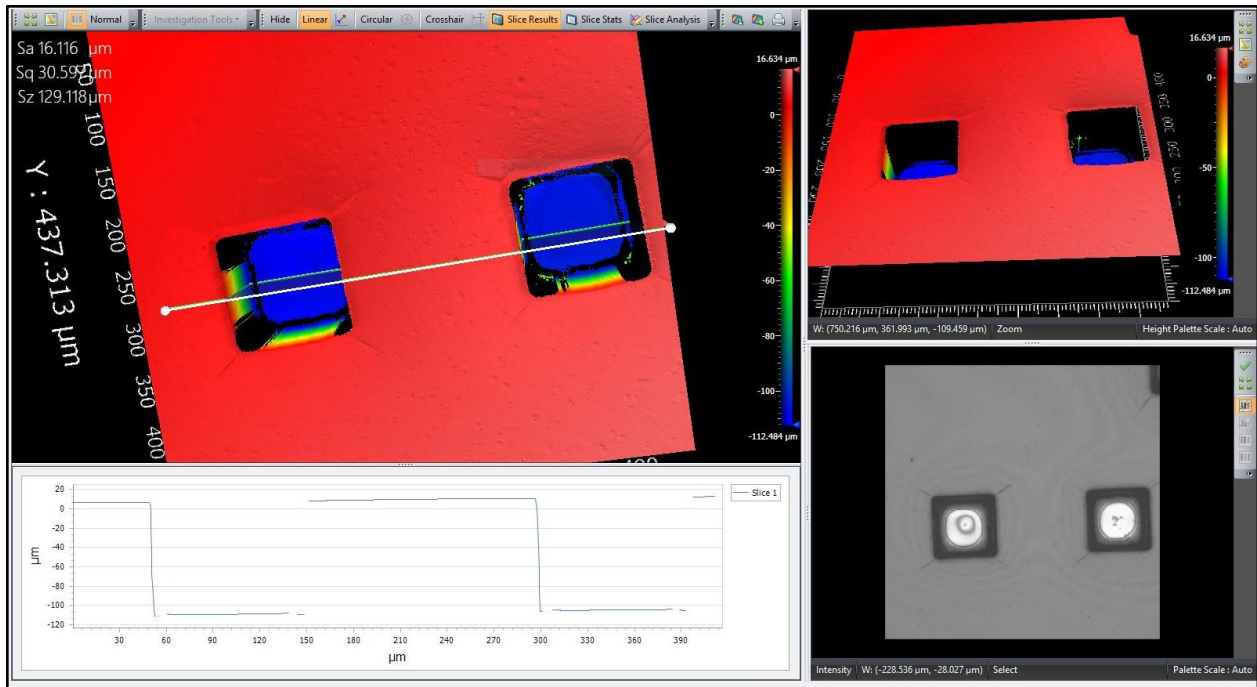
Figure 19: Imaging of 120 µm Device using Zygo Optical Profilometer. The graph on the bottom left shows the depth of the pillars, the X-axis being length left to right, and the Y-axis showing depth. The wafer was found to be approximately 115 µm deep. Images on the top show a three-dimensional model of the device. Image on the bottom right shows a microscope image of the square pillars in the device. The circular shape within the pillar, indicates the top of the pillar tapering into a rounded shape.

Following the success of the 120 µm wafer characterization, the same analysis was performed on a 200 µm wafer. However, due to light being unable to penetrate the depth of the pillar holes, this characterization was unsuccessful. The results displayed in Figure 20 show that the software was only able to pick up the top surface of the wafer and completely unable to determine the depth of the pillars.
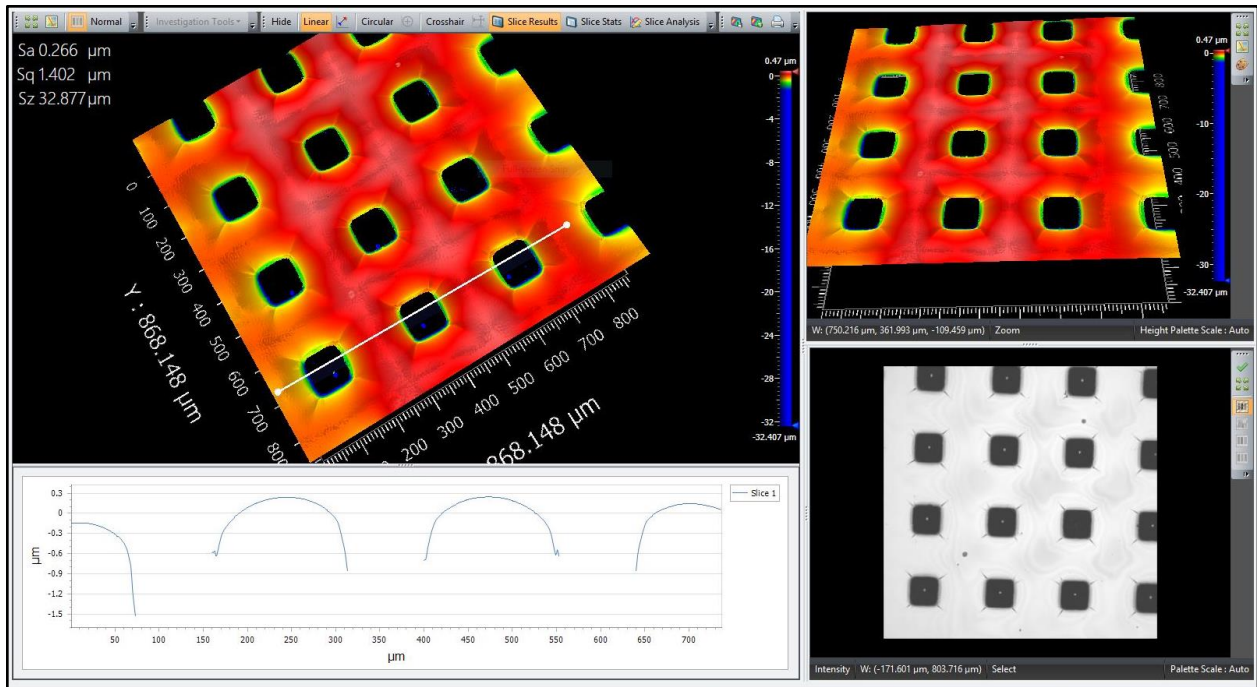
Figure 20: Imaging of 200 µm Device using Zygo Optical Profilometer. The graph on the bottom left shows the depth of the pillars, the x axis being length left to right, and the y axis showing depth. This showed slight variation in the top surface of the wafer, but was unable to accurately read the depth of the pillar negatives. Images on the top show a three-dimensional model of the device, where the black squares indicate pillar holes that light could not reach into the depths of. Image on the bottom right shows a microscope image of the square pillars in the device.

Finally, characterization of the silicon wafers was also conducted with a Zeiss Stemi 2000-C Stereo Microscope. Images were captured highlighting the discrepancies between the desired pillar geometries and the actual geometries of the silicon wafer. Figure 21 shows the square inner pillars and trapezoidal outer pillars. Rounded edges are present on both shapes, but more extreme on the trapezoidal pillars. Fading of the trapezoidal pillars along the span of the microfluidic device negative were also seen, as highlighted in Figure 22.
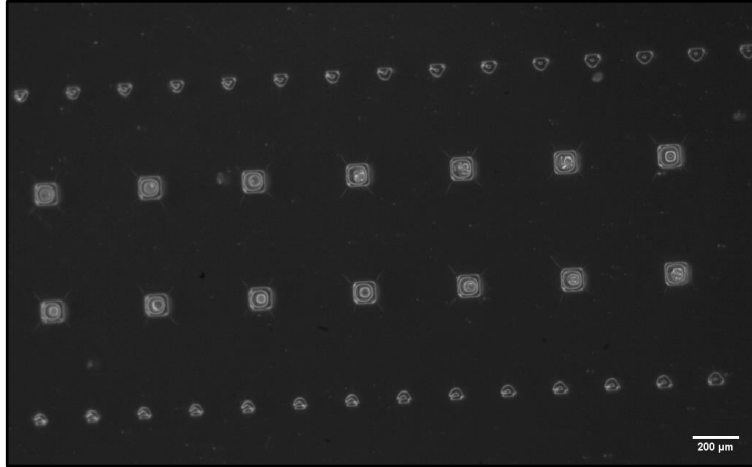
Figure 21: Silicon Wafer with Damaged Pillars. Within this design, there are trapezoidal pillars (top and bottom rows) and square interior pillars (middle rows). Each pillar is 100 µm at the base.
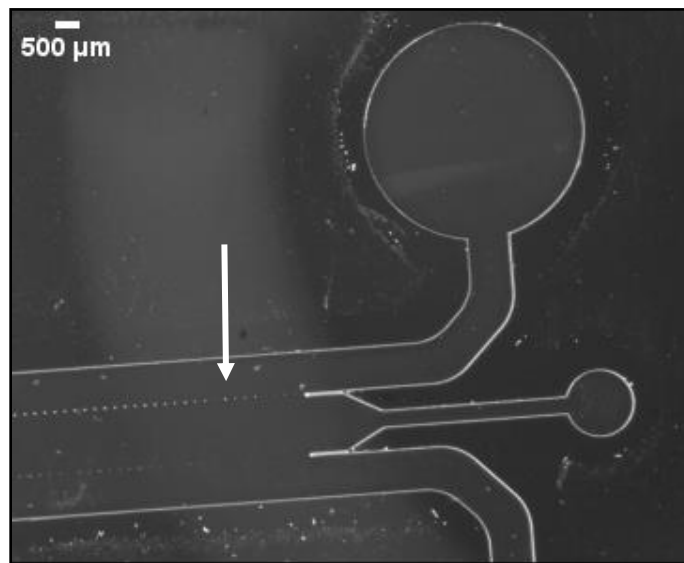

Figure 22: Silicon Wafer with Damaged Pillars from Spin Coat. Within this design, there are trapezoidal pillars indicated by the arrow. However, as the pillars get closer to the gel inlet, they become much smaller to the point where they are not visible.

Ultimately, these analyses confirmed that the desired pillar dimensions and geometries were not being produced in the silicon wafer. Thus, these discrepancies were translated to the microfluidic devices during the PDMS casting process. Based on these results, it was determined that a more advanced wafer fabrication process would be necessary to produce the desired pillar geometries.

F. Commercial Device Tested Upon

Upon testing of our device, as explained in 'Design Testing: Gel Placement,' and imaging of the designs, as explained in 'Characterization of Silicon Wafer,' it became apparent

that modifications to designs were necessary. As the printing process resulted in pillars being tapered off and becoming very narrow at the top, the design was modified to have trapezoidal pillars that were 300 µm at the base, rather than 100 µm. This would allow the pillars to hold their shape better and have more surface area at the top to adhere to a cover slip. We also need to utilize a different, or more advanced, type of technology to print the initial wafer to ensure the pillars are printing properly to the desired height of 200 µm.

To increase the accuracy of a silicon wafer print, we considered using a more advanced technology for photolithography than what was originally available to the team. Another option was to 3D print the mold and cast PDMS on that to create the devices. Finally, xurography was considered, which enables micro production by structuring thin foils with a knife plotter.

While waiting for the next steps in printing a new design, further gel placement testing is being performed on chips from AIM Biotech, called idenTx3 devices, shown in Figure 23 below. These devices have similar characteristics as our initial designs including trapezoidal pillars on the outer edge of the chamber (pillars are 300 µm at the base), 500 µm wide fluid channels and a gel inlet and outlet. This device has a height of 250 µm.
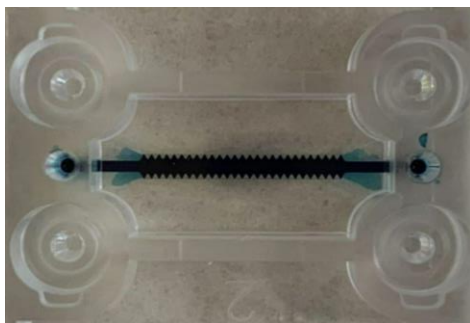

Figure 23: idenTx3 PDMS Devices from AIM Biotech. This device has two fluid channels and a gel chamber connected to a gel inlet and outlet, indicated by blue. Within the gel chamber, there are exterior trapezoidal pillars that are spaced out 100 µm. The height of this device is 250 µm.

G. Flow Through Decellularization Initial Testing

In the microfluidic device, the goal is to be able to place fibrin gels seeded with cells inside of the PDMS device, allow the cells to remodel the fibrin scaffold on the gel, then decellularize the gel *in situ*, leaving behind only the remodeled extracellular matrix. Ideally, decellularization will be achieved by flowing 1% SDS and 1% Triton X-100 through the gels to lyse the cells, then rinse away the cell fragments with PBS. We first tested the viability of this flow through decellularization method by placing the fibroblast seeded fibrin gels in a transwell plate. Transwell plates have a culture plate with a permeable bottom thus the decellularizing solutions were placed above the gel and allowed to flow through the gel due to the pressure gradient created.

In this experiment, two different heights of gels were used and placed in each transwell and two different pressures were used on the gels. The low pressure (P1) used was 50 Pa, as it has been used to induce interstitial flow through a similarly sized fibrin gel in a similar device

(Vickerman et al., 2008). Fibrin gels will tear under high mechanical forces, so we chose 80 Pa for the higher pressure (P2) as we did not want to greatly exceed 50 Pa (De Jesús & Sander, 2014). The low height (H1) used was 1 mm, because this is the approximate width of the gel in our device and accurately represents how far the decellularization fluid will have to travel through the gel. The higher height (H2) we chose was 4 mm, because we know that fibrin gels will compact as a result of extracellular remodeling (Rowe et al., 2007). Figure 24 below shows a schematic of the setup in the transwell. Combinations of each gel height and pressure were tested.
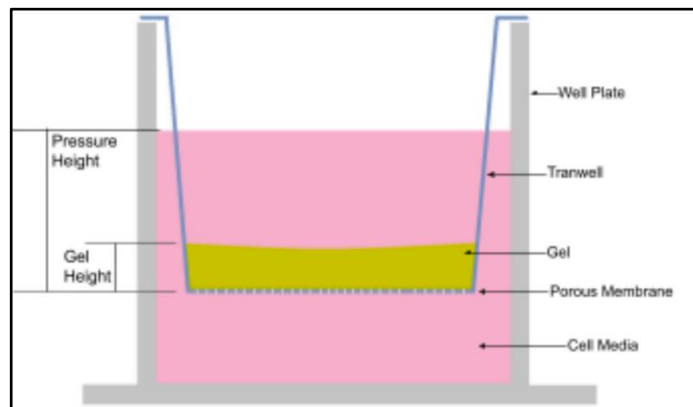

Figure 24: Gel Seeded in a Transwell. The gel is placed in the transwell, surrounded by cell media. The porous membrane of the transwell allows for solution to flow through. The pressure height refers to the height of cell media over the gel. The gel height refers to the thickness of the gel.

In this experiment, two 24 transwell plates were used, each holding 12 samples. For our controls, we decided to use a fibrin gel that was not seeded with any cells and a cellular fibrin gel that was not treated with surfactants to decellularize it. The purpose of the acellular control was to compare the ECM that was remodeled by the cells vs the structure of the fibrin without them. The purpose of the cellular gel that was not decellularized was to see how well the experimental gels were decellularized and if there was a visual similarity between them. The acellular gel was developed after multiple days after the other gels were made and they were made at H2 and P2. This was because by the time they were made, it was discovered that H2 gels will be easier to see than H1 after compaction. P2 was chosen for the acellular gels to see a higher compaction factor on the gels. For the gels that were not decellularized, H1 and P1 were used. This was because H1 at the time seemed to be a standard value. P1 for these gels were chosen to not reduce the gels significantly compared to a higher pressure.

When fabricating the gels, fibrinogen was first added to the wells. Next, a solution of thrombin supplemented with a cell suspension of 2 million cells/mL was mixed and added to the fibrinogen in the well. This was quickly moved into the transwells at the appropriate heights, as the gels cure in approximately 30 seconds. The total concentration of cells in the gel was 1 million cells/mL. The transwell plates were then placed in the incubator to gelate for one hour.

After the hour, cell media was added to the wells and the plates were stored in the incubator. More on this procedure can be found in Appendix F.

The gels were left to remodel for ten days. In that time, the media was replaced approximately every three days to replenish the nutrients for the cells. At the end of the experiment, we decellularized the gels with 1% SDS for 6 hours and 1% Triton X-100 for 30 mins, replacing the solution at 10 minute intervals. Gels were rinsed 3x with PBS. After decellularization, gels were fixed using paraformaldehyde (PFA) for 15 minutes. The gels were rinsed again, then measured. Gels were then permeabilized with 0.25% Triton X-100 for 10 minutes and stained with Hoechst 33342 for 10 minutes. Hoechst is a blue fluorescent dye that stains DNA. The gels were then transferred to a 96 well plate to be imaged using a BZ Keyence microscope. This procedure can be found in Appendix G.

Upon completion of this experiment, at initial glance, some gels had been aspirated from the transwells, but the majority of the gels held securely in their plates and decellularization was successful. The gels seeded at height one were less likely to stay in one piece and we weren't able to see them by eye. This could be a result of them either having broken into pieces, or being compacted to very small height.

To calculate the actual heights of the gels, ImageJ Software was utilized by taking an image of each well with a gel, alongside a scale bar and uploading the image to ImageJ. ImageJ allows for an easy comparison between the scale bar and the gel. For each gel, three heights were found and the average was taken for accuracy. Figure 25 shows an example of an image taken of a transwell. This transwell had a gel at height 2, of 4 mm and a pressure 1 at 50 Pa.
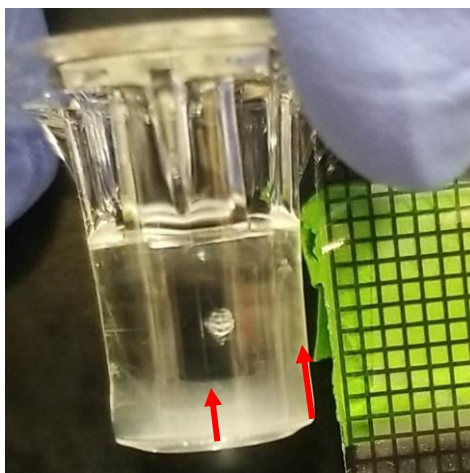

Figure 25: Decellularized Gel at H2 of 4 mm and P1 of 50 Pa in Transwell Plate. The scale bar on the right has boxes that are 1 mm in length. The gel has a concave meniscus, where the center of the meniscus and edge are indicated by red arrows.

As previously stated, some gels were no longer fixed to the transwell, which could have been a result of it being pulled from the well during aspiration. Figure 26 shows an image of a gel at height 2 and pressure 1, that had been lifted from the transwell. As this gel is lifted, it shows a top profile of the gel, which is a circular shape. The diameter of the circle is much less

than the diameter of the transwell, as a result of it being compacted over time due to the pressure of the solution on it. This proves that the gels are being compacted from the pressure.
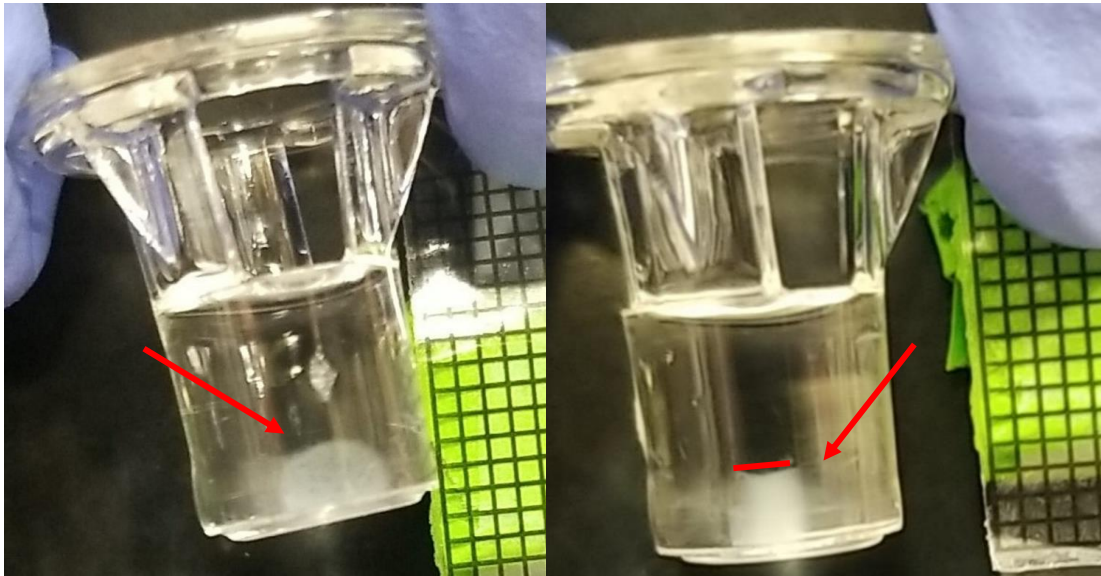

Figure 26: Gel Detached from Transwell at H2 of 4 mm and P1 of 50 Pa. The scale bar shown has boxes of 1 mm. The image on the left shows what was the top of the gel, in a circular shape. The image on the right shows the gel on its side. The width of the gel can then be measured and is shown by the red line.

From scientific literature, we expected the gel to compact due to the nature of the fibrin gel and ECM remodeling (Rowe et al., 2007). Compaction was found in the samples. The majority of the visible wells compacted downwards, but stayed bound to the sides of the transwell. Some lifted off the transwell and in those the width compacted as well.

Many of the gels at the lower height were not visible, likely a result of them already being at a low height and then compacting greatly. The comparison of initial gel height and final gel height after being compacted is necessary in understanding their compaction rates when we place them in our devices. Figure 27 shows the relation for each of the gel heights found. The percentages show what percent of the initial gel height that the final gel height was at. Analyzing this figure, it can be determined, that under conditions of H1P1, the gels compacted to be 50% of the original height, under conditions of H2P1, the gels compacted to be 45% of the original height and under conditions of H2P2, the gels compacted to be 41% of the original height (excluding the outlier of the acellular gel). The acellular gel compacted to be 15% the original height, which is likely due to the fact that there were no cells present. The cells therefore contributed to reducing the amount of gel compaction.
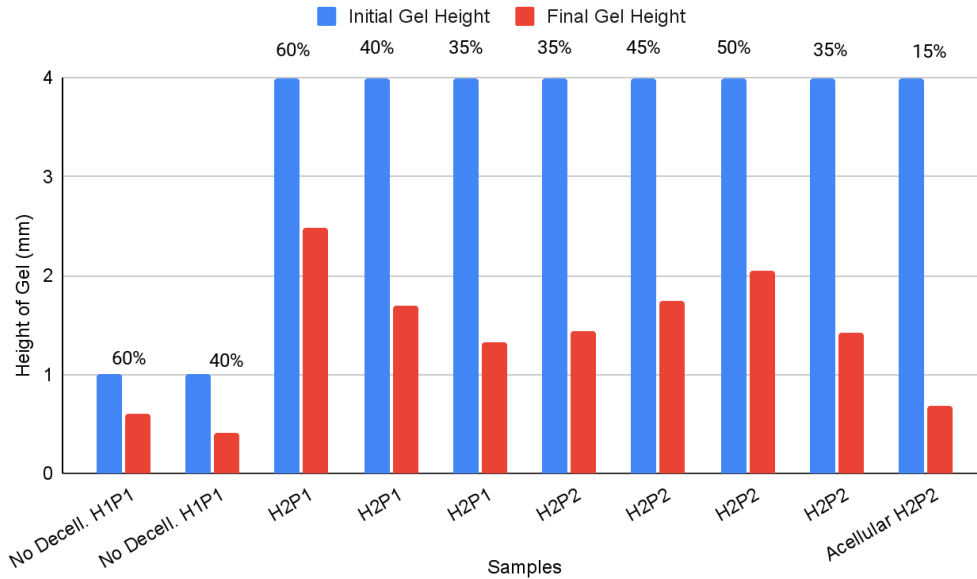
Figure 27: Relationship Between Initial Gel Heights and Final Gel Heights. H1 refers to a gel height of 1 mm, H2 refers to a gel height of 4 mm, P1 refers to a pressure gradient of 50 Pa, and P2 refers to a pressure gradient of 80 Pa. The blue bars show the initial gel heights when they were placed in the transwell. The red bars show the final gel heights after 10 days. The percentages show the amount of compaction between initial gel height and final gel height. Samples that the gel was not visible are not included in this graph.

To determine the success of the decellularization, the gels had to be stained and imaged to visualize any remaining cell nuclei. This was done using Hoechst dye to stain DNA. This procedure can be found in Appendix H. Imaging was done on an All-In-One Fluorescence BZ Keyence microscope. Figures 28 and 29 below show a decellularized gel and a gel that was not decellularized, respectively.
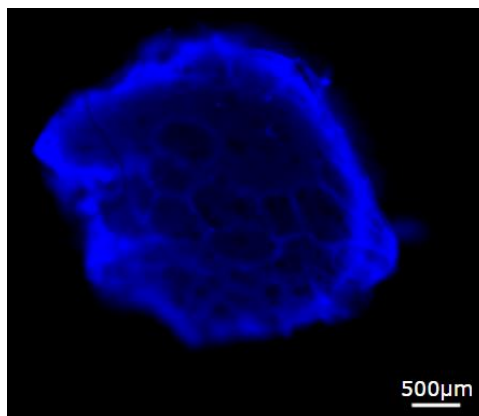

Figure 28: Stitched Image of Gel after being stained with Hoechst Dye at 4 mm Height.. Gel at height 2, pressure 2 was measured to be 1.43 mm thick. The microscope was set to 4x and the scale bar is 500 µm. In this gel sample the extracellular matrix within the gel can be seen in dark blue. There are gaps or holes

in the extracellular matrix indicates where nuclei would be present if there were any. Because of this, it is assumed that all cells were removed during the decellularization process.
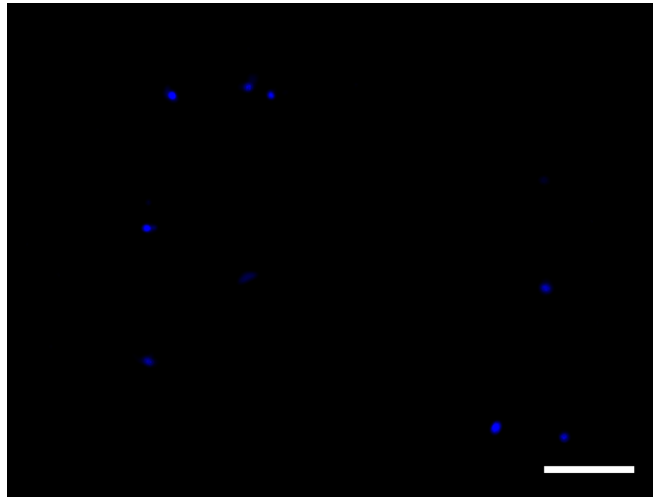

Figure 29: Sticked Image of Gel after Being Stained with Hoechst Dye at 1 mm Height. Gel 6 of 1 mm Height Without Decellularization. Small blue fluorescent dots are assumed to be cell nuclei. 4x image with a 100 µm scale bar.

Decellularization was successful because no remaining cell DNA could be seen in the images. In the control that was not decellularized, cells were seen. The difference between these images shows that the cells were present before decellularization, but not after decellularization, meaning that the experiment was successful.

The gel samples were further analyzed through histological staining. Hematoxylin and eosin (H&E) and trichrome staining were applied to separate samples. Detailed descriptions of the H&E staining procedure and results can be found in Appendix I, and the procedure and results for trichrome staining can be found in Appendix J. Briefly, the fixed samples are processed in a tissue processor, embedded in paraffin, sliced into sections 3-8 microns in thickness, placed onto a microscopic slide, and stained as desired. (Heinbockel & Shields, 2018).

In H&E staining, pink represents connective tissues and blue represents nuclei of cells. In trichrome staining the blue represents collagen, pink represents the cytoplasm of cells and brown/black represents cell nuclei. The gels were fixed and stained using standard histology procedures as outlined in the Histology and Cellular Staining section of this paper. From histology imaging, there were none or very few nuclei present in all of the samples. Unfortunately, the no decellularization control was not sliced properly, so there is no way to properly evaluate the decellularized gels. Figure 30 and Figure 31 below show some imaging results found from H&E staining and trichrome staining.
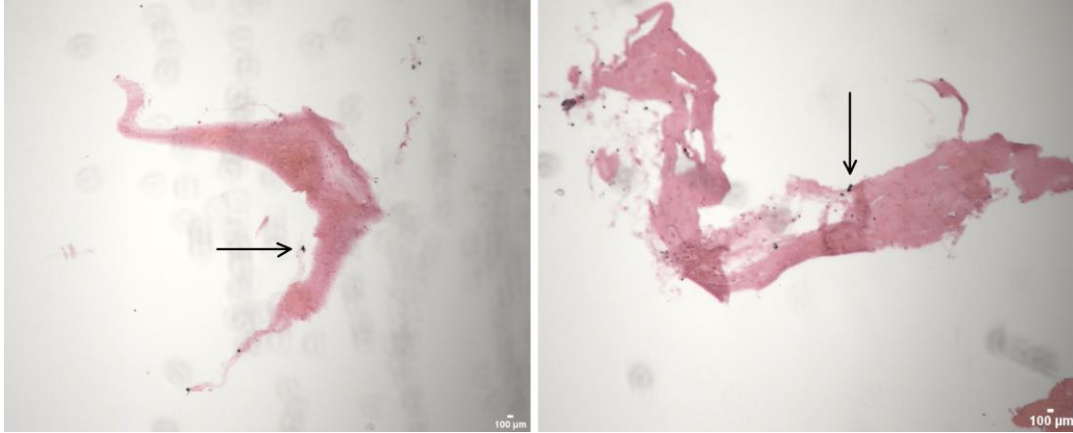
Figure 30: Microscope Image of Fibrin Gel After Decellularization and H&E Staining. Image on left shows a gel at height 2 of 4 mm and pressure 1 of 50 Pa. Image on right shows a gel at height 2 of 4 mm and pressure 2 of 80 Pa. Images were taken at 10X magnification. A few blue dots, indicated by an arrow, could potentially be a cell nucleus.
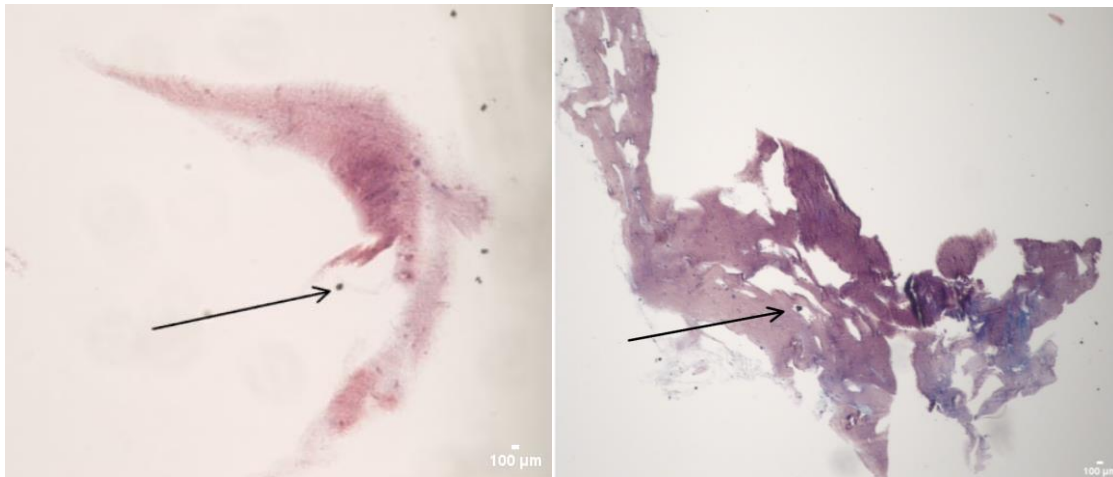

Figure 31: Microscope Image of Fibrin Gel After Decellularization and Trichrome Staining. Image on left shows a gel at height 2 of 4 mm and pressure 1 of 50 Pa. Image on right shows a gel at height 2 of 4 mm and pressure 2 of 80 Pa. Images were taken at 20X magnification. A few blue dots, indicated by an arrow, could potentially be a cell nucleus.

From the H&E figures of the staining above, there is only a very small amount of potential cell nuclei visible. From the trichrome staining, it was concluded that the 'spots' were not dyed brown/black and were not cell nuclei. This proves that the decellularization method was successful, and could next be tested in the microfluidic devices.

H. Decellularization in AIM Biotech idenTx 3 Chip

1. Experimental Setup

As the microfluidic devices produced via photolithography and PDMS casting proved to be ineffective at holding the hydrogel in the gel chamber, the idenTx 3 Chip from AIM Biotech were employed to test the concept of flow-through decellularization in a microfluidic device. As outlined previously, these devices are of a similar concept to our proposed design. The main differences between the idenTx 3 chip and our initial proposed design are dimension based and are outlined in Table 3. As these chips contain a gel inlet port for easy hydrogel insertion, pillars for capillary action, and media channels for the application of fluid flow, these devices fulfill the requirements for this procedure.

Table 3: Dimensional Comparison of Our Design and AIM Biotech idenTx 3 chip

	Our Design	AIM Biotech idenTx 3
Trapezoidal Pillar Dimensions	100 µm at base	300 µm at base
Pillar Spacing	100 µm	100 µm
Height	200 µm	250 µm
Media Channel Width	500 µm	500 µm
Gel Chamber Width	1,300 µm (1.3 mm)	1,300 µm (1.3 mm)
Gel Chamber Length	8,000 µm (8 mm)	10,500 µm (10.5 mm)

In addition to testing interstitial flow decellularization, the goal of this procedure was to determine if the concentration of fibrinogen, thrombin, neonatal dermal fibroblast cell suspension, or media supplement concentrations would affect the efficacy of *in situ* decellularization. Different combinations of media were selected based on TEHV based experiments conducted by as Syedain *et al.* as well previous experiments carried out by the Billiar Lab at Worcester Polytechnic Institute. Media supplements consisted of insulin, aprotinin, TGF-β, ascorbic acid, and aprotinin. These supplements were added to complete media (10% FBS, 1% Antibiotic-Antimycotic, 4.5 g/L D-Glucose, L-Glutamine, 110 mg/mL sodium pyruvate) at the desired concentrations, as outlined in Table 4. Additionally, the different concentrations of the fibrin gel components are provided in Table 5.

Six copies of each media and fibrin gel composition combination were produced; three to be decellularized, and three to serve as non decellularized controls. Additionally, three acellular gels (one of composition A, one of composition B, and one of composition C) were produced. The specific media and fibrin gel composition combinations are outlined in Table 6.

Table 4: Concentration of Supplements Added to Complete Media

	Media A (Billiar Lab)	Media B (Syedain *et al.*)	Purpose of Supplement
Insulin	5 µg/mL	2 µg/mL	Increase glucose intake to support cell ECM secretion
Ascorbic Acid	250 µg/mL	50 µg/mL	promote collagen synthesis and secretion by fibroblasts (Guo et al., 2007)
Aprotinin	500 KIU/mL	N/A	Inhibit fibrin degradation (Mühleder et al., 2018)
TGF-β	10 ng/mL (added on day 3)	10 ng/mL (added on day 3)	Increase ECM protein secretion by cells, it also lowers cell proliferation and was thus added on day 3 (Zhu et al., 2021)

Table 5: Concentrations for Fibrin Hydrogel Composition

	Concentration A	Concentration B	Concentration B1	Concentration B2
Fibrinogen	3.3 mg/mL	4 mg/mL	6 mg/mL	4 mg/mL
Thrombin	1 U/mL	0.38 U/mL	0.38U/mL	0.38 U/mL
Cell Suspension	$1 * 10^6$ cells/mL	$1 * 10^6$ cells/mL	$1 * 10^6$ cells/mL	$0.5 * 10^6$ cells/mL
Purpose of testing this concentration	Billiar Lab formula	Syedain *et al.* formula	Higher fibringen concentration	Lower cell concentration

Table 6: Media and Fibrin Gel Compositions Tested

Media and Fibrin Composition	Number of Devices
Media A + Concentration A	6
Media B + Concentration B	6
Media B + Concentration B1	6
Media B + Concentration B2	6
Media B + Acellular	3

2. Placing Gels in idenTx Devices

First, cell suspensions of $1 * 10^6$ cells/mL and $0.5 * 10^6$ cells/mL of neonatal dermal fibroblasts were produced from a cell line at passage 11. Next, fibrinogen and thrombin were diluted in Dulbecco's phosphate-buffered saline (DPBS) to create the desired concentration for each condition. Thrombin and cell suspension solutions were then combined at a 1:1 volume ratio. Next, 5 L of the thrombin/cell suspension solution was combined with a 5µ of fibrinogen solution. The resulting solution was quickly repeat pipetted and placed into a single device, with half of the volume (5µL) going in one gel inlet and the other half going in the opposite gel inlet. This was repeated for each device and each concentration.

After gel placement, the gels were placed in a humidified chamber created with a micropipette box. The gels were incubated for 1 hour at 37°C to permit gelation. After this period, the specified media for each device was added to the media channels. 70 µL of media was added to one port, and 50 µL was added to the connected port. This was repeated for every media channel.

The devices were stored in humidified chambers created by placing a small cell culture dish filled with sterile water next to the idenTx 3 devices in a larger cell culture dish. The cells were incubated at 37°C and allowed to remodel for 8 days prior to decellularization. Cells within the devices were fed daily following a procedure provided by AIM Biotech. Briefly, media was aspirated from the media ports. Then 70 µL of media was injected into one port with a micropipette and 50 µL was injected into the connecting port. This is repeated for the opposite media channel, and then the whole procedure is repeated for every device. Devices were fed Media A or Media B based on their assignment laid out.

Before and after the daily media changes, the cell embedded hydrogels were imaged to ensure that the gels were still in the chambers. The gels remained in the chambers throughout the experiment, however as the cell population increased some cells did migrate into the channels (Figure 32). This phenomenon was most prevalent on the higher cell density trials ($1 * 10^6$ cells/mL), but was present in some samples for each experimental group. However, as there were still cells within the hydrogel chambers, these devices were still suitable for testing the decellularization process.
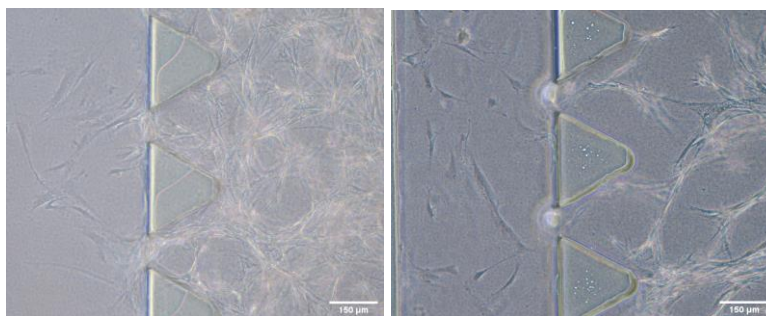

Figure 32: Devices with Fibrin Gel and Fibroblasts. Devices from Experimental Groups B1 (left, $1 * 10^6$ cells/mL) and B2 (right, $0.5 * 10^6$ cells/mL Embedded After 8 Days Incubation. Cells have migrated into the media flow chambers in both cases, however cells are still present in the hydrogel.

3. Determining Decellularization Pressure

On day 7, an abbreviated decellularization test was conducted on one idenTx 3 chip (3 microfluidic devices) to determine the ideal pressure to apply to the devices during the application of the decellularizing solutions. One chip from the Media A + Concentration A group was selected for this procedure as the cell densities for the three devices on these chips varied significantly (5% confluent - 80% confluent), suggesting that the fibrin gel solution was not mixed sufficiently during the placement in these devices. The starting cell densities and pressure tested are outlined in Table 7.

Media was removed from the media ports on each of the devices, and the devices were washed with PBS three times. A rubber stopper was placed into each of the gel inlets to prevent fluid from draining from these ports. 1000 µL pipette tips were then added to each media port to serve as the SDS reservoirs, as shown in Figure 33. SDS was added at the pressure differences specified and allowed to flow through for 3 hours. Every 15 minutes the height differences were reestablished by pipetting the volume that had flown into the second reservoir back into the first reservoir. Cells were imaged with a Nikon TS2-S-SM microscope before and after decellularization.

Table 7: Preliminary Pressures Tested

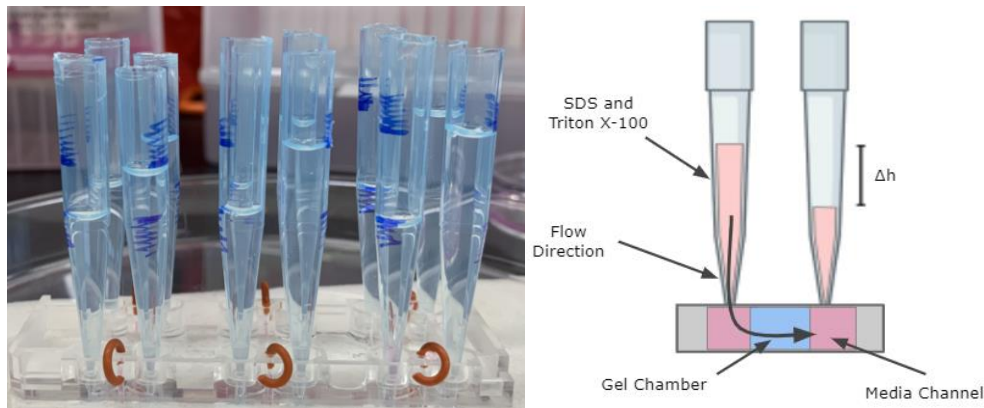| Device	Starting Cell Density	Pressure Tested (Pa)
1	5%	60
2	60%	90
3	80%	120

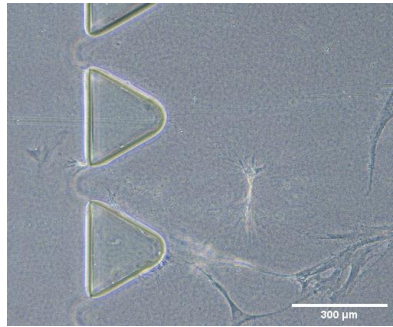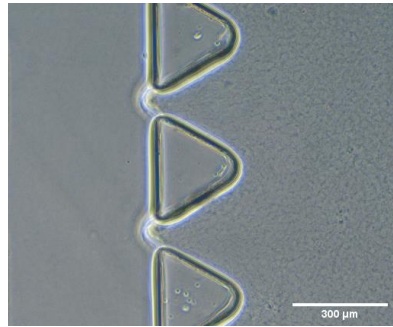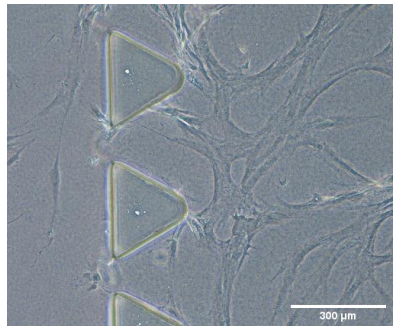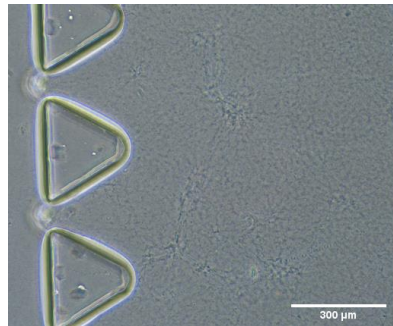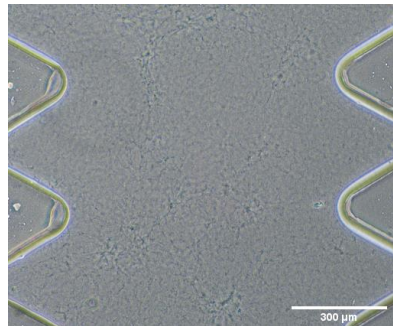Figure 33. Setup for Testing Decellularization Pressures. 1000 µL pipette tips were used as the SDS reservoirs. Three pressures were tested: from left to right 60 Pa, 90 Pa, 120 Pa. The schematic on the right shows a side view of the setup. Image created with BioRender.com.

After 3 hours of SDS application, the hydrogels in all of the devices appeared to remain in the chambers as indicated by visible meniscus between the pillars, as shown in Table 8. Additionally, any visible indication of fibroblast presence was not viable in any of the devices, suggesting that even through an abbreviated procedure, decellularization was achieved. From these results, 120 Pa pressure was selected to decellularize the remaining devices as most of the other devices had a cellular density that was similar to this device.

Table 8: Images of Chip A Taken at 20X Before and After Undergoing the Decellularization Process.

	Before Decellularization	After Decellularization
Device 1		
Device 2		
Device 3		

4. Decellularization

To begin the decellularization process, the devices were removed from the incubator and the gel inlets were plugged with rubber stoppers as in previous testing for determining the necessary pressure. Media was removed from the ports and the hydrogels were washed with PBS three times before the micropipette tip reservoirs were added. Non decellularized gels were fixed

in paraformaldehyde (PFA). For the gels being decellularized, 1% SDS was applied at a height difference of 1.2 cm to produce a pressure difference of approximately 1.2 Pa ($\Delta P = \rho \Delta hg$). The SDS was allowed to flow through the gels for 6 hours. Every 15 minutes, the heights on the reservoir inlets would be recalibrated to ensure that the pressure difference and corresponding interstitial flow remained as consistent as possible.

After 6 hours, the SDS was removed from the reservoirs and 1% Triton X-100 was added to the reservoirs at the same 1.2 cm height difference. The Triton-X 100 was left for 10 minutes, and this was repeated a total of 3 times. Next, the gels were washed with PBS 3 times and fixed with paraformaldehyde, imaged, and stored in the refrigerator. A select number of hydrogels which were representative of the non decellularized control, the acellular control, and the decellularized gel were selected for fluorescence staining and imaging. The gels were stained with Hoechst and Phalloidin. The full staining procedure can be seen in Appendix K. Images of these gels are provided in Figure 34.
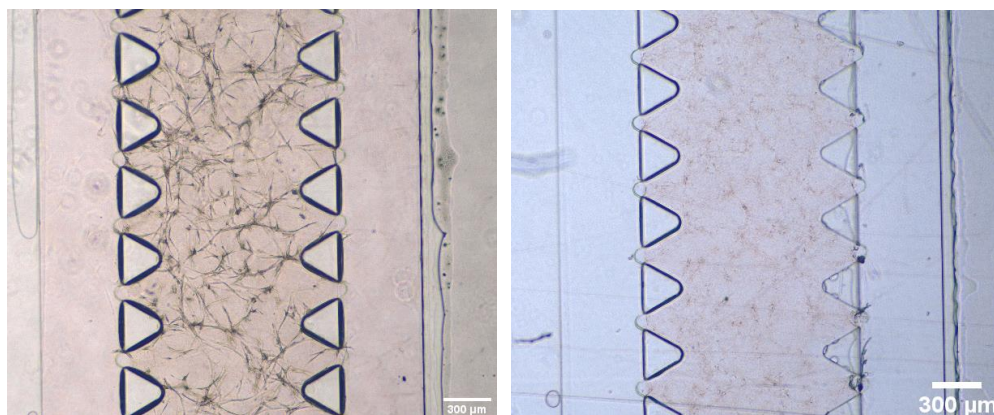

Figure 34: Fibroblast-Embedded Hydrogel Before (left) and After (right) Decellularization. Image was taken at 4x on the Nikon TS2-S-SM.

Over the course of the experiment, all hydrogels remained within the gel chamber in the device. Furthermore, none of the decellularized hydrogels showed any visible indication of cellular presence within the gel at the conclusion of the procedure. However along the outer pillar region some potential cellular debris appeared to be gathered. Overall, the results indicated that decellularization through interstitial flow of detergents is possible in a microfluidic platform. The different fibrinogen, cell, and aprotinin concentrations did not seem to affect the success of the decellularization as gel were successfully decellularized from all samples (see Appendix L).

The non-decellularized gel stained with Hoechst and Phalloidin (Figure 35) shows a clear presence of cell nuclei (blue) and cell cytoskeleton (green) throughout the gel. Conversely, the decellularized gel does not show any indication of cells within the gel (Figure 36). There are some areas of fluorescent concentration around the posts, however this is likely due to the stains not fully washing out of the gel, or due to the presence of autofluorescence. This is confirmed by examining the acellular gels, which also show fluorescence around the posts (Figure 37).

Figure 35: Fluorescent Image of Non Decellularized Gel. Hoechst (blue, nuclei) and Phalloidin (green, f-actin) staining of non-decellularized gel (B1) taken at 4x on the Keyence BZ-X800.
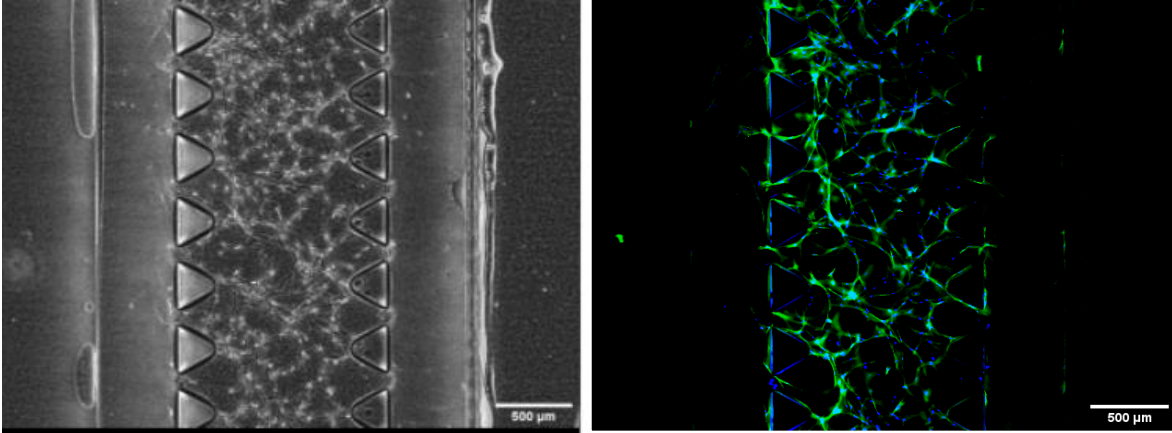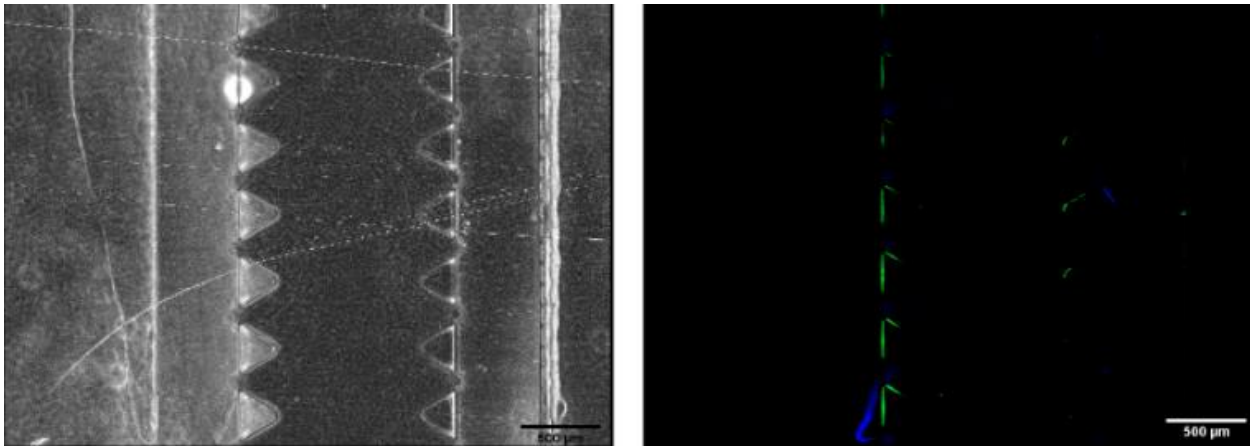

Figure 36: Fluorescent Image of Decellularized Gel. Hoechst (blue, nuclei) and Phalloidin (green, f-actin) staining of decellularized gel (B1) taken at 4x on the Keyence BZ-X800.
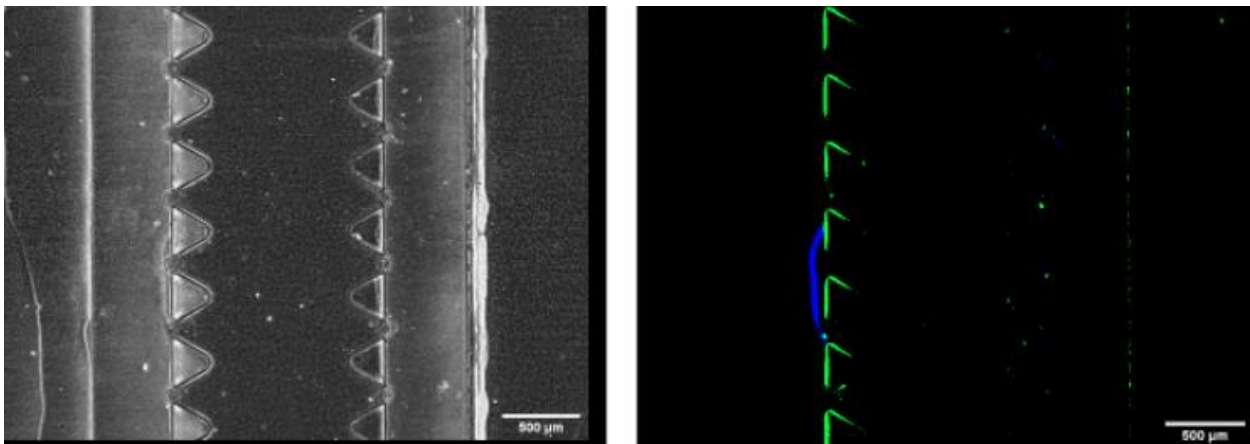

Figure 37: Fluorescent Image of Acellular Gel. Hoechst (blue, nuclei) and Phalloidin (green, f-actin) staining of acellular gel (B1) taken at 4x on the Keyence BZ-X800.

I. Producing a Microfluidic Gravity Pump

In order to produce the desired steady and oscillatory flow rates and patterns in the PDMS microfluidic device, a suitable pumping system is required. Various pumping systems are employed for microfluidic applications as outlined in the Literature Review and Appendix B. A modified gravity pump was selected for the final device design.

A gravity pump is relatively simple and only requires tubing and connectors at varying heights to produce a range of flow rates. A singular gravity pump is capable of producing steady flow, so modifications are needed to produce oscillatory flow. Thus, two gravity pumps are employed in this design; one to create forward flow and one to create backflow. This change in flow direction will be accomplished by turning the gravity pumps on one at a time. To turn the pump on and off, solenoid pinch valves programmed by Arduino software will 'pinch' or 'close' one end of the tubing to prevent flow. A basic setup of the gravity pump is shown schematically in Figure 38. When the two green solenoid pinch valves of group 1 are open, fluid flows from inlet 1 to outlet 1 (i.e. flow through the microfluidic is from the left to the right). When the two red solenoid pinch valves of group 2 are open, fluid flows from inlet 2 to outlet 2 (i.e. flow through the microfluidic is from the right to the left). By programming the solenoid pairs to switch between open and closed states, the flow can be systematically reversed and oscillatory flow can be produced.
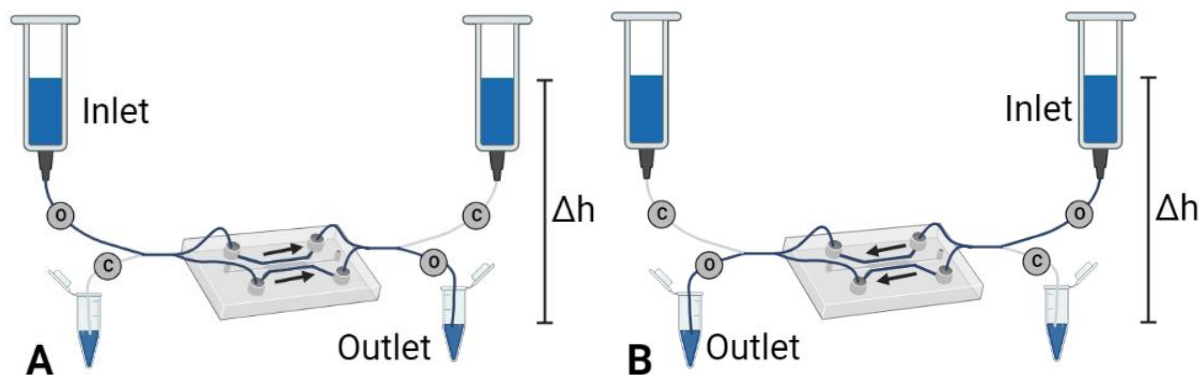
Figure 38: Schematic of Gravity Pump for Oscillatory Flow. The gray circles represent solenoid pinch valves, which open (O) and close (C) periodically to reverse the flow from one direction (A) to the other direction (B). Pressure differences were varied by altering the heights of inlet and outlet wells. The microfluidic device is pictured in the center. Image created with BioRender.com.

The gravity pump needs to be able to produce the necessary flow values to create the desired wall shear stress (0.2 Pa and 2.0 Pa) along the gel chamber where the endothelial cells will be seeded. Additionally, for the oscillatory flow, a range of 60 to 72 oscillations per minute must be met. Resistance of the microfluidic tubing and the fluidic channels in the device influence the relationship between the shear stress flow rates. In the final device design, the internal fluid channels are rectangular and 500 μm wide. Additionally, 250 μm radius tubing was

selected for use in this design. This tubing was selected to minimize variations in flow rates at the transition between the microfluidic device and the tubing. Developing a gravity pump and testing various flow rates will allow for a comparison between theoretical and experiment values.

The gravity pump was assembled by attaching all components to a peg board, as shown in Figure 39. 30 ml syringes with the plunger removed were used as pressure wells. 3-way valves were used to connect the syringes to the tubing, as well as integrate a priming syringe. The solenoids would not activate with the smaller diameter tubing we had initially selected. The larger tubing that came with the solenoids were then spliced into the smaller tubes using metal fittings. These same fittings were used to attach the tubing to the microfluidic device. Y connectors were used to connect the inlet and outlet tubing with the microfluidic device, and split the flow into the device so that fluid flows on each side of the gel chamber.
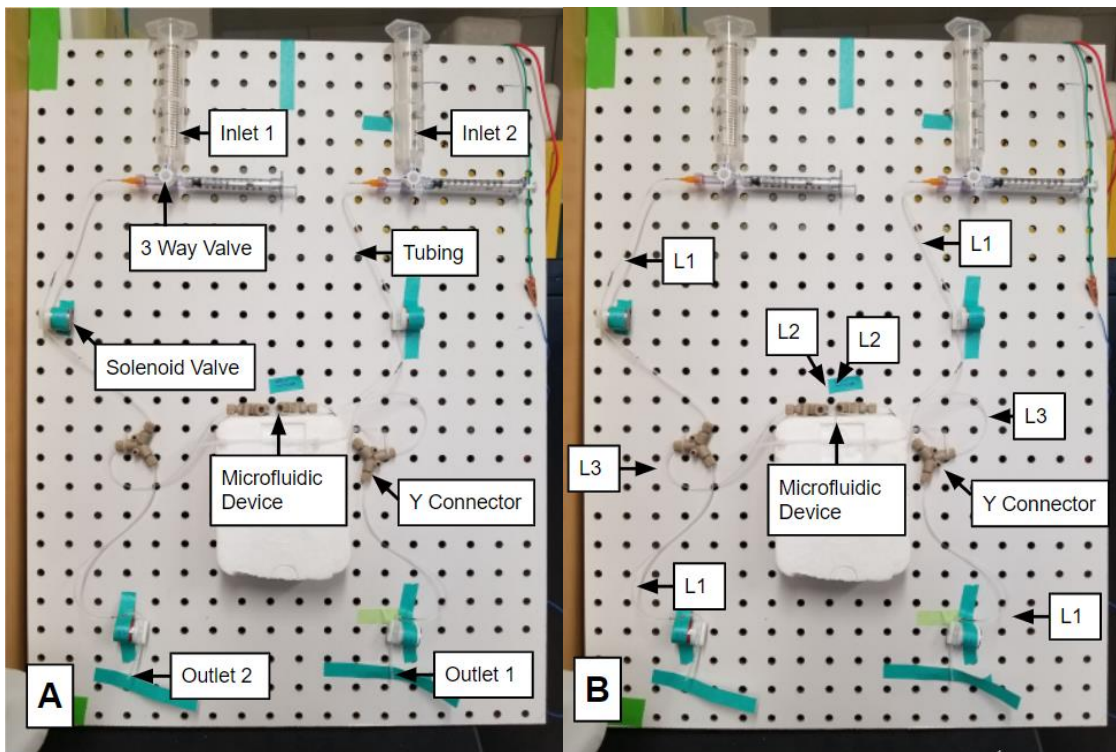
Figure 39: Setup for Testing of the Double Gravity Pump System. A) Labeled components of the system. B) Labeled tubing lengths; L1 corresponds to 20 cm, L2 corresponds to 10 cm and L3 corresponds to 20cm.

A theoretical flow rate of 3 µl/s was tested by placing the inlet and outlet at a height difference of approximately 47.6 cm. These values were found using the following equations:

Determining Flow Rate Using Wall Shear Stress

$$\tau = \frac{6Q\mu}{h^2 w} \tag{1}$$

Fluidic resistance in the tubing was found by using Equation 2. An example calculation can be found below. The radius of the tubing was 250 µm, dynamic viscosity was assumed to be 1mPa*s, and the length of the tubing was variable, but here 60 cm is used.

Tubing Resistance Modeled as a Circular Pipe

$$R = \frac{8\mu L}{\pi r_o^4} \tag{2}$$

$$R = \frac{8 * 1mPa * s * 60cm}{\pi * 250\mu m^4}$$

$$R = 391.7 \frac{Pa * s}{mm^3}$$

Rectangular channel resistance was calculated using the surface of the gel chamber in the device as the width, and the depth of the channels in the device as the heights. This was done to find the correct resistance for the surface that endothelial cells were cultured on. Per the device, height was 500 µm and width was 200 µm. Dynamic viscosity was assumed to be 1 mPa/s and the length of the device was 30 mm. An example calculation is shown in Equation 2 below.

Rectangular Channel Resistance in the Device

$$R = \frac{12\mu L}{wh^3} * \frac{1}{1-(.63*\frac{h}{w})} \tag{3}$$

$$R = \frac{12*(0.0001mPa/s)*(0.03m)}{0.0002m*0.0005m^3} * \frac{1}{1-(.63*\frac{0.0005m}{0.0002m})}$$

$$R = 3.73 \frac{Pa * s}{mm^4}$$

The resistance of all lengths of tubing and the device were summed together to find the total resistance of the system. Once this value was determined, it could be used in combination with our necessary flow rate to find the total amount of pressure needed to produce the desired shear stress. An example of this calculation can be found in Equation 4.

Total Pressure in System

$$\Delta P = R \; x \; Q \tag{4}$$

$$\Delta P = 693 \frac{Pa*s}{mm^2} * 3.0 \frac{\mu L}{s}$$

$$\Delta P = 4150 \; Pa$$

The total pressure in the system was used to find the desired change in heights, as shown in Equation 5.

Determining Height Based on Pressure

$$\Delta P = \rho g \Delta h \tag{5}$$

$$693.17 \; \frac{Pa * s}{mm^2} = 1 \; mPa * s \; * \; 9.81 \frac{m}{s^2} * \Delta h$$

$$\Delta h \; = 42.5 \; cm$$

The tubing and device were primed and any air bubbles were removed prior to the start of the flow test. The solenoids were attached to the tubing in the desired spots. The three-way valves were then opened. A timer was prepared to measure a flow rate, and then the battery was attached to begin the test. Five trials were conducted, at varying rates of oscillation, measured in beats per minute. The outlet tubes were measured using a micropipette. The data from these trials are shown below.

Table 9: Experimental Flow Rates from Double Gravity Pump Setup

	BPM	Volume 1 (μl)	Volume 2 (μl)	Flow Rate 1 (μl/s)	Flow Rate 2 (μl/s)	Total Flow Rate (μl/s)
Trial 1	40	75	730	.75	3.65	2.683
Trial 2	10	339	710	3.39	3.55	3.496
Trial 3	20	335	680	3.35	3.4	3.383
Trial 4	40	325	690	3.25	3.45	3.383
Trial 5	60	327	680	3.27	3.4	3.356

As can be seen in the data, there was some variation in the flow rates. For instance, Volume 1 of Trial 1 was much less due to the pump not having been primed initially. This piece of data was not used in calculating the average flow rate as it was an outlier, but it proved the need of priming the entirety of the pump prior to usage. However, the data gathered remained consistent enough to validate the system's functionality. The average flow rate, excluding Trial 1 as an outlier, was 3.4045 μl/s, which was higher than our target of 3 μl/s, which could be fixed by reducing the height difference, or experimentally refining the flow rates. Additionally, in this experiment, we were able to prove the success of the flow rate at 60 BPM.

J. Programming of Solenoid Pinch Valves

Four solenoid pinch valves were purchased from Clippard (2-Way N.C. Pinch Valve, 0.75" Dia., 0.030" ID-0.065" OD Tubing, 24 VDC). An Arduino Uno was also acquired for use in programming these valves. Arduino code was written to open two of the pinch valves at a time, while simultaneously closing the other two pinch valves, as previously shown. To create the desired oscillation, the first pair of solenoids are opened for 1000 milliseconds, while the second pair is closed. Immediately after, the second pair of solenoids are opened for approximately 500 milliseconds, while the first pair are closed. This timing was later updated to 666 milliseconds and 333 milliseconds. The varied timing of the different pairs of solenoids is to ensure that fresh media is being circulated to the cells in the microfluidic device without stopping the oscillation. This code is provided in Appendix M.

A circuit to power a single solenoid is displayed in Figure 40. A 22 V external battery was required to provide enough voltage for the four 24 V solenoid pinch valves and a transducer is used to help control the current. To produce the final circuit, four of these individual circuits are connected to one Arduino board and battery. This system has been tested and is capable of turning on and off the solenoids at the desired rate.
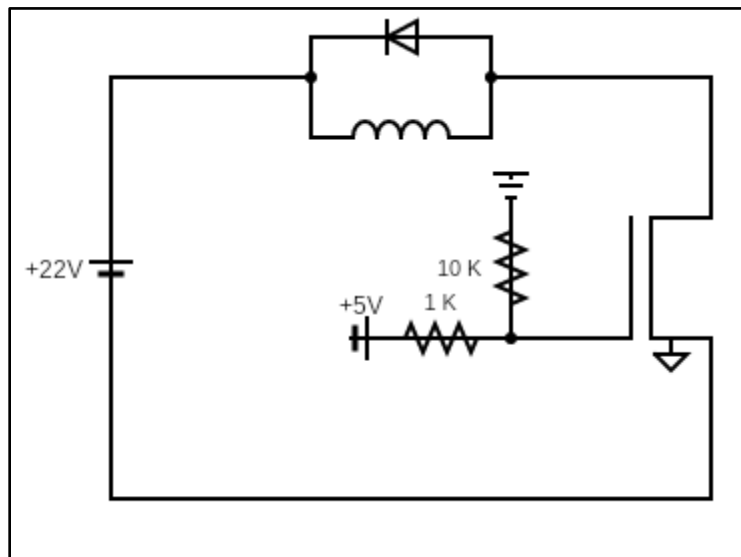

Figure 40: Circuit Diagram for a Single Solenoid Pinch Valve. The solenoid, shown as an inductor in parallel with a diode on the top, is triggered by the activation of the transducer, seen on the right. Four of these circuits are connected to the singular 22 V voltage source to power the solenoids.

V. Additional Considerations

A. Ethical Concerns

This device makes use of human dermal fibroblasts and endothelial cells which need to be sourced responsibly. Human fibroblasts can be sourced from skin biopsies and endothelial cells can be sourced from the umbilical vein (Bezenah et al., 2019, Fernandes et al., 2016). While both fibroblasts and endothelial cells can be expanded *in vitro*, thus limiting the number of sourced cells required, it is important to use the cells in a conscientious manner and make effective use of them.

In future applications of these processes, TEHV may be produced using porcine heart valves. Adherents to certain faiths, lifestyles, and cultures do not consume products which come from pigs, so this could create conflict and controversy in the development of the treatment. However, if porcine hearts destined for human implantation are sourced from existing meat processing plants, it may cut down on the byproducts of pork production, as the heart is not typically sold in North America.

B. Environmental Concerns

As with standard microfluidic devices which involve cells, both the microfluidic devices we produced and the microfluidic devices purchased from AIM Biotech cannot be reused after experimentation. Our devices are produced out of PDMS and a glass coverslip, which then must be discarded after use. However, the silicon wafer used to produce the devices, can be reused to make more devices through PDMS casting. Furthermore, PDMS has been demonstrated to have no adverse effects on terrestrial or aquatic life during the degradation process (Fendinger, 2005). The gravity pump system also needs to be considered in this context. The steady and oscillatory pump makes use of plastic reservoirs and microfluidic tubing. Over time, these components will need to be replaced. As such, a significant use of single-use equipment is required to operate the device, and thus all resources should be used with great care and consideration.

Additionally, all waste products should be disposed of responsibly. Most notably, PFA which is utilized to fix the cells in the devices, must be disposed of by following the chemical waste disposal procedure for the facility.

C. Societal Impacts

The implications of this system on the future of TEHV research are significant. By utilizing the decellularization *in situ* protocol, a more accurate model can be generated. This remodeled hydrogel is more accurate to native heart valves and will therefore have more accurate results in terms of attachment and migration. This would improve our current understanding of EndMT, which would allow for TEHV to be implemented with higher success rates. By furthering TEHV research, a treatment for heart valve disease can be developed which is more

cost effective and may not require the use of a medication. This would also make pediatric valve replacements more viable as a TEHV would be able to grow and adapt with the patient.

D. Health and Safety Concerns

Proper operation of the device does not impose any critical health or safety concerns. However, proper care should be taken when handling the devices when they contain cells. This includes wearing proper laboratory attire (gloves, lab coat, eye protection, etc.) and adhering to standard aseptic technique protocol. Furthermore, when performing any fixing procedures that use PFA, the chemical hood should be used. Additionally, the oscillatory pump requires an electrical circuit powered with a 22 V battery which the user must ensure is properly grounded before operation to prevent the risk of injury.

E. Economics and Manufacturability

The device can be effectively manufactured from a reusable silicon wafer through PDMS casting. By designing the silicon wafer to have repeated patterns of the same design on it, multiple devices can be produced from each PDMS cast, thus increasing manufacturing efficiency. The silicon wafer is manufactured through photolithography. While in this project, the wafer was produced in WPI facilities, future iterations of the device may require more advanced photolithography, which could require outsourcing the production of the silicon wafer.

The production of the gravity pump required the purchase of four Y connectors, four solenoid pinch valves, microfluidic tubing, a breadboard, and an Arduino microprocessor. These components require fairly significant user interaction to produce the proper gravity pump setup. However, once one becomes familiar with the setup process, it can be accomplished efficiently.

F. Engineering Standards

ISO standard 22916:2022, titled "Microfluidic devices - Interoperability requirements for dimensions, connections and initial device classification" details specific requirements for microfluidic devices to ensure seamless incorporation with additional microfluidic components such as connectors. Another relevant ISO standard, "IWA 23:2016: Interoperability of microfluidic devices - Guidelines for pitch spacing dimensions and initial device classification" provides definitions related to microfluidic devices. Both of these standards can be applied to the microfluidic device produced in this project in future applications.

VI.   Future Directions

  The next step of this project is to explore the use of a more advanced photolithography process to produce the desired pillar dimensions and geometry. This would be advantageous over using the AIM Biotech devices as it allows for greater customization, and results in a reusable silicon wafer from which a large number of devices can be produced at a low cost. One potential method of improving the accuracy of the photolithography process would be to outsource the production of the silicon wafer to a larger facility such as the Minnesota Nano Center at the University of Minnesota.

  Further design modifications can also be considered to increase the throughput and improve the ease of experimental designs. For instance, some of the preliminary designs produced through this project were able to apply shear to multiple gel chambers at once. Additionally, modification in pillar geometries, dimensions, and layout can be further explored to optimize the design for our application.

  Finally, the next step of the implementation of the device is to seed endothelial cells onto the cell derived matrix and measure endothelial cell migration and phenotype expression under the application of shear stress. Standard staining procedures can be utilized to visualize cells after the experimental period. This work has the potential to contribute to the research and development of tissue engineered heart valves.

VII.   Appendices

## Appendix A: Function and Structural Description of Heart Valve Components

The following table lists heart valve components; extracellular matrix, valvular interstitial cells (ICs) and valvular endothelial cells (ECs), along with their descriptions.

Heart Valve Component	Description
Valvular Extracellular Matrix (ECM)	Proteins including collagen, elastin and glycosaminoglycans arrange strategically to form a stratified ECM structure that can withstand the forces of blood flow while still being flexible enough to allow the movement of the valve leaflets (Walker et al., 2004).
Valvular Interstitial Cells (ICs)	Spindle shaped valvular ICs are found throughout the heart valve. They play a role in valve remodeling and maintain the structural integrity of the leaflet by secreting ECM components (Peeters et al., 2018; Walker et al., 2004). In healthy valves, little to no α-smooth muscle actin (α-SMA) is expressed by these cells (Walker et al., 2004).
Valvular Endothelial Cells (ECs)	These cells form the outer layer of the valve wall which makes contact with the blood. As the blood inflicts shear stress onto the ECs, the cells align perpendicularly to the direction of flow (Arjunon et al., 2013). Functions of ECs include regulation of valve permeability, paracrine signaling and inflammatory cell adhesion (Peeters et al., 2018). Note that valvular ECs are genetically different from vascular ECs and have a greater tendency to experience endothelial to mesenchymal transition (Arjunon et al., 2013).

Appendix B: Fluidic Pumps

Peristaltic Pumps

Peristaltic pumps function by tubing being wrapped around a motor that spins. Rollers push the fluid through the tubing at a controlled rate. To generate steady flow, the motor rotates in one direction at a constant rate. To generate pulsatile flow, the motor rotates at a steady pace in one direction for a given period of time, then stops for a given period of time and this continues. To generate oscillatory flow, the motor rotates in one direction for a given period of time, then rotates in the opposite direction for a given period of time (Byun et al., 2014). Peristaltic pumps can be produced with multiple motors and tubing sections to increase throughput.
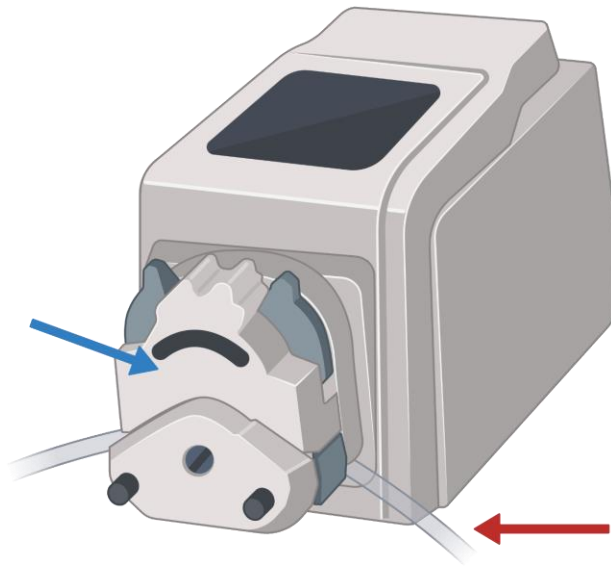
Peristaltic pump diagram. Flow is generated by rollers that pinch the tubing and push the fluid through them. The red arrow indicates the tubing, and the blue arrow indicates the housing where the rollers sit. Image created with Biorender.com.

Syringe Pumps

Syringe Pumps function by a piston pushing on a syringe that is connected to tubing. In the image below, the piston, indicated by the red arrow, is programmed to generate pressure, which twists a screw, located by the blue arrow. While the screw is being twisted, it pushes the plunger of the syringe and fluid in the syringe is pushed into tubing connected to the syringe tip (Alizadehgiashi et al., 2018; Byun et al., 2014).
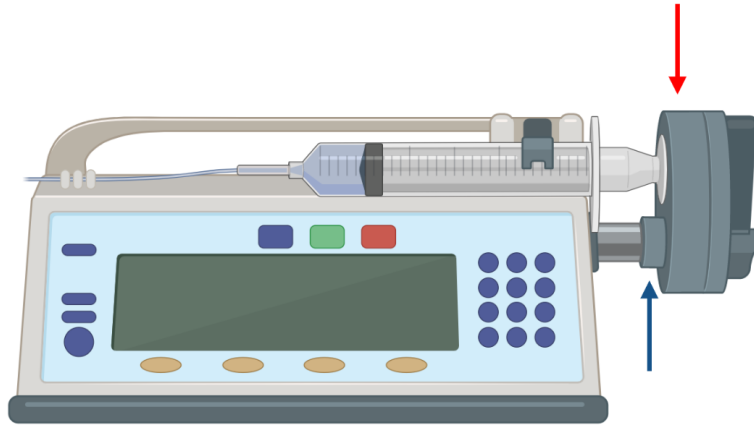
Syringe pump diagram. Flow is generated by pushing the syringe plunger, which expels liquid from the syringe into the connected tubing. The red arrow indicates the piston, and the blue arrow indicates the screw. Image created with Biorender.com.

Gravity Pump

Gravity pumps can be found set up in a range of ways, as they are essentially just tubing connecting an inlet and outlet reservoir. Fluid flows through the tubing by gravity and the flow rate can be controlled by changing the height difference between the inlet and outlet reservoirs. Steady flow can be generated by filling the inlet reservoir and letting the system run by gravity. Pulsatile flow can be generated by adding a valve, or pinching the tubing periodically. Oscillatory flow can be generated by producing a second gravity pump setup and using Y-tubing connectors and valves or pinching tubing. This setup, although more complicated, can be used by altering what inlet reservoir is open or closed (Byun et al., 2014).
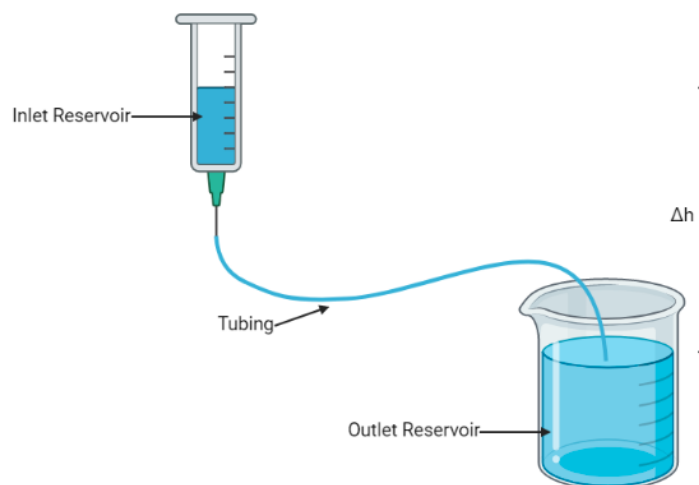
Basic setup for a gravity pump, consisting of an inlet and outlet reservoir connected by tubing, and separated by a height difference. Image created with BioRender.com.

Pressure Pump

Pressure pumps function by an external pressure source of gas. As shown in this image, a flow controller is used, however a pressure pump device or air tank can also be used. The flow controller (or pressure pump device or air tank) pushes air, at a given pressure, into the conical tube. In the image on the left, it can be seen that pressure is pushed inside the tube and the liquid gets pushed into the tubing as a result. Steady flow can be generated by pushing a constant pressure into the conical. Pulsatile flow can be generated by periodically pushing pressure into the conical, then stopping. Oscillatory flow can be generated by connecting another external pressure source of air on the other end of the tubing and altering the pressure being exerted from each source (Casquillas G., 2021).
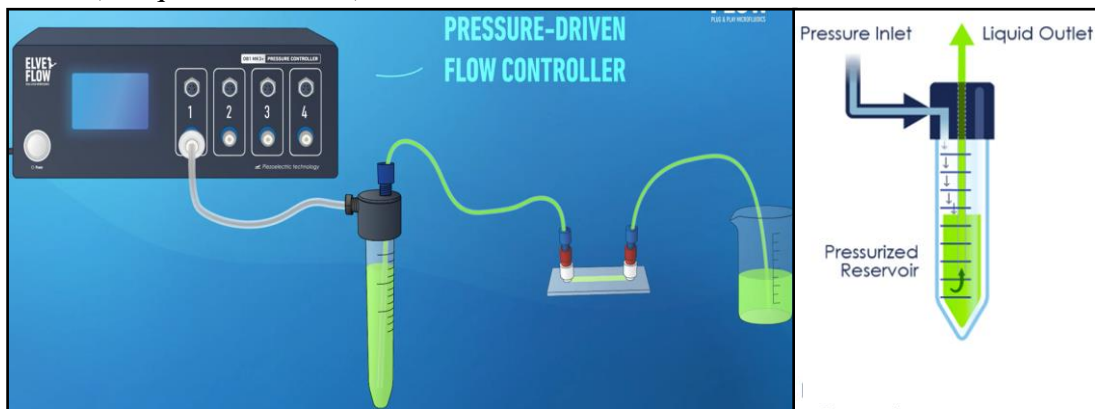
Depiction of a pressure pump, showing the controller, reservoir, microfluidic device, and outlet container. The controller pushes air into the reservoir, and maintains a constant level of pressure. This pressure produces fluid flow through the tubing and into the device. Copyright permission granted from Elveflow, an Elvesys brand. Image produced by Marie Gemey. (Casquillas G., 2021).

Vacuum Pump

A vacuum pump works similarly to a pressure pump, however the pressure created in the conical tubing, would be a negative pressure. This pulls the fluid through the device, rather than pushing it through. Steady flow can be generated by pushing a constant negative pressure into the conical. Pulsatile flow can be generated by periodically pushing negative pressure into the conical, then stopping. Oscillatory flow can be generated by connecting another vacuum pump on the other end of the tubing and altering the pressure being exerted from each source (Seo et al., 2019).

## Appendix C: Comparison of Types of Fluidic Bioreactors

The following table shows a comparison of devices used to test fluid applied shear research. This table provides details on a macro fluidic device, the Cone and Plate and three unique microfluidic devices. The table states the device name, the purpose of use, or what it was used to study, its strengths and limitations.

Device Name	Purpose of Use	Strengths	Limitations
Cone and Plate - (Kouzbari et al., 2019; Sucosky et al., 2008).	- Studying shear stress on heart cells	- Multiple trials simultaneously - Steady and oscillatory flow - Easy microscopy of cells	- Cannot generate pulsatile flow - Flow rates are not uniform throughout the device - Closed system- replacing liquid requires stopping of the device
PDMS microfluidic device with staggered micro pillars - (Vickerman et al., 2008)	- Measuring cell migration for capillary morphogenesis	- Micro pillars will hold the gel in place in the chamber	- Placing the gel in the device requires precision - Limited throughput as only one trial can run at a time
PDMS microfluidic device with long gel chamber - (Polacheck et al., 2014)	- Migration of Mammary adenocarcinoma cells	- Placing the gel is easy with the use of the gel inlet and channel - Trapezoidal pillars will hold the gel in place in the chamber	- Longer gel chamber requires more gel to fill - Limited throughput as only one trial can run at a time
PDMS microfluidic device with three fluid channels - (Chung et al., 2009)	- Measure migration of endothelial cells in collagen	- Multiple channels allows co-culture of two different cell types simultaneously - Easy addition of cell suspension - Placing the gel is easy with the use of the gel inlet and channel - Can run two trials simultaneously - Singular micro pillars can aid in holding the gel in place	- Only one larger pillar in the gel chamber blocks the surface of the collagen from coming in contact with liquid
PDMS microfluidic device with one wide fluid channel - (Mina et al., 2016)	- Measure migration of endothelial cells in gel	- Imaging of cells is within the device is easy - A deeper gel chamber can aid in holding the gel in place	- Limited throughput as only one trial can run at a time

Appendix D: Initial Wafer Designs

Within the silicon wafer, the top row holds two copies each of three different designs, Design 1, Design 2 and Design 3. The second row is two copies of another design, Design 4. The bottom two rows are each a unique design of gel chambers, Design GC1 through Design GC9 (where GC stands for Gel Chamber). These modifications of the gel chamber are to test the ease of gel placement and how well the gels stay in place. Each of the designs have a gel chamber that is 3mm by 1mm and has fluid channels on either side. They also all have 500µm wide gel inlet and outlet channels. The following figures show the different modifications to the gel chamber, while Designs 1-4 are explained in detail in the Initial Device Design Alternatives.

Design GC1 (gel chamber 1) has trapezoidal pillars, with a length of 100µm, that are spaced out by 100µm. The point where the gel inlet channel meets the gel chamber has a curved corner, with a radius of 0.05mm.
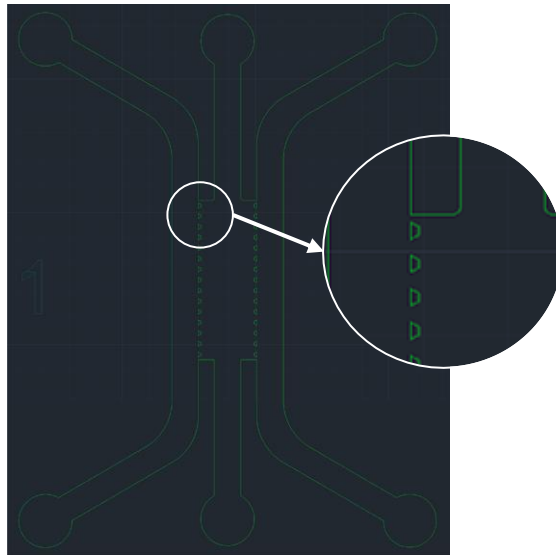
AutoCAD Design GC1. Trapezoidal pillars are at a length of 100µm on the longest side and are spaced out 100µm. The radius of the curve connecting the gel channel to the gel chamber is 0.05mm.

Design GC2 has trapezoidal pillars, with a length of 100µm, that are spaced out by 100µm. The point where the gel inlet channel meets the gel chamber has a curved corner, with a radius of 0.3mm.
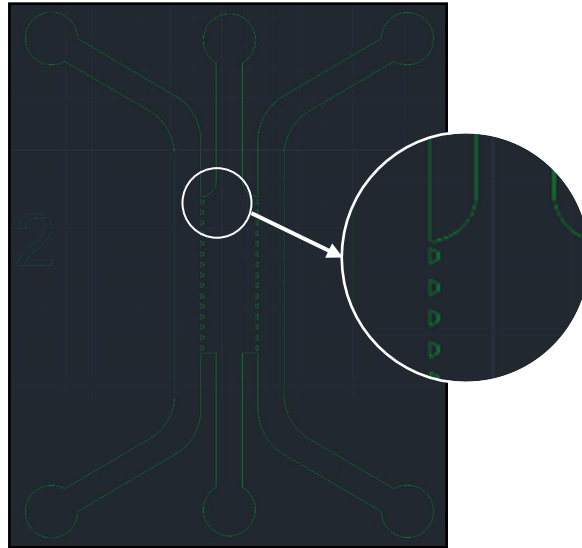
AutoCAD Design GC2. Trapezoidal pillars are at a length of 100µm on the longest side and are spaced out 100µm. The radius of the curve connecting the gel channel to the gel chamber is 0.3mm.

Design GC3 has trapezoidal pillars, with a length of 100µm, that are spaced out by 125µm. The point where the gel inlet channel meets the gel chamber has a curved corner, with a radius of 0.05mm.

AutoCAD Design GC3. Trapezoidal pillars are at a length of 100µm on the longest side and are spaced out 125µm. The radius of the curve connecting the gel channel to the gel chamber is 0.05mm.

Design GC4 has trapezoidal pillars, with a length of 100µm, that are spaced out 150µm. The point where the gel inlet channel meets the gel chamber has a curved corner, with a radius of 0.05mm.

AutoCAD Design GC4. Trapezoidal pillars are at a length of 100µm on the longest side and are spaced out 150µm. The radius of the curve connecting the gel channel to the gel chamber is 0.05mm.

Design GC5 has trapezoidal pillars, with a length of 100µm, that are spaced out 100µm. The point where the gel inlet channel meets the gel chamber has a curved corner, with a radius of 0.05mm. Inside the chamber, are square pillars that are 100µm in height and rows are spaced out 100µm. There are four columns of square pillars spaced out approximately 136µm between columns. This will allow for testing with more device surface area to hold the gels in place.
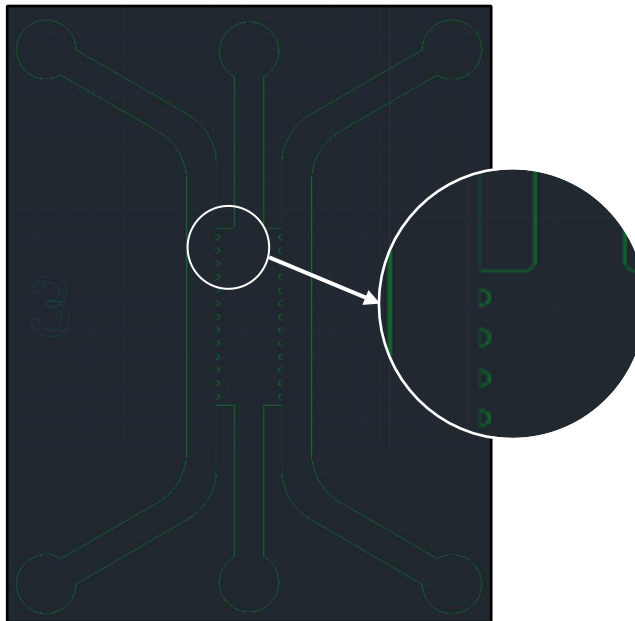

AutoCAD Design GC5. Trapezoidal pillars are at a length of 100µm on the longest side and are spaced out 100µm. The radius of the curve connecting the gel channel to the gel chamber is 0.05mm. There are interior square pillars that are 100µm in height. The space between the square pillar rows is 100µm and the space between the square pillar columns is approximately 136µm to fit four columns.

Design GC6 has trapezoidal pillars, with a length of 100µm, that are spaced out 100µm. The point where the gel inlet channel meets the gel chamber has a curved corner, with a radius of 0.3mm. Inside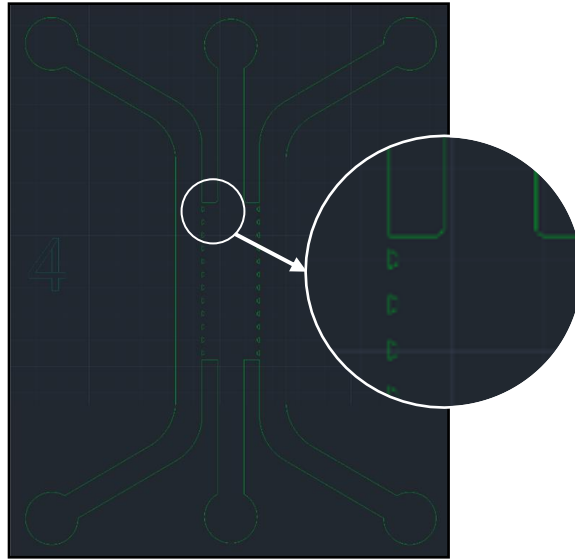 the chamb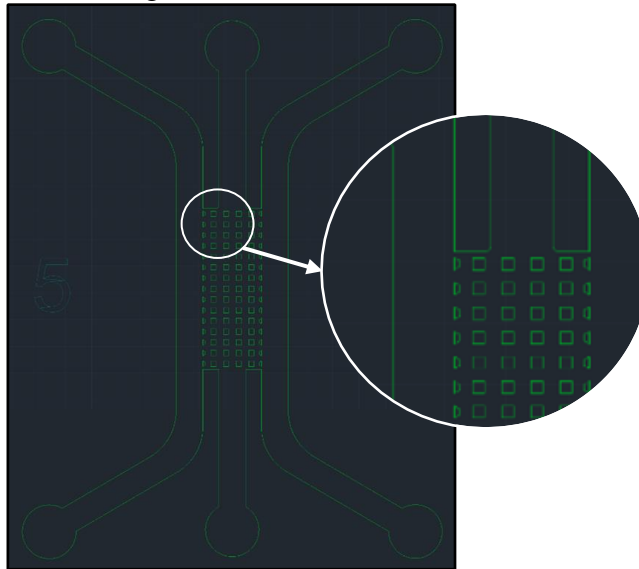er, are square pillars that are 100µm in height and rows are spaced out by 100µm. There are four columns of square pillars spaced out approximately 136µm between columns.

AutoCAD Design GC6. Trapezoidal pillars are at a length of 100µm on the longest side and are spaced out 100µm. The radius of the curve connecting the gel channel to the gel chamber is 0.3mm. There are interior square pillars that are 100µm in height. The space between the square pillar rows is 100µm and the space between the square pillar columns is approximately 136µm to fit four columns.

Design GC7 has trapezoidal pillars, with a length of 100µm, that are spaced out 125µm. The point where the gel inlet channel meets the gel chamber has a curved corner, with a radius of 0.05mm. Inside the cha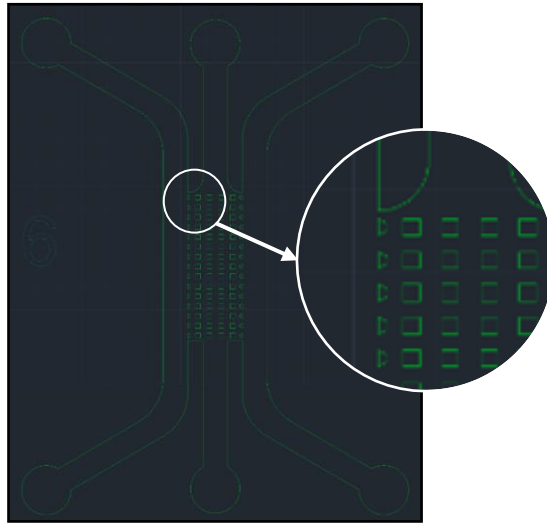mber, are square pillars that are 100µm in height and rows are spaced out 125µm. There are four columns of square pillars spaced out approximately 136µm between columns.

AutoCAD Design GC7. Trapezoidal pillars are at a length of 100µm on the longest side and are spaced out 125µm. The radius of the curve connecting the gel channel to the gel chamber is 0.05mm. There are interior square pillars that are 100µm in height. The space between the square pillar rows is 125µm and the space between the square pillar columns is approximately 136µm to fit four columns.

Design GC8 has trapezoidal pillars, with a length of 100µm, that are spaced out 150µm. The point where the gel inlet channel meets the gel chamber has a curved corner, with a radius of 0.05mm. Inside the chamber, are square pillars that are 100µm in height and rows are spaced out 150µm. There are four columns of square pillars spaced out approximately 136µm between columns.
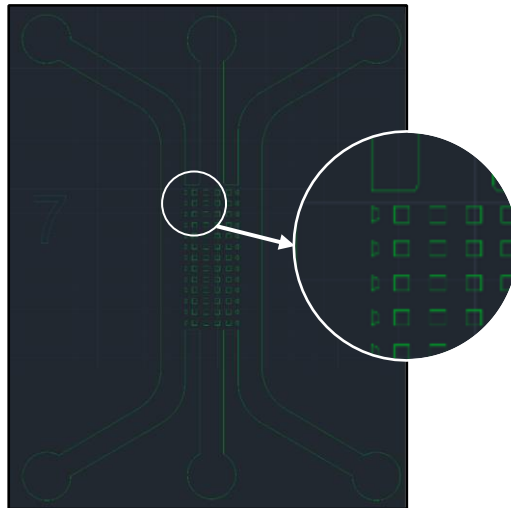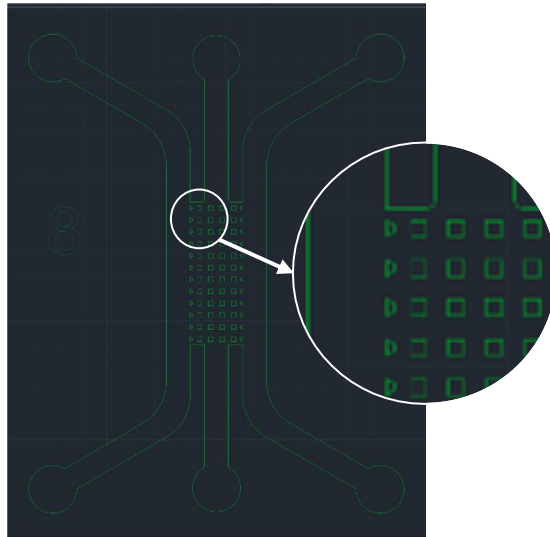

AutoCAD Design GC8. Trapezoidal pillars are at a length of 100µm on the longest side and are spaced out 150µm. The radius of the curve connecting the gel channel to the gel chamber is 0.05mm. There are interior square pillars that are 100µm in height. The space between the square pillar rows is 150µm and the space between the square pillar columns is approximately 136µm to fit four columns.

Design GC9 has trapezoidal pillars, with a length of 100µm, that are spaced out 125µm. The point where the gel inlet channel meets the gel chamber has a curved corner, with a radius of 0.05mm. Inside the chamber, are square pillars that are 100µm in height and rows are spaced out 125µm. There are three columns of square pillars spaced out approximately 230µm between columns.
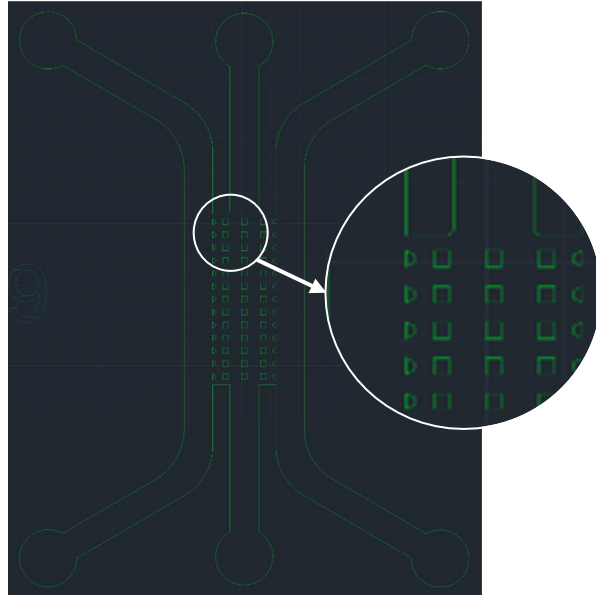
AutoCAD Design GC9. Trapezoidal pillars are at a length of 100µm on the longest side and are spaced out 125µm. The radius of the curve connecting the gel channel to the gel chamber is 0.05mm. There are interior square pillars that are 100µm in height. The space between the square pillar rows is 125µm and the space between the square pillar columns is approximately 230µm to fit three columns.

Appendix E: Procedure for PDMS Casting and Plasma Treatment

PDMS Casting

Materials:

- Oven (to work at 65 degrees Celsius)
- PDMS silicone elastomer base Sylgard
- PDMS curing agent Sylgard
- Mass scale
- Weigh boat
- Metal stirring scoop
- Vacuum chamber
- Pre-made silicon wafer mold in petri dish
- Pre-made tape molds
- 100mL diameter petri dish

Methods:

*procedure based on Reidinger, Z. (n.d.). (rep.). *BME 3811 PDMS and Hydrophobicity*. Worcester, MA.

1. Measure approximately 60grams of PDMS silicone elastomer base onto a weigh boat to make a 10:1 ratio.
2. Add 6.0 grams of PDMS curing agent to base.
3. Mix the elastomer base and curing agent vigorously with the metal stirring scoop.
4. Place weigh boat in a vacuum chamber for approximately 30 minutes, until all air bubbles are released.
5. Pour contents of uncured PDMS into petri dish containing the silicon wafer
6. Place petri dishes in an oven set at 65 degrees Celsius overnight (our team is leaving it over a weekend ~72 hours), until PDMS is solidified.
7. Store PDMS in a dust free container for further use.

Plasma Treatment

Materials:

- PDMS molds from Making PDMS Tape Molds
- Scalpel
- Razor blade
- 1mL biopsy punches
- Tweezers
- Plasma cleaner
- Kim tech wipes
- 70% ethanol
- Pressurized air
- Scotch tape
- Glass coverslips

Methods:

1. Using a scalpel, cut on the wafer and glass slide to cut out the PDMS cast. Remove the casts.
2. Using a razor blade, cut out each of the designs.
3. Using the biopsy punch, make holes for the inlet and outlets on the designs, with the design facing downwards.
4. Use tweezers to ensure the inlets and outlet PDMS are removed.
5. For each PDMS piece, spray both sides with 70% ethanol, then wipe with a Kim tech wipe, then spray again with 70% ethanol, then spray with pressurized air.
6. Immediately cover the PDMS piece in Scotch tape to prevent dust build up.
7. Repeat step 5, for each of the glass cover slips.
8. Turn on the plasma cleaner switch on the left.
9. Remove the tape off of one side of 2 cover slips and off the design side of two of the PDMS pieces.
10. Place the 2 coverslips and 2 designs into the plasma cleaner, tape side down.
11. Holding the cover of the vacuum in place, turn the plasma cleaner switch on the right to ON. After about 60 seconds, the lid should be vacuum sealed in place.
12. Turn the plasma cleaner knob to high and set a timer for 60 seconds.
13. After 60 seconds, turn the plasma cleaner knob to OFF and slowly release the plasma cleaner lid to let air in.
14. Once the vacuum refills with air, remove the cover and turn the switch on the right to OFF.
15. Take out the plasma treated pieces very carefully using tweezers. (Make sure not to touch the plasma treated sides of the pieces.)
16. Carefully turn the coverslip upside down and place it onto the PDMS piece designs to adhere.

Appendix F: Procedure for Making Fibrin Gels in Transwell Plates

Materials:
- Fibrinogen
  - Want 6.6mg/mL in DPBS, stock is 16.7mg/mL
  - Stored in -20, keep on ice
- Thrombin
  - Want 2 units/mL in DPBS, stock is 25units/mL
  - Stored in -80, keep on ice, most temp sensitive
- Ascorbic Acid
  - Want 250 ug/mL in media
  - Stored at -20, keep at RT, can thaw at 37
- Insulin
  - 5ug/mL in media
  - Stored at 4, keep on ice
- TGF-beta
  - 10ng/mL in media
  - Stored at -20, keep on ice
- Aprotinin
  - 500 KUI/mL in media
  - Stored at -20, keep at RT, can thaw at 37
- DPBS(-)
- DMEM w everything added to make complete media
- Ice Bucket

Methods:

*procedure based on personal notes from Rozanne Mungai and referencing a procedure from Ying's Lei

-Everything is done in the biosafety cabinet using aseptic technique

1. Passage and count cells. Resuspend in media at 4x10^6 cells/mL.
2. Add fibrinogen to empty wells (no transwell).
   a. H1=25uL
   b. H2=75uL
3. Begin thawing thrombin.
4. In a separate tube, mix 1:1 thrombin at 2 units/mL in DBPS and cell suspension.
   a. We used 0.75mL of each.
5. One by one, add thrombin/cell mixture to the fibrinogen in an empty well and pipette to mix. Very quickly transfer the whole mixture to the transwell plate. Gelling will occur in ~30s. Extra fibrin and thrombin was added to each well. Only transfer the amount needed.
   a. Add 25uL T/C for H1 (total 50uL)
      i. Place 33uL in transwell
   b. 75uL T/C for H2 (total 150uL)
      i. Place 133uL
6. Place in a 37°C incubator to gelate for 1 hour.

7. Add media to wells.
    a. 600uL in bottom of well plate, 100uL on top of the gel

Plate was setup to have two controls

- Control 1: No cells/Acellular
- Control 2: Gels that do not undergo decellularization

Plate was set up to run trials of two different gel heights/thicknesses

- Height 1: 1mm (~33.18 uL)
- Height 2: 4mm (~132.73 uL)

Appendix G: Procedure for Decellularizing and Fixing Gels

Decellularization

    Materials:
- 1x PBS
- 1% SDS in DI water
- 1% Triton X-100 in DI water
- Fibrin gels prepared from Making Fibrin Gels in Transwell Plates

    Methods:

        *procedure based on Mungai, R. & Lei, Y. (n.d.) *Making cell-seeded fibrin hydrogels.* Retrieved November 29, 2021. and Tranquillo Lab Syedain et. al. Biomaterials 2019

1. Aspirate solution from transwell plates.
2. Fill transwells with 1x PBS to rinse the gels and place on a rocker plate for 5 minutes at speed of 4. Repeat three times.
3. Treat with 1% SDS, allow to sit on gels for 6 hours at room temp.
   a. If needed, replace after 1, 2, 4 hours (keep pressures constant)
   b. P1= 5mm SDS
      i. 165.92 microliter /well
      For 12 wells: 1991.04 uL
   c. P2= 8mm SDS
      i. 265.46 microliter /well
      For 12 wells: 3185.52 uL
4. Wash with 1% Triton X-100 3 times for 10 mins each time at room temp.
   a. P1= 2.5mm Triton
      i. 82.96 microliter /well
      For 12 wells: 995.52 microliter
   b. P2= 4mm Triton
      i. 132.73 microliter /well
      For 12 wells: 1592.76 uL
5. Rinse three times with 1x PBS
   a. Fill well with PBS, place on shaker plate for 5 minutes, aspirate and repeat
6. Add enough 4% PFA to fill the top portion of the transwell without it overflowing while in the chemical hood
   a. Allow to sit for 15 minutes
   b. Get a waste container prepared
   c. Aspirate out the PFA from the wells
7. Rinse three times with 1x PBS
   a. Fill well with PBS, place on shaker plate for 5 minutes, aspirate and repeat
8. Store in 1x PBS at 4 deg C. Wrap plates in parafilm to prevent cell media evaporation

Fixing Gels

    Materials:

- 24 well plate
- 4% PFA
- 1x PBS
- Parafilm

    Methods:

1. Fix gels that are not being decellularized and gels that have already been decellularized.
   a. Remove the desired transwells and add to a new well plate.
   b. Add enough 4% PFA to fill the top portion of the transwell without it overflowing while in the chemical hood.
   c. Allow to sit for 15 minutes.
   d. Get a waste container prepared.
   e. Aspirate out the PFA from the wells, place it into a waste container.
   f. Rinse with PBS three times. This can be done outside of the fume hood.
   g. Add PBS to the transwells to fill.
   h. Wrap the well plate in parafilm and store in the refrigerator.

Appendix H: Procedure for Hoechst Staining and Imaging Decellularized Gels

Materials:
- Our transwell plates with gels
- DI water
- 1% triton x-100
- 1xPBS
- Shaker plate
- Hoechst dye
- Aluminum foil
- Tweezers
- 96 well plate
- BZ Keyence microscope

Methods:
- Perform in tubes on shaker plate with 1 mL volume each
- Cells were recently rinsed in 1xPBS so the procedure is beginning with permeabilizing.

Staining:
1. Make 8mL 0.25% Triton X-100 by adding 2mL of 1% Triton x-100 and 6mL distilled water.
2. Permeabilize in 0.25% Triton x-100 in 1x PBS for 10 minutes.
3. Rinse with 1xPBS for 10 minutes on a shaker plate. Do this step three times.
4. Add Hoechst dye at 1:1000 with PBS for 10 minutes. 8mL of solution was made. Hoechst should only be opened in the dark and the mixing conical should be wrapped in aluminum foil.
5. Wash in 1xPBS for 5 minutes.
6. Use tweezers and/or a wide transfer pipet to *gently* move the samples to a 96-well plate.
   a. The plate should have a smooth flat bottom for imaging and a lid.

Microscope Tips
- Navigation button can be used to scan the whole well to find when the gel is
- Full focus button can be used to find the plane which is best focused for the image

Appendix I: Procedure & Results for H & E Staining and Imaging of Samples

Materials:
- Dryer
- Xylene
- 100% ETOH
- 95% ETOH
- 70% ETOH
- Harris Hematoxylin
- Coffee filters
- Acid alcohol (10mL concentrated HCl in 1000mL 70% ETOH)
- Ammonia water (2-3mL ammonium hydroxide in 500mL distilled water)
- Eosin Y (1 gm Eosin Y (water soluble) in 100mL distilled water, working eosin- 100mL stock Eosin, 10mL stock Phloxine, 780 mL 95% ETOH, adjust pH to 4.5 with glacial acetic acid)
- Distilled water
- Staining tray with buckets
- Gel samples from Wax Embedding and Sectioning Lab
- Glass coverslips
- Cytoseal glue
- Microscope

Methods:
*procedure based on personal notes from Jyotsna Patel
1. Place samples in the cell dryer for 20 minutes.
2. Setup staining tray with all required solutions.
3. Begin dipping the tissues in each of the solutions for the required amount of time as follows:
    a. Xylene 1 for 3 minutes
    b. Xylene 2 for 2 minutes
    c. Xylene 3 for 1 minute
    d. 100% ETOH for 3 minutes
    e. 100% ETOH for 3 minutes
    f. 95% ETOH for 1 minute
    g. 70% ETOH for 1 minute
    h. Rinse in running water for 5 minutes
    i. Harris Hematoxylin (filter in coffee filter before and after use) for 5 minutes
        *after this step is completed, pour solution back in bottle, then put the bucket in the sink and add half bleach, half water to clean it
    j. Rinse in running water until clear

     k. Differentiate in acid alcohol for 2 to 3 quick dips
     l. Rinse in running water for 30 seconds
     m. Blue sections in ammonia water for 1 minute
     n. Rinse in warm running water for 5 minutes
     o. 95% ETOH for 30 seconds
     p. Counterstain in Eosin Y for 1 minute
     q. 95% ETOH for 30 seconds
     r. 95% ETOH for 30 seconds
     s. 100% ETOH for 1 minute
     t. 100% ETOH for 1 minute
     u. 100% ETOH for 1 minute
     v. Xylene 4 for 1 minute
     w. Xylene 5 for 1 minute
     x. Xylene 6 for 1 minute

4. Once completed, leave the samples in solution and not out in the open air to prevent contamination.
5. Obtain glass coverslips. Put one drop of glue on the slide with a sample and place the coverslip on the slide at 45 degree angle.
6. Image samples under microscope.

Appendix J: Procedure & Results for Trichrome Staining and Imaging of Samples

Part 1:

Materials:
- Dryer
- Xylene
- 100% ETOH
- 95% ETOH
- 70% ETOH
- Distilled water
- Staining tray with buckets
- Gel samples from Wax Embedding and Sectioning Lab
- Bouin's fixative

Methods:
1. Place samples in the cell dryer for 30 minutes.
2. Setup staining tray with all required solutions.
3. Begin dipping the tissues in each of the solutions for the required amount of time as follows:
    1. Xylene 1 for 3 minutes
    2. Xylene 2 for 2 minutes
    3. Xylene 3 for 1 minute
    4. 100% ETOH for 3 minutes
    5. 100% ETOH for 3 minutes
    6. 95% ETOH for 1 minute
    7. 70% ETOH for 1 minute
4. Once completed, the samples can sit in distilled water.
5. Place a sample holder on a paper towel to remove excess solution.
6. Move samples into a bucket of Bouin's fixative overnight.

Part 2:

Materials:
- Gel samples in Bouin's fixative from Trichrome Staining Gels Samples Part 1
- 2 mL Alcoholic Hematoxylin
- 2 mL 29% Ferric Chloride
- Gomoris 1 Step Solution
- 0.5% Acetic Acid
- Pipette
- Conical Tube

Methods:

1. Rinse samples in running water until the color from the Bouin's fixative is removed from the slides
2. Combine 2 mL Alcoholic Hematoxylin with 2 mL 29% ferric chloride in a conical tube
3. Pipette out enough of the solution to cover each slide.
4. Let the slides sit for 10 minutes
5. Rinse slides under running water for 10 minutes
6. Apply the trichrome stain by submerging the slides in the gomori's one step stain for 15 to 20 minutes
7. Wash in running water for 2 minutes
8. Wash the sample in 0.5% acetic acid for 2 minutes
9. Dehydrate and clear in xylene by following steps o-w of the H&E protocol
10. Apply cover slip
11. Image

Appendix K: Hoechst and Phalloidin Staining Procedure

Materials:
- AIM Chips with fixed gels
- DI water
- 1% Triton x-100
- 1xPBS
- Shaker plate
- Hoechst 33342
- Alexa Fluor Phalloidin 488
- Aluminum foil
- BZ Keyence microscope

Methods:

Making 0.25% Triton X-100
1. We have 27 devices total, which will each need 240 uL each (.24 mL) = 6.48 mL. 8mL will be made.
2. Combine 2mL of 1% Triton x-100 and 6mL distilled water to make 8mL Triton X-100.

Making Phalloidin Dilution (1:100)
1. Add 20mg BSA to 2mL on PBS
    ○ Allow the solution to dissolve, this will take a few minutes
2. Add 20uL Phalloidin 488

Making Hoechst Dilution (1:1000)
1. Add 2uL Hoechst to 2mL PBS

Permeabilizing
1. Remove PBS from all 4 ports carefully
2. Add 70 μl of 0.25 % Triton X-100 into one of the ports and then add 50 μl into the opposite connected port. Repeat for the other channel.
3. Incubate for 10 min at RT
4. Wash with PBS once (Add 70 μl of 1X PBS into one port and then add

50 μl into the opposite connected port of a media channel) for 5 minutes
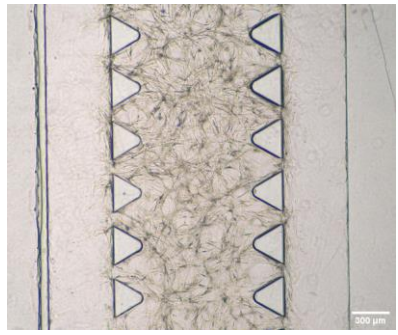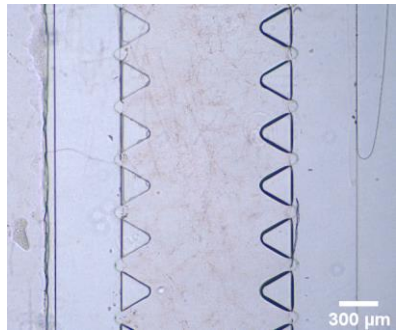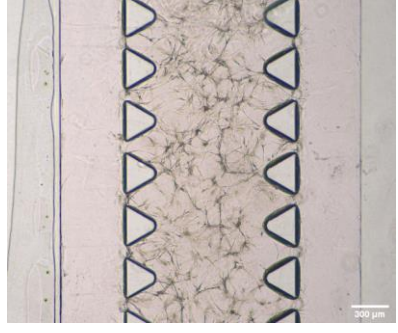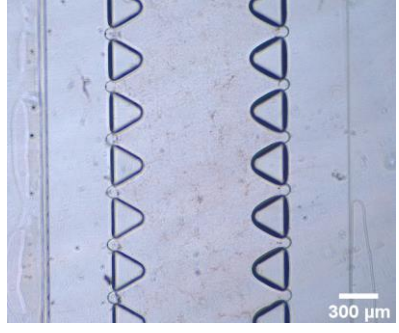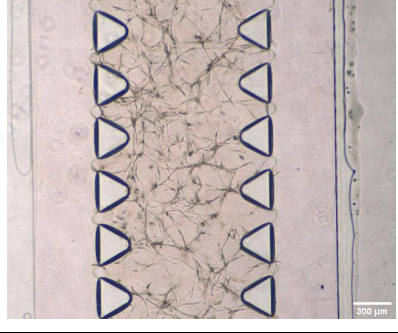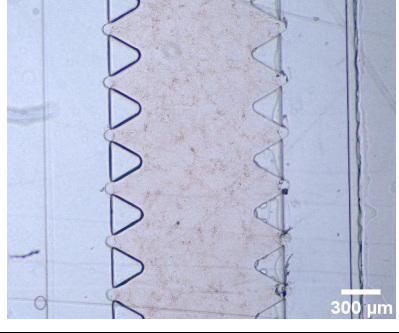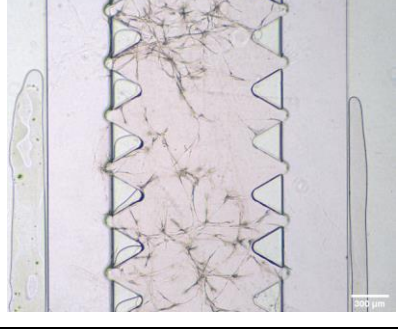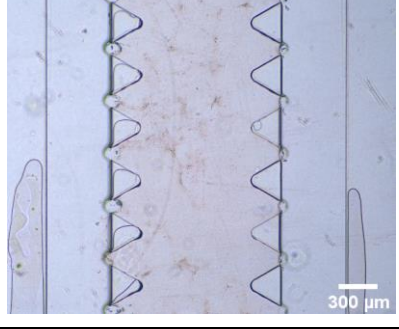
Staining
1. Aspirate out PBS from devices
2. Add 70uL Phalloidin solution to inlets and 50uL Phalloidin to outlets.
3. Incubate for 30 min at room temp. Cover devices with aluminum foil.
4. Aspirate out Phalloidin solution.
5. Add 70uL Hoechst to inlets and 50uL Hoechst to outlets
6. Let sit at room temp for 5-10 minutes

7. Rinse channels with 1x PBS 5 times with a 5 min incubation between each by adding 70uL into inlets, and 50uL into outlets

8. Store devices in parafilm/aluminum foil and keep at 4 degrees Celsius until imaged

Image cells with BZ Keyence microscope. This can be done with the gels still in the AIM Biotech chip.

Appendix L: Before and After Decellularization Images

       Images taken at 4x on the Nikon TS2-S-SM do not indicate any differences in success of decellularization in the different concentration and media groups tested.

Concentration	Before Decellularization	After Decellularization
Media A + Composition A		
Media B + Composition B		
Media B + Composition B1		
Media B + Composition B1		

| Acellular Media B + Composition A | | |
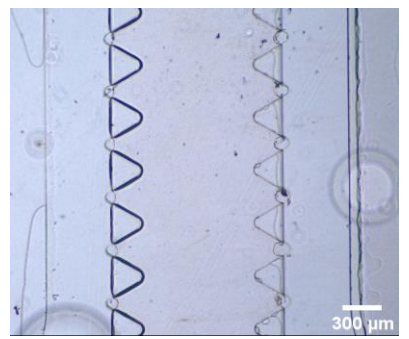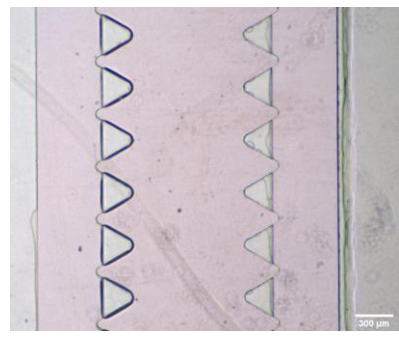
Appendix M: Arduino Code for Solenoid Pinch Valves

```
int x=1000;
int b1=4;
int g1=3;
int b2=5;
int g2=6;
void setup() {
  // put your setup code here, to run once:
pinMode(b1, OUTPUT);
pinMode(b2, OUTPUT);
pinMode(g1, OUTPUT);
pinMode(g2, OUTPUT);
}

void loop() {
  // put your main code here, to run repeatedly:
//activate solenoids 1 and 4
digitalWrite(b1, HIGH);
digitalWrite(b2, HIGH);
//deactivate 2&3
digitalWrite(g1, LOW);
digitalWrite(g2, LOW);
//hold for x secs
delay(x);             //2 steps ahead
//deactivate 1&4
digitalWrite(b1, LOW);
digitalWrite(b2, LOW);
//activate 2&3
digitalWrite(g1, HIGH);
digitalWrite(g2, HIGH);
//hold for x seconds
delay(x/2);           //1 step back
}
```

The script used to run the solenoid pinch valves. The integer 'x' represents the time of the "two steps forward" phase, where fresh media is cycled in. The "one step back" phase, where the oscillation occurs is represented by 'x/2'.

References

Ahmed, M. (2017, August 21). Heart Valve Surgery - Mechanical Vs. Bioprosthetic – Which Is Better? • MyHeart. *MyHeart*. https://new.myheart.net/articles/heart-valve-surgery-mechanical-vs-bioprosthetic-which-is-better/

Al-Halhouli, A., El Far, B., Albagdady, A., & Al-Faqheri, W. (2020). Development of Active Centrifugal Pump for Microfluidic CD Platforms. *Micromachines*, *11*(2), 140. https://doi.org/10.3390/mi11020140

Alizadehgiashi, M. (2018). *Shear-Induced Alignment of Anisotropic Nanoparticles in a Single-Droplet Oscillatory Microfluidic Platform | Langmuir*. https://pubs.acs.org/doi/full/10.1021/acs.langmuir.7b03648

Arjunon, S., Rathan, S., Jo, H., & Yoganathan, A. P. (2013). Aortic Valve: Mechanical Environment and Mechanobiology. *Annals of Biomedical Engineering*, *41*(7), 1331–1346. https://doi.org/10.1007/s10439-013-0785-7

Avram, R., Tison, G. H., Aschbacher, K., Kuhar, P., Vittinghoff, E., Butzner, M., Runge, R., Wu, N., Pletcher, M. J., Marcus, G. M., & Olgin, J. (2019). Real-world heart rate norms in the Health eHeart study. *NPJ Digital Medicine*, *2*, 58. https://doi.org/10.1038/s41746-019-0134-9

Badylak, S. F., Freytes, D. O., & Gilbert, T. W. (2009). Extracellular matrix as a biological scaffold material: Structure and function. *Acta Biomaterialia*, *5*(1), 1–13. https://doi.org/10.1016/j.actbio.2008.09.013

Baguneid, M., Murray, D., Salacinski, H. J., Fuller, B., Hamilton, G., Walker, M., & Seifalian, A. M. (2004). Shear-stress preconditioning and tissue-engineering-based paradigms for generating arterial substitutes. *Biotechnology and Applied Biochemistry*, *39*(2), 151–157. https://doi.org/10.1042/BA20030148

Barker, S., Rhoads, E., Lindquist, P., Vreugdenhil, M., & Müllner, P. (2016). Magnetic Shape Memory Micropump for Submicroliter Intracranial Drug Delivery in Rats. *Journal of Medical Devices*, *10*(4). https://doi.org/10.1115/1.4034576

Bengtsson, K., Christoffersson, J., Mandenius, C.-F., & Robinson, N. D. (2018). A clip-on electroosmotic pump for oscillating flow in microfluidic cell culture devices. *Microfluidics and Nanofluidics*, *22*(3), 27. https://doi.org/10.1007/s10404-018-2046-4

Behrens, M. R., Fuller, H. C., Swist, E. R., Wu, J., Islam, M. M., Long, Z., Ruder, W. C., & Steward, R. (2020). Open-source, 3D-printed Peristaltic Pumps for Small Volume Point-of-Care Liquid Handling. *Scientific Reports*, *10*(1), 1543. https://doi.org/10.1038/s41598-020-58246-

Bezenah, J. R., Rioja, A. Y., Juliar, B., Friend, N., & Putnam, A. J. (2019). Assessing the ability of human endothelial cells derived from induced-pluripotent stem cells to form functional microvasculature in vivo. *Biotechnology and Bioengineering*, *116*(2), 415–426. https://doi.org/10.1002/bit.26860

Bogdanov, A. A., Lin, C. P., & Kang, H.-W. (2007). Optical Imaging of the Adoptive Transfer of Human Endothelial Cells in Mice Using Anti-Human CD31 Monoclonal Antibody. *Pharmaceutical Research*, *24*(6), 1186–1192. https://doi.org/10.1007/s11095-006-9219-7

Brecs, I., Sekretarjovs, J., Stradins, P., Skuja, S., Groma, V., Pavars, J., & Lacis, R. (2018). Activation of valvular interstitial cells and remodeling of extracellular matrix in calcific aortic valve stenosis. *Atherosclerosis*, *275*, e131. https://doi.org/10.1016/j.atherosclerosis.2018.06.380

Brennan, J. M., Edwards, F. H., Zhao, Y., O'Brien, S., Booth, M. E., Dokholyan, R. S., Douglas, P. S., & Peterson, E. D. (2013). Long-Term Safety and Effectiveness of Mechanical Versus Biologic Aortic Valve Prostheses in Older Patients. *Circulation*, *127*(16), 1647–1655. https://doi.org/10.1161/CIRCULATIONAHA.113.002003

Bucevičius, J., Lukinavičius, G., & Gerasimaitė, R. (2018). The Use of Hoechst Dyes for DNA Staining and Beyond. *Chemosensors*, *6*(2), 18. https://doi.org/10.3390/chemosensors6020018

Butcher, J. T., Mahler, G. J., & Hockaday, L. A. (2011). Aortic valve disease and treatment: The need for naturally engineered solutions. *Advanced Drug Delivery Reviews*, *63*(4), 242–268. https://doi.org/10.1016/j.addr.2011.01.008

Byun, C. K., Abi-Samra, K., Cho, Y.-K., & Takayama, S. (2014). Pumps for microfluidic cell culture. *ELECTROPHORESIS*, *35*(2–3), 245–257. https://doi.org/10.1002/elps.201300205

Campbell, S. B., Wu, Q., Yazbeck, J., (2020). *The Fabrication of Microfluidics, 3D Cell Culture, Organ-on-a-Chip. (2020, December 7). 3DHeals. https://3dheals.com/fabrication-of-microfluidics-3d-cell-culture-organ-on-a-chip*

Casale, J., & Crane, J. S. (2021). Biochemistry, Glycosaminoglycans. In *StatPearls*. StatPearls Publishing. http://www.ncbi.nlm.nih.gov/books/NBK544295/

Casquillas, G. (2021, June 16). *Pressure-Driven Flow Control*. Elveflow. Retrieved November 17, 2021, from https://www.elveflow.com/microfluidic-applications/setup-microfluidic-flow-control/pressure-driven-flow-control/.

Chan, J. K. C. (2014). The Wonderful Colors of the Hematoxylin–Eosin Stain in Diagnostic Surgical Pathology. *International Journal of Surgical Pathology*, *22*(1), 12–32. https://doi.org/10.1177/1066896913517939

Chen, C., Hirdes, D., & Folch, A. (2003). Gray-scale photolithography using microfluidic photomasks. *Proceedings of the National Academy of Sciences*, *100*(4), 1499–1504. https://doi.org/10.1073/pnas.0435755100

Chen, H.-M., Lai, Z.-Q., Liao, H.-J., Xie, J.-H., Xian, Y.-F., Chen, Y.-L., Ip, S.-P., Lin, Z.-X., & Su, Z.-R. (2018). Synergistic antitumor effect of brusatol combined with cisplatin on colorectal cancer cells. *International Journal of Molecular Medicine*, *41*(3), 1447–1454. https://doi.org/10.3892/ijmm.2018.3372

Cheung, D. Y., Duan, B., & Butcher, J. T. (2015). Current Progress in Tissue Engineering of

Heart Valves: Multiscale Problems, Multiscale Solutions. *Expert Opinion on Biological Therapy*, *15*(8), 1155–1172. https://doi.org/10.1517/14712598.2015.1051527

Chung, S., Sudo, R., Mack, P. J., Wan, C.-R., Vickerman, V., & Kamm, R. D. (2009). Cell migration into scaffolds under co-culture conditions in a microfluidic platform. *Lab on a Chip*, *9*(2), 269–275. https://doi.org/10.1039/B807585A

Coyan, G. N., D'Amore, A., Matsumura, Y., Pedersen, D. D., Luketich, S. K., Shanov, V., Katz, W. E., David, T. E., Wagner, W. R., & Badhwar, V. (2019). In vivo functional assessment of a novel degradable metal and elastomeric scaffold-based tissue engineered heart valve. *The Journal of Thoracic and Cardiovascular Surgery*, *157*(5), 1809–1816. https://doi.org/10.1016/j.jtcvs.2018.09.128

Cukierman, E., Pankov, R., Stevens, D. R., & Yamada, K. M. (2001). Taking cell-matrix adhesions to the third dimension. *Science (New York, N.Y.)*, *294*(5547), 1708–1712. https://doi.org/10.1126/science.1064829

De Jesús, A. M., & Sander, E. A. (2014). Observing and Quantifying Fibroblast-mediated Fibrin Gel Compaction. *Journal of Visualized Experiments : JoVE*, *83*, 50918. https://doi.org/10.3791/50918

Ellis, M. E. (2014, July 18). *Symptoms and Complications of Blood Clots*. Healthline. https://www.healthline.com/health/symptoms-and-complications-blood-clots

Encyclopædia Britannica. (2021). *Histology*. Britannica School. Retrieved December 11, 2021, from https://school-eb-com.ezpv7-web-p-u01.wpi.edu/levels/high/article/histology/40592

Farahat, W., Wood L., Zervantonakis I., Schor A., Ong S., Neal D., Kamm R., Asada H. (2012). Ensemble analysis of angiogenic growth in three-dimensional microfluidic cell cultures. *PLOS ONE,* https://pubmed.ncbi.nlm.nih.gov/22662145/

Feldman, A. T., & Wolfe, D. (2014). Tissue Processing and Hematoxylin and Eosin Staining. In C. E. Day (Ed.), *Histopathology: Methods and Protocols* (pp. 31–43). Springer. https://doi.org/10.1007/978-1-4939-1050-2_3

Fendinger, N. J. (2005). Polydimethylsiloxane (PDMS): Environmental Fate and Effects. In *Organosilicon Chemistry Set* (pp. 626–638). John Wiley & Sons, Ltd. https://doi.org/10.1002/9783527620777.ch103c

Fernández-Pérez, J., & Ahearne, M. (2019). The impact of decellularization methods on extracellular matrix derived hydrogels. *Scientific Reports*, *9*(1), 14933. https://doi.org/10.1038/s41598-019-49575-2

Flanagan, T. C., Sachweh, J. S., Frese, J., Schnöring, H., Gronloh, N., Koch, S., Tolba, R. H., Schmitz-Rode, T., & Jockenhoevel, S. (2009). In vivo remodeling and structural characterization of fibrin-based tissue-engineered heart valves in the adult sheep model. *Tissue Engineering. Part A*, *15*(10), 2965–2976. https://doi.org/10.1089/ten.TEA.2009.0018

Fernandes, I. R., Russo, F. B., Pignatari, G. C., Evangelinellis, M. M., Tavolari, S., Muotri, A. R., & Beltrão-Braga, P. C. B. (2016). Fibroblast sources: Where can we get them? *Cytotechnology*, *68*(2), 223–228. https://doi.org/10.1007/s10616-014-9771-7

Gilpin, A., & Yang, Y. (2017). Decellularization Strategies for Regenerative Medicine: From Processing Techniques to Applications. *BioMed Research International*, *2017*, 9831534. https://doi.org/10.1155/2017/9831534

Goding, J. W. (1996). 12—Immunofluorescence. In J. W. Goding (Ed.), *Monoclonal Antibodies (Third Edition)* (pp. 352–399). Academic Press. https://doi.org/10.1016/B978-012287023-1/50060-2

Gottlieb, D., Kunal, T., Emani, S., Aikawa, E., Brown, D. W., Powell, A. J., Nedder, A., Engelmayr, G. C., Melero-Martin, J. M., Sacks, M. S., & Mayer, J. E. (2010). In vivo monitoring of function of autologous engineered pulmonary valve. *The Journal of Thoracic and Cardiovascular Surgery*, *139*(3), 723–731. https://doi.org/10.1016/j.jtcvs.2009.11.006

Grizzle, W. (2009). Special symposium: Fixation and tissue processing models. *Biotechnic & Histochemistry*, *84*(5), 185–193. https://doi.org/10.3109/10520290903039052

Harris, C., Croce, B., & Cao, C. (2015). Tissue and mechanical heart valves. *Annals of Cardiothoracic Surgery*, *4*(4), 399. https://doi.org/10.3978/j.issn.2225-319X.2015.07.01

Harris, E. S., & Nelson, W. J. (2010). VE-Cadherin: At the Front, Center, and Sides of Endothelial Cell Organization and Function. *Current Opinion in Cell Biology*, *22*(5), 651–658. https://doi.org/10.1016/j.ceb.2010.07.006

Hasan, A., Ragaert, K., Swieszkowski, W., Selimović, Š., Paul, A., Camci-Unal, G., Mofrad, M. R. K., & Khademhosseini, A. (2014). Biomechanical properties of native and tissue engineered heart valve constructs. *Journal of Biomechanics*, *47*(9), 1949–1963. https://doi.org/10.1016/j.jbiomech.2013.09.023

Hasan, A., Soliman, S., El Hajj, F., Tseng, Y.-T., Yalcin, H. C., & Marei, H. E. (2018). Fabrication and In Vitro Characterization of a Tissue Engineered PCL-PLLA Heart Valve. *Scientific Reports*, *8*(1), 8187. https://doi.org/10.1038/s41598-018-26452-y

Hata, A., & Chen, Y.-G. (2016). TGF-β Signaling from Receptors to Smads. *Cold Spring Harbor Perspectives in Biology*, *8*(9), a022061. https://doi.org/10.1101/cshperspect.a022061

Heart Valve Disease. Heart Foundation NZ. (2021). Retrieved October 7, 2021, from https://www.heartfoundation.org.nz/your-heart/heart-conditions/heart-valve-disease.

Heinbockel, T., & Shields, V. D. C. (2018). Introductory Chapter: Histological Microtechniques. In *Histology*. IntechOpen. https://doi.org/10.5772/intechopen.82017

Hinton, R. B., & Yutzey, K. E. (2011). Heart Valve Structure and Function in Development and Disease. *Annual Review of Physiology*, *73*(1), 29–46. https://doi.org/10.1146/annurev-physiol-012110-142145

Huesa, C., Helfrich, M. H., & Aspden, R. M. (2010). Parallel-plate fluid flow systems for bone cell stimulation. *Journal of Biomechanics*, *43*(6), 1182–1189. https://doi.org/10.1016/j.jbiomech.2009.11.029

Hsu, C.-P. D., Hutcheson, J. D., & Ramaswamy, S. (2020). Oscillatory fluid-induced mechanobiology in heart valves with parallels to the vasculature. *Vascular Biology*, *2*(1), R59–R71. https://doi.org/10.1530/VB-19-0031

Ibrahim, D. M., Kakarougkas, A., & Allam, N. K. (2017). Recent advances on electrospun scaffolds as matrices for tissue-engineered heart valves. *Materials Today Chemistry*, *5*, 11–23. https://doi.org/10.1016/j.mtchem.2017.05.001

IdenTx 3 chip. AIM Biotech. (2022, January 28). Retrieved March 2, 2022, from https://aimbiotech.com/product/identx-3-chip/

Intelligent peristaltic pump (n.d.). Retrieved December 14, 2021, from https://www.crpumpshop.com/the-intelligent-peristaltic-pump-with-the-maximum-liquid-transfer-flow-of-1740mlmin-was-obtained-p3744582.html

Isailovic, B., Rees, B., & Kradolfer, M. (2015). Fluid Dynamics of a Single-Use, Stirred-Tank Bioreactor for Mammalian Cell CultureBioProcess International. https://bioprocessintl.com/upstream-processing/bioreactors/fluid-dynamics-of-a-single-use-stirred-tank-bioreactor-for-mammalian-cell-culture-2/

Islam, M. R., & Hossain, M. E. (2021). Chapter 2—State-of-the-art of drilling. In M. R. Islam & M. E. Hossain (Eds.), *Drilling Engineering* (pp. 17–178). Gulf Professional Publishing. https://doi.org/10.1016/B978-0-12-820193-0.00002-2

Jana, S., Lerman, A., & Simari, R. D. (2015). In Vitro Model of a Fibrosa Layer of a Heart Valve. *ACS Applied Materials & Interfaces*, *7*(36), 20012–20020. https://doi.org/10.1021/acsami.5b04805

Joshi, S., & Yu, D. (2017). Chapter 8—Immunofluorescence. In M. Jalali, F. Y. L. Saldanha, & M. Jalali (Eds.), *Basic Science Methods for Clinical Researchers* (pp. 135–150). Academic Press. https://doi.org/10.1016/B978-0-12-803077-6.00008-4

Ju, J., Park, J. Y., Kim, K. C., Kim, H., Berthier, E., Beebe, D. J., & Lee, S.-H. (2008). *Backward flow in a surface tension driven micropump*. *18*(8), 087002. https://doi.org/10.1088/0960-1317/18/8/087002

Kai, D. (2013). Electrospun synthetic and natural nanofibers for regenerative medicine and stem cells. *Biotechnology Journal.*, *8*(1), 59–72. https://doi.org/10.1002/biot.201200249

Khan, S. S., Trento, A., DeRobertis, M., Kass, R. M., Sandhu, M., Czer, L. S., Blanche, C., Raissi, S., Fontana, G. P., Cheng, W., Chaux, A., & Matloff, J. M. (2001). Twenty-year comparison of tissue and mechanical valve replacement. *The Journal of Thoracic and Cardiovascular Surgery*, *122*(2), 257–269. https://doi.org/10.1067/mtc.2001.115238

Kim, S.-O., Kim, J., Okajima, T., & Cho, N.-J. (2017). Mechanical properties of paraformaldehyde-treated individual cells investigated by atomic force microscopy and

scanning ion conductance microscopy. *Nano Convergence*, *4*, 5. https://doi.org/10.1186/s40580-017-0099-9

Kim, S.-J., Zhu, X., & Takayama, S. (2017). Gravity-Driven Fluid Pumping and Cell Manipulation. In W. Lee, P. Tseng, & D. Di Carlo (Eds.), *Microtechnology for Cell Manipulation and Sorting* (pp. 175–192). Springer International Publishing. https://doi.org/10.1007/978-3-319-44139-9_6

Kouzbari, K., Hossan, M. R., Arrizabalaga, J. H., Varshney, R., Simmons, A. D., Gostynska, S., Nollert, M. U., & Ahamed, J. (2019). Oscillatory shear potentiates latent TGF-β1 activation more than steady shear as demonstrated by a novel force generator. *Scientific Reports*, *9*(1), 6065. https://doi.org/10.1038/s41598-019-42302-x

Kovacic, J. C., Dimmeler, S., Harvey, R. P., Finkel, T., Aikawa, E., Krenning, G., & Baker, A. H. (2019). Endothelial to Mesenchymal Transition in Cardiovascular Disease. *Journal of the American College of Cardiology*, *73*(2), 190–209. https://doi.org/10.1016/j.jacc.2018.09.089

Lee, J.-Y., & Kong, G. (2016). Roles and epigenetic regulation of epithelial–mesenchymal transition and its transcription factors in cancer initiation and progression. *Cellular and Molecular Life Sciences*, *73*(24), 4643–4660. https://doi.org/10.1007/s00018-016-2313-z

Lincoln, J., & Garg, V. (2014). Etiology of Valvular Heart Disease. *Circulation Journal*, *78*(8), 1801–1807. https://doi.org/10.1253/circj.CJ-14-0510

Liu, Y., Deng, B., Zhao, Y., Xie, S., & Nie, R. (2013). Differentiated markers in undifferentiated cells: Expression of smooth muscle contractile proteins in multipotent bone marrow mesenchymal stem cells. *Development, Growth & Differentiation*, *55*(5), 591–605. https://doi.org/10.1111/dgd.12052

Lloyd-Jones, D., Adams, R. J., Brown, T. M., Carnethon, M., Dai, S., De Simone, G., Ferguson, T. B., Ford, E., Furie, K., Gillespie, C., Go, A., Greenlund, K., Haase, N., Hailpern, S., Ho, P. M., Howard, V., Kissela, B., Kittner, S., Lackland, D., … Wylie-Rosett, J. (2010). Heart Disease and Stroke Statistics—2010 Update: A Report From the American Heart Association. *Circulation*, *121*(7). https://doi.org/10.1161/CIRCULATIONAHA.109.192667

Lund, O., Nielsen, T. T., Emmertsen, K., Flø, C., Rasmussen, B., Jensen, F. T., Pilegaard, H. K., Kristensen, L. H., & Hansen, O. K. (1996). Mortality and worsening of prognostic profile during waiting time for valve replacement in aortic stenosis. *The Thoracic and Cardiovascular Surgeon*, *44*(6), 289–295. https://doi.org/10.1055/s-2007-1012039

Luo, Z., Bian, Y., Su, W., Shi, L., Li, S., Song, Y., Zheng, G., Xie, A., & Xue, J. (2019). Comparison of various reagents for preparing a decellularized porcine cartilage scaffold. *American Journal of Translational Research*, *11*(3), 1417–1427.

Mahler, G. J., Frendl, C. M., Cao, Q., & Butcher, J. T. (2014). Effects of shear stress pattern and magnitude on mesenchymal transformation and invasion of aortic valve endothelial cells. *Biotechnology and Bioengineering*, *111*(11), 2326–2337.

https://doi.org/10.1002/bit.25291

Makkar, R. R., Fontana, G. P., Jilaihawi, H., Kapadia, S., Pichard, A. D., Douglas, P. S., Thourani, V. H., Babaliaros, V. C., Webb, J. G., Herrmann, H. C., Bavaria, J. E., Kodali, S., Brown, D. L., Bowers, B., Dewey, T. M., Svensson, L. G., Tuzcu, M., Moses, J. W., Williams, M. R., … Leon, M. B. (2012). Transcatheter Aortic-Valve Replacement for Inoperable Severe Aortic Stenosis. *New England Journal of Medicine*, *366*(18), 1696–1704. https://doi.org/10.1056/NEJMoa1202277

Mavrogiannis, N., Ibo, M., Fu, X., Crivellari, F., & Gagnon, Z. (2016). Microfluidics made easy: A robust low-cost constant pressure flow controller for engineers and cell biologists. *Biomicrofluidics*, *10*(3), 034107. https://pubmed.ncbi.nlm.nih.gov/27279931/

McMillan, A. (2017, November 28). *Flow Control in Microfluidics*. Darwin Microfluidics. https://darwin-microfluidics.com/blogs/reviews/flow-control-in-microfluidics *Peristaltic Pumps*. Cole. (2021, October 18). Retrieved November 16, 2021, from https://www.coleparmer.com/tech-article/multiple-channel-pumping.

Mc Morrow, R., Kriza, C., Urbán, P., Amenta, V., Amaro, J. A. B., Panidis, D., Chassaigne, H., & Griesinger, C. B. (2020). Assessing the safety and efficacy of TAVR compared to SAVR in low-to-intermediate surgical risk patients with aortic valve stenosis: An overview of reviews. *International Journal of Cardiology*, *314*, 43–53. https://doi.org/10.1016/j.ijcard.2020.04.022

Medfusion 4000 Syringe Infusion Pump | Biomedix Medical, Inc. (n.d.). Retrieved December 14, 2021, from https://www.biomedixmedical.com/product/medfusion-4000-syringe-infusion-pump/

Mendelson, K., & Schoen, F. J. (2006). Heart Valve Tissue Engineering: Concepts, Approaches, Progress, and Challenges. *Annals of Biomedical Engineering*, *34*(12), 1799–1819. https://doi.org/10.1007/s10439-006-9163-z

Merryman, D. (2015). Frontiers of Engineering: Reports on Leading-Edge Engineering from the 2014 Symposium. Vanderbilt University. https://doi.org/10.17226/18985

Mina, S., Wang, W., Cao, Q., Huang, P., T. Murray, B., & J. Mahler, G. (2016). Shear stress magnitude and transforming growth factor-βeta 1 regulate endothelial to mesenchymal transformation in a three-dimensional culture microfluidic device. *RSC Advances*, *6*(88), 85457–85467. https://doi.org/10.1039/C6RA16607E

Motta, S. E., Fioretta, E. S., Lintas, V., Dijkman, P. E., Hilbe, M., Frese, L., Cesarovic, N., Loerakker, S., Baaijens, F. P. T., Falk, V., Hoerstrup, S. P., & Emmert, M. Y. (2020). Geometry influences inflammatory host cell response and remodeling in tissue-engineered heart valves in-vivo. Scientific Reports, 10(1), 19882. https://doi.org/10.1038/s41598-020-76322-9

Muylaert, D. E. P., de Jong, O. G., Slaats, G. G. G., Nieuweboer, F. E., Fledderus, J. O., Goumans, M.-J., Hierck, B. P., & Verhaar, M. C. (2016). Environmental Influences on Endothelial to Mesenchymal Transition in Developing Implanted Cardiovascular Tissue-Engineered Grafts. *Tissue Engineering Part B: Reviews*, *22*(1), 58–67.

https://doi.org/10.1089/ten.teb.2015.0167

Nienow, A., Isailovic, B., & Barrett, T. (2016, November 17). Design and Performance of Single-Use, Stirred-Tank Bioreactors. *BioProcess International*. https://bioprocessintl.com/2016/design-performance-single-use-stirred-tank-bioreactors/

Peeters, F. E. C. M., Meex, S. J. R., Dweck, M. R., Aikawa, E., Crijns, H. J. G. M., Schurgers, L. J., & Kietselaer, B. L. J. H. (2018). Calcific aortic valve stenosis: Hard disease in the heart. *European Heart Journal*, *39*(28), 2618–2624. https://doi.org/10.1093/eurheartj/ehx653

Peterson, D. (2014). Microfluidic Bioreactors. *SpringerLink*. https://doi.org/10.1007/978

Pober, J. S., & Sessa, W. C. (2007). Evolving functions of endothelial cells in inflammation. Nature Reviews Immunology, 7(10), 803–815. https://doi.org/10.1038/nri2171

Polacheck, W. J., German, A. E., Mammoto, A., Ingber, D. E., & Kamm, R. D. (2014). Mechanotransduction of fluid stresses governs 3D cell migration. *Proceedings of the National Academy of Sciences*, *111*(7), 2447–2452. https://doi.org/10.1073/pnas.1316848111

Ramaswamy, S., Boronyak, S. M., Le, T., Holmes, A., Sotiropoulos, F., & Sacks, M. S. (2014). A novel bioreactor for mechanobiological studies of engineered heart valve tissue formation under pulmonary arterial physiological flow conditions. *Journal of Biomechanical Engineering*, *136*(12), 121009. https://doi.org/10.1115/1.4028815

Reardon, M. J., Van Mieghem, N. M., Popma, J. J., Kleiman, N. S., Søndergaard, L., Mumtaz, M., Adams, D. H., Deeb, G. M., Maini, B., Gada, H., Chetcuti, S., Gleason, T., Heiser, J., Lange, R., Merhi, W., Oh, J. K., Olsen, P. S., Piazza, N., Williams, M., … Kappetein, A. P. (2017). Surgical or Transcatheter Aortic-Valve Replacement in Intermediate-Risk Patients. *New England Journal of Medicine*, *376*(14), 1321–1331. https://doi.org/10.1056/NEJMoa1700456

Reimer, J., Syedain, Z., Haynie, B., Lahti, M., Berry, J., & Tranquillo, R. (2017). Implantation of a Tissue-Engineered Tubular Heart Valve in Growing Lambs. Annals of Biomedical Engineering, 45(2), 439–451. https://doi.org/10.1007/s10439-016-1605-7

Resto, P. J., Mogen, B. J., Berthier, E., & Williams, J. C. (2010). An automated microdroplet passive pumping platform for high-speed and packeted microfluidic flow applications. *Lab on a Chip*, *10*(1), 23–26. https://doi.org/10.1039/b917147a

Rowe, S. L., Lee, S., & Stegemann, J. P. (2007). Influence of Thrombin Concentration on the Mechanical and Morphological Properties of Cell-seeded Fibrin Hydrogels. *Acta Biomaterialia*, *3*(1), 59–67. https://doi.org/10.1016/j.actbio.2006.08.006

Sabbagh-yazdi, S., Rostami, F., Rezaei-manizani, H., & Mastorakis, N. E. (2007). *Comparison of the Results of 2D and 3D Numerical Modeling of Flow over Spillway Chutes with Vertical Curvatures*. *1*(4), 7.

Schoen, F. J. (2012). Mechanisms of Function and Disease of Natural and Replacement Heart Valves. Annual Review of Pathology: Mechanisms of Disease, 7(1), 161–183. https://doi.org/10.1146/annurev-pathol-011110-130257

Seo, J., Wang, C., Chang, S., Park, J., & Kim, W. (2019). A hydrogel-driven microfluidic suction pump with a high flow rate. *Lab on a Chip*, *19*(10), 1790–1796. https://doi.org/10.1039/C9LC00062C

Shinoka, T., & Miyachi, H. (2016). Current Status of Tissue Engineering Heart Valve. *World Journal for Pediatric and Congenital Heart Surgery*, *7*(6), 677–684. https://doi.org/10.1177/2150135116664873

Sin, A., Reardon, C. F., & Shuler, M. L. (2004). A self-priming microfluidic diaphragm pump capable of recirculation fabricated by combining soft lithography and traditional machining. *Biotechnology and Bioengineering*, *85*(3), 359–363. https://doi.org/10.1002/bit.10787

Stassen, O. M. J. A., Muylaert, D. E. P., Bouten, C. V. C., & Hjortnaes, J. (2017). Current Challenges in Translating Tissue-Engineered Heart Valves. *Current Treatment Options in Cardiovascular Medicine*, *19*(9), 71. https://doi.org/10.1007/s11936-017-0566-y

Streets, A. M., & Huang, Y. (2013). Chip in a lab: Microfluidics for next generation life science research. *Biomicrofluidics*, *7*(1), 011302. https://doi.org/10.1063/1.4789751

Sucosky, P., Padala, M., Elhammali, A., Balachandran, K., Jo, H., & Yoganathan, A. P. (2008). Design of an ex vivo culture system to investigate the effects of shear stress on cardiovascular tissue. *Journal of Biomechanical Engineering*, *130*(3), 035001. https://doi.org/10.1115/1.2907753//www.horiba.com/gbr/semiconductor/applications/photolithography/ (accessed Dec. 04, 2021).

Super simple gravity-fed AT0—Reef Central Online Community. (n.d.). Retrieved December 14, 2021, from http://www.reefcentral.com/forums/showthread.php?t=1557960

Syedain, Z., Reimer, J., Schmidt, J., Lahti, M., Berry, J., Bianco, R., & Tranquillo, R. T. (2015). 6-month aortic valve implantation of an off-the-shelf tissue-engineered valve in sheep. *Biomaterials*, *73*, 175–184. https://doi.org/10.1016/j.biomaterials.2015.09.016

Syedain Z., Haynie B., Johnson S., Lahti M., Berry J., Carney J., Li J., Hill R., Hansen K., Thrivikraman G., Bianco R., Tranquillo R. T. (2021). Pediatric tri-tube valved conduits made from fibroblast-produced extracellular matrix evaluated over 52 weeks in growing lambs. *Sci Transl Med, 13,* 585. https://pubmed.ncbi.nlm.nih.gov/33731437/

Tag, H. M. (2015). Hepatoprotective effect of mulberry (Morus nigra) leaves extract against methotrexate induced hepatotoxicity in male albino rat. *BMC Complementary and Alternative Medicine*, *15*, 252. https://doi.org/10.1186/s12906-015-0744-y

Taylor, D. A., Sampaio, L. C., Ferdous, Z., Gobin, A. S., & Taite, L. J. (2018). Decellularized matrices in regenerative medicine. *Acta Biomaterialia*, *74*, 74–89. https://doi.org/10.1016/j.actbio.2018.04.044

Tissue Engineering—An overview | ScienceDirect Topics. (n.d.). Retrieved October 2, 2021, from https://www.sciencedirect.com/topics/engineering/tissue-engineering

Tonk, C. H., Witzler, M., Schulze, M., & Tobiasch, E. (2020). Mesenchymal Stem Cells. In B. Brand-Saberi (Ed.), *Essential Current Concepts in Stem Cell Biology* (pp. 21–39). Springer International Publishing. https://doi.org/10.1007/978-3-030-33923-4_2

Transwell with 8.0 µm Pore Polycarbonate Membrane Insert, (n.d.). Retrieved December 15, 2021, from https://ecatalog.corning.com/life-sciences/b2c/US/en/Permeable-Supports/Inserts/Transwell%C2%AE-Permeable-Supports,-Polycarbonate-(PC)-Membrane/p/3422

Torino, S., Corrado, B., Iodice, M., & Coppola, G. (2018). PDMS-Based Microfluidic Devices for Cell Culture. *Inventions*, *3*(3), 65. https://doi.org/10.3390/inventions3030065

Vahanian, A., Baumgartner, H., Bax, J., Butchart, E., Dion, R., Filippatos, G., Flachskampf, F., Hall, R., Iung, B., Kasprzak, J., Nataf, P., Tornos, P., Torracca, L., Wenink, A., Priori, S. G., Blanc, J.-J., Budaj, A., Camm, J., Dean, V., … Authors/Task Force Members, E. C. for P. G. (CPG), Document Reviewers. (2007). Guidelines on the management of valvular heart disease: The Task Force on the Management of Valvular Heart Disease of the European Society of Cardiology. *European Heart Journal*, *28*(2), 230–268. https://doi.org/10.1093/eurheartj/ehl428

VeDepo, M. C., Detamore, M. S., Hopkins, R. A., & Converse, G. L. (2017). Recellularization of decellularized heart valves: Progress toward the tissue-engineered heart valve. Journal of Tissue Engineering, 8, 2041731417726327. https://doi.org/10.1177/2041731417726327

Vesely, I. (2005). Heart Valve Tissue Engineering. Circulation Research, 97(8), 743–755. https://doi.org/10.1161/01.RES.0000185326.04010.9f

Vickerman, V., Blundo, J., Chung, S., & Kamm, R. D. (2008). Design, Fabrication and Implementation of a Novel Multi Parameter Control Microfluidic Platform for Three-Dimensional Cell Culture and Real-Time Imaging. *Lab on a Chip*, *8*(9), 1468–1477. https://doi.org/10.1039/b802395f

Weber, M., Gonzalez de Torre, I., Moreira, R., Frese, J., Oedekoven, C., Alonso, M., Rodriguez Cabello, C. J., Jockenhoevel, S., & Mela, P. (2015). Multiple-Step Injection Molding for Fibrin-Based Tissue-Engineered Heart Valves. *Tissue Engineering Part C: Methods*, *21*(8), 832–840. https://doi.org/10.1089/ten.tec.2014.0396

What is Computational Fluid Dynamics/3D Hydraulic Modeling? (2019, July 24). *Ayres*. https://www.ayresassociates.com/what-is-computational-fluid-dynamics-3d-hydraulic-modeling/

Walker, G., Masters, K., Shah, D., Anseth, K., & Leinwand, L. (2004, June 11). *Valvular Myofibroblast Activation by Transforming Growth Factor-β*. https://doi.org/10.1161/01.RES.0000136520.07995.aa

Working principle peristaltic pumps. (2017, June 26). Verder Liquids. https://www.verderliquids.com/us/en/pumps-by-principle/how-do-peristaltic-pumps-work/working-principle-peristaltic-pumps/

Yao, S., & Santiago, J. G. (2003). Porous glass electroosmotic pumps: Theory. *Journal of Colloid and Interface Science*, *268*(1), 133–142. https://doi.org/10.1016/s0021-9797(03)00731-8

Zhu, W., Cao, L., Song, C., Pang, Z., Jiang, H., & Guo, C. (2021). Cell-derived decellularized extracellular matrix scaffolds for articular cartilage repair. *The International Journal of Artificial Organs*, *44*(4), 269–281. https://doi.org/10.1177/0391398820953866

Zhu, A. S., & Grande-Allen, K. J. (2018). Heart valve tissue engineering for valve replacement and disease modeling. Current Opinion in Biomedical Engineering, 5, 35–41. https://doi.org/10.1016/j.cobme.2017.12.006